



WP2

Wednesday, 5th of November 2009

**D07 PART B: ADVANCED MOBILE
BROADCAST SYSTEM – DVB-NGH**

-

WP2 SYSTEM ARCHITECTURE

-

NOVEMBER 2009

I EXECUTIVE SUMMARY – INTRODUCTION

This deliverable aims at evaluating some key technologies that are worth investigating for advanced mobile broadcast system, i.e. DVB-NGH standard. Among these technologies, we find multi-antenna or MIMO (Multiple-In Multiple-Out) aspects.

The first study (see section II) proposes a new spatial coding scheme called 3D MIMO that is a hybrid combination of space-time block codes (STBC) and Golden code MIMO schemes. It is shown that such a code is very efficient in a single frequency network (SFN) context where the double layer structure of the code allows inter-cell and intra-cell space-time coding across the multiple antennas of the network. Another field of application is also proposed with the possible hybrid reception of satellite and terrestrial links. In both transmission scenarios, the proposed code outperforms other classical STBC approaches since it does not only take advantage of the robustness of the Alamouti structure but also of the full rate capability of the Golden code. As a consequence, such a code allows high spectral efficiencies to be achieved while ensuring robust transmission in many broadcasting contexts.

The second MIMO topic (see section VI) proposes and evaluates the combination of the rotated constellation, introduced in DVB-T2, with MIMO schemes. This evaluation shows the interest of the iterative receivers to benefit from the diversity gains brought either by the MIMO or/and by the rotated constellations. The first part of the study concerns the performance of iterative receivers for MIMO systems when the DVB-T2 error correcting (LDPC) code is considered. Several STBCs are considered, ranging from the classical spatial multiplexing scheme to more complex linear precoding-based STBCs. Unlike the previous work performed in TF206 and presented in deliverable D2.6.1, the system design and the performance evaluation take into account the presence of the powerful LDPC error correcting encoder/decoder. Moreover, through synthesis charts, this study shows the improvements in terms of spectral efficiency and/or BER performance brought by the MIMO system compared to a SIMO (Single-In Multiple-Out) or SISO (Single-In Single-Out) system. It was observed that:

- compared to the SISO system, the proposed MIMO scheme allows for a performance gain greater than 2 dB for low spectral efficiencies and even 6 dB for high spectral efficiencies;
- compared to the SIMO system, the proposed MIMO scheme allows for a performance gain, greater than 2 dB whatever the couple code rate/modulation.

In the second part of the study, the principle of rotated constellations adopted in the DVB-T2 standard was extended to a SIMO system. The simulation results showed that when erasure events are taken into account during the transmission, the rotated scheme largely outperformed the non-rotated one. The gap between both schemes can range from several tenth of dB to several dBs when the performance of the non-rotated scheme leads to an error floor. In the case of transmission over Rayleigh fading channel, an iterative process between the decoder and the demapper should be performed in order to efficiently exploit the signal space diversity provided by the rotated constellation.

A proposal of a new preamble design (see section III) is also evaluated for coarse frequency synchronization for cyclic prefix (CP) OFDM systems. The presented approach allows for a fast synchronisation to the data stream. In case of OFDM this procedure especially incorporates the detection of signals and the coarse frequency synchronisation to the data stream. Additionally, the flexibility of the overall signal bandwidth is important, as the available frequency resources get more and more fragmented. One example for a completely flexible signal bandwidth is DVB's second generation standard for cable transmission: DVB-C2. This system does not rely on any channel raster and the bandwidth of the signal is completely flexible. However, this requires a new synchronisation scheme to the signals. The scheme presented in this document could also be

applied for the next generation handheld system, DVB-NGH. As shown in the document, the proposed technique cannot be applied to the preamble only, but it is also feasible for the frequency domain pilots within the payload OFDM symbols. This is especially reached by the fact that the receiver knows the sequence it has to expect. Additionally, it allows for a method to transmit Layer 1 signalling within the preamble, which can be received even if the receiver is not completely tuned to the correct frequencies. Hence, it also allows for variable bandwidth without any need for a fixed channel structure.

In order to increase the spectral efficiency, a system without pilot symbols for channel estimation is proposed; in this scenario a SISO (see section IV) and MISO (see section V) system are evaluated. So, DVB-T2 offers a special mode in which the overhead due to the pilots is minimized. Using this Pilot Pattern (PP) 8, the receiver has to employ additional means to estimate the channel. One means, for which the PP8 scheme of DVB-T2 was mainly designed, is the so-called and well known CD3 algorithm. Using this algorithm, the data is used as pilots in order to estimate the channel. However, the data symbols have to be known prior the equalization process in order to estimate the channel correctly. As this is practically impossible, the algorithm introduces a delay of at least one OFDM symbol. Hence, the receiver does not use the correct channel estimates to equalize the channel, but previous ones. This may be uncritical for stationary reception, but gets important for mobile or portable receivers. Additionally, there may be the effect of error propagation. If the PP8 scheme is used for DVB-T2, the application of time interleaving is prohibited, because this would lead to even longer delays than 1 OFDM symbol. However, if the receiver is not able to correct one LDPC FEC block completely, the following channel estimation will include errors that leads to reduced channel estimation performance. This will naturally propagate to the next OFDM symbols, and so on. In extreme situations, this may even lead to loss of synchronization until the next reference symbol is sent. However, due to the decreased overhead this technique may be a candidate for DVB-NGH as well, especially for slow mobility (< 40 Hz Doppler).

Since the beginning of the B21C project, Orange Labs proposed the OFDM/OQAM modulation scheme in order to be more resistant than CP-OFDM in mobile environments. The main interests of OQAM are the improvement of throughput thanks to the absence of the guard interval, the performance against Doppler and the confinement of the spectrum. Of course these advantages are not free since the modem complexity is greater than for CP-OFDM and the performance against long echoes is less than conventional OFDM scheme. During previous studies within the B21C project, it has been shown that OFDM/OQAM is suitable for Doppler environments but suffers from large channel delay spreads typical of SFN environments. In addition, we have seen that regarding to the environment, the OFDM/OQAM prototype filter can be adapted, since some filters are more suitable for Doppler environments (TFL prototype) whereas others are appropriate to large delay spread values (FS prototype). The idea of introducing OFDM/OQAM in a new standard should be very useful for mobile scenarios, i.e. DVB-NGH, and for networks having delay spread value no more than 10% of the symbol duration. So, the idea is not to entirely stand in conventional CP-OFDM for OFDM/OQAM but to put in as optional to get more robustness in mobile environments (train ...). However, combining OFDM/OQAM with STBCs such Alamouti codes leads to some troubles that are detailed in this document. Thus a comparison and evaluation of OFDM/OQAM in a SISO environment regarding to CP-OFDM with MIMO Alamouti scheme, either performed in time or in frequency domain, is carried out with regards to Doppler effect and SFN environment. The conclusion shows that for mobile environments, OQAM leads to better resistance than CP-OFDM even if MIMO Alamouti is implemented. However, OQAM suffers from large delay spreads typical of SFN environments.

Table of Content

I	Executive summary – Introduction	2
II	3D MIMO	7
II.1	Introduction	7
II.2	System Model in Terrestrial Single Frequency Networks.....	7
II.2.1	Open area environment	8
II.2.2	Gap Area Environment.....	9
II.2.3	Transmission Model	9
II.3	System Model in Hybrid Satellite Terrestrial Transmission.....	11
II.3.1	Land Mobile Satellite Channel Model	11
II.3.2	Transmission Model	12
II.4	Receiving Model.....	13
II.4.1	Received Signal	13
II.4.2	STBC detector	15
II.4.3	LLR computation	16
II.5	Choice of MIMO Schemes: Terrestrial Transmission.....	17
II.5.1	Single Layer case: inter-cell ST coding	19
II.5.2	Double Layer case	20
II.5.2.1	Open area environment.....	21
II.5.2.2	Gap area environment.....	23
II.5.3	Choice of MIMO Schemes: Hybrid SATT Transmission.....	23
II.6	Conclusion.....	25
II.7	REFERENCES	25
III	New preamble for efficient coarse frequency synchronization in OFDM	27
III.1	Concept of Absolute OFDM.....	27
III.2	Preamble Realisation.....	28
III.3	Synchronisation Procedure	29
III.4	Transmission of Layer 1 Signalling Data	30
III.5	Example Tuning Procedure.....	31
III.6	Simulation Results	31
III.7	Conclusions	32

III.8	References	33
IV	Performance of channel estimation without pilots.....	34
IV.1	Description of Basic Algorithm	34
IV.2	Simulation Results	35
IV.2.1	Static Channel Simulation Results.....	35
IV.2.2	Mobile Channel Simulation Results.....	37
IV.2.3	Error Propagation Simulation Results	38
IV.3	Conclusion	38
IV.4	References	39
V	Channel MISO channel estimation without pilots	40
V.1	Estimation of the Channel Transfer Functions	40
V.2	Performance Results	41
V.3	Conclusions	42
V.4	References	42
VI	Extension of rotated constellations for MIMO systems over erasure channels.....	43
VI.1	Introduction	43
VI.2	Performance of iterative receivers for MIMO system with DVB-T2 LDPC code	43
VI.2.1	Transmission model	43
VI.2.2	Description of the space-time codes.....	44
VI.2.3	Receiver model.....	46
VI.2.3.1	SIMO receiver	46
VI.2.3.2	MIMO iterative receiver	46
VI.2.3.3	Symbol to LLR conversion.....	48
VI.2.3.4	LLR to symbol conversion	49
VI.2.4	Performance bounds.....	49
VI.2.4.1	MRC receiver	49
VI.2.4.2	MIMO Iterative receiver.....	50
VI.2.5	Simulation results	50
VI.2.6	Iterative receivers for a MIMO system with DVB-T2 LDPC code: Conclusion	57
VI.3	Extension of rotated constellations for a SIMO system over erasure channels	58
VI.3.1	System model.....	58
VI.3.2	Simulation results	59
VI.3.2.1	Over i.i.d. Rayleigh fading channel	60
VI.3.2.2	Over i.i.d. Rayleigh fading channel with erasures	60
VI.3.2.3	Summary of performance over i.i.d. Rayleigh fading channel with erasures	63

- VI.3.2.4 Comparison with SISO..... 64
- VI.3.3 Rotated constellations for a SIMO system over erasure channels: Conclusion 67
- VI.4 Conclusions 67
- VI.5 References 67
- VII MIMO and OFDM/OQAM..... 69
- VII.1 INTRODUCTION 69
- VII.2 OFDM/OQAM and Alamouti 69
 - VII.2.1 OFDM/OQAM: Brief recall of the basic principles 69
 - VII.2.2 Alamouti scheme: General case 72
 - VII.2.3 OFDM/OQAM with Alamouti scheme..... 73
- VII.3 SISO OFDM/OQAM versus MISO Alamouti CP-OFDM..... 76
 - VII.3.1 Context 76
 - VII.3.2 Simulation chain description 76
 - VII.3.3 Presentation of the different OFDM/MISO/Alamouti schemes 77
 - VII.3.4 Time approach (classical) 77
 - VII.3.5 Frequency approach (included in DVB-T2) 78
 - VII.3.6 Performances results..... 78
 - VII.3.6.1 Results with Doppler shift..... 78
 - VII.3.6.2 Results with SFN channel 79
- VII.4 Conclusion 80
- VII.5 References 81

II 3D MIMO

II.1 INTRODUCTION

The proposed system is based on a 3D MIMO-OFDM scheme taking advantage of the particular characteristics of the SFN. More precisely, the contribution of this work is multifold.

If the system implements terrestrial sites only, the MIMO techniques will be applied between different sites' antennas and thus it will allow a higher diversity than co-located antennas. An investigation of potential distributed MIMO techniques in terrestrial transmission will be one of the main targets of this work. First of all, we investigate the possibility of applying a space-time block code (STBC) encoder between the antennas of two sites in the SFN architecture. Second, a generalized framework is proposed for modelling the effect of unbalanced powers received from different transmitting antennas in MIMO-OFDM systems. This is a critical problem in SFN with mobile and portable reception. Then, we analyze and compare some of the most promising STBC schemes in the context of broadcasting for future terrestrial digital TV with equal and unequal received powers. Once compared, we propose a new 3D space-time-space (STS) block code for SFN environment. The use of a second space dimension will be justified as being particularly adapted and efficient in the case of SFN transmission. The proposed code is based on a double level construction of ST codes resulting from the combination of two coding schemes. The first layer corresponds to an inter-cell ST coding while the second one corresponds to an intra-cell ST coding.

If the system implements a satellite component, the combination of satellite and terrestrial sites' antennas using a MIMO technique will be investigated. In this hybrid transmission, a detailed study will focus on MIMO channel model combining the terrestrial and satellite components. The land mobile satellite (LMS) channel model proposed by Fontan and adopted in DVB-SH is a starting point for further research in this domain.

II.2 SYSTEM MODEL IN TERRESTRIAL SINGLE FREQUENCY NETWORKS

Classically, in SFN architectures, the different antennas transmit at the same moment the same signal on the same frequency. From the reception viewpoint, one has to distinguish two cases: the open area and the gap area environments [1][2]. Open areas correspond to the areas which benefit from an unobstructed view of transmitting antennas. Gap areas correspond to the areas where the direct signal is shadowed by obstacles. In the open area case, the transmitted signal is reflected from a large number of objects in the surroundings of the receiver. These signal components are received with independently time varying amplitudes and phases. In gap areas, there is no direct signal path and the transmitted signal might be easily lost due to the obstacles. To cope with gap areas, repeaters are usually implemented in those regions. The role of these repeaters, known as gap fillers, is to adequately amplify and retransmit the signal in the gap areas. Therefore, a receiver in the gap area could operate similarly as a receiver in the open area.

On the other hand, for the SFN to work properly the resulting total delay spread τ_{\max} of the different received signals must be less than the duration of the guard interval time inserted at the beginning of each OFDM symbol. Moreover, due to the path loss, the power received by each antenna is related to this resulting delay spread as it will be shown in next subsection. As a starting point, let us assume that each site holds one antenna ($M_T=1$ in Figure 2) and that the receiver receives signals from both antennas. Then, two receiving environments could be presented: the open area environment and the gap area environment.

II.2.1 OPEN AREA ENVIRONMENT

In the case of an open area environment, the time offset between the signals received from each site antennas could be seen as a superposition of the time offset between transmitters' signals (the signal time delay between the transmitting antennas) and the signal time offset between each transmitter and the receiver. The first offset is generally negligible since the transmitters are synchronized with an ultra stable reference like the global positioning system (GPS). The second offset could be seen as follows. When the mobile terminal (MT) moves within one cell, it receives signal from its own cell antenna but also from the neighbouring cell antenna. Since the MT is not equidistant to both antennas, the signal received from each one will be delayed according to the position of the MT. This results into a delay $\Delta\tau$ between the two received signals from both antennas or equivalently between the channel impulse responses (CIR) between the transmitters and the receiver. The delays are directly related to the distances between the transmitters and the receiver and thus to the signal strength ratio at the receiver. Assuming an equal transmitted power P_0 at each antenna, the received power from the i^{th} antenna is:

$$P_i = \frac{P_0}{d_i^\alpha} \quad (1)$$

where d_i is the distance between the receiver and the i^{th} transmitter and α is the propagation constant which depends on the transmission environment.

The delay of each CIR between the i^{th} transmitter and the receiver is:

$$\tau_i = \frac{d_i}{c} \quad (2)$$

where c is the light celerity.

Without loss of generality, let us assume that the first transmitter site is the reference site. Substituting d_i from (2) in (1), the CIR delay of the i^{th} link (i.e. between the i^{th} transmitter and the receiver) with respect to the reference antenna can be expressed by:

$$\Delta\tau_i = \tau_i - \tau_1 = \left(10^{\frac{-\beta_i}{10\alpha}} - 1 \right) \frac{d_1}{c} \quad (3)$$

d_1 is the distance between the reference transmitter (first one) and the receiver. β_i is the received power difference (expressed in dB) between the signal received from the reference site and the signal received from the i^{th} transmitter. It is given by:

$$\beta_i [dB] = -10 \cdot \alpha \cdot \log_{10} \left(\frac{d_i}{d_1} \right) \quad (4)$$

In the sequel, we will assume that the power received from the reference antenna is equal to 0 dB and the distance d_i is greater than d_1 whatever i . It is a real situation where the MT is closer to its own cell antenna than other antennas. In this case, β_i is neither than the power attenuation factor between the i^{th} transmitter and the MT. As a consequence, the transmission model becomes equivalent to a system with unbalanced powers received from each site antennas. Figure 1 shows an example of the relation between the power attenuation factor β and the timing offset between the CIR of the second link and the reference link in a system having two transmitting antennas located in two different sites.

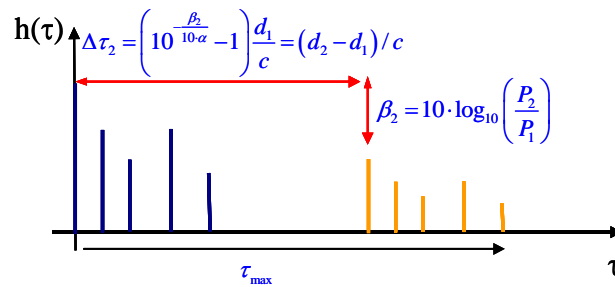


Figure 1- delays and powers in SFN

If we now consider that the number of Tx in one site is greater than one i.e. $M_T > 1$, the choice of an adequate MIMO scheme should then be based on this imbalance in an SFN open area environment. Moreover, it should be adequate for inter-cell (i.e. between antennas signals of each site) and intra-cell (i.e. between antennas signals in each site) environments.

II.2.2 GAP AREA ENVIRONMENT

In this case, the gap filler receives the signals from both antennas with a power difference according to equation (4). Then, it amplifies each one and retransmits them to the MT. Since the gap areas spread, in general, over a smaller region than that of the cell area, the delays between the signals received by the MT could be assumed equal to those between the signals received by the gap filler. Nevertheless, the signals received by the gap filler with a power imbalance of β_i could be re-amplified with different power gains which compensate this imbalance. As a consequence, the MT could receive the different signals with the same power. In other words, due to the gap filler, the delays between the received signals from both sites' antennas could be independent of the parameters β_i in the gap area environment. Thus, when designing a STBC for MIMO transmission, we should also consider this case of transmission environment.

Based on this discussion on SFN transmission, it is clear that the STBC should be chosen adequately to cope with the open area environment but also with the gap area environment.

II.2.3 TRANSMISSION MODEL

In this work, we propose to apply a MIMO communication scheme between the antennas located in the different sites of the SFN architecture. Such a system could be implemented using M_T transmit antennas (Tx) by site as shown in Figure 2. Without loss of generality, we will consider in our study the transmission behaviour of two neighbouring cells using a total of $(2 \times M_T)$ Tx and M_R receive antennas (Rx). However, the proposed double layer scheme could be adapted to more than two neighbouring cells.

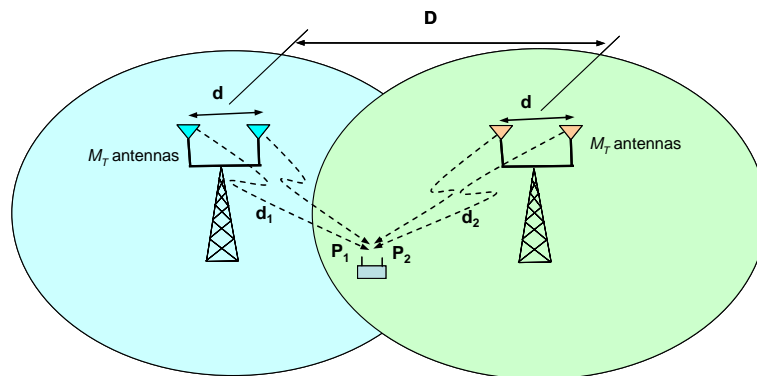


Figure 2- SFN with unequal received powers

The double layer proposed here has to cope with the open area environment but also with the gap area environment in the SFN architecture. Particularly, in contrast with the gap area where the powers received from each site are equal, the double layer has to deal with the equal and unequal received powers in the open area environment. The first layer in our proposed code corresponds to the inter-cell ST coding while the second corresponds to the intra-cell ST coding. We recall that we restrict our study to two sites only and the generalisation could be done in different forms.

Figure 3 depicts the transmitter modules at each site. Information bits b_k are first channel encoded, randomly interleaved, and fed to a quadrature amplitude modulation (QAM) module. The SFN transmission system involving the two sites (described in Figure 2) could therefore be seen as a double layer scheme in the space domain. The first layer is seen between the two sites separated by D km. The second layer is seen between the antennas separated by d meters within one site. For the first layer, a space time block code (STBC) scheme is applied between the 2 signals transmitted by each site antennas. In the second layer, we use a second STBC encoder for each subset of M_T signals transmitted from the same site. For the first layer (respectively the second layer), the STBC encoder takes L (respectively M) sets of data complex symbols and transforms them into a $(2, U)$ (respectively (M_T, V)) output matrix according to the STBC scheme. This output is then fed to $2 \times M_T$ OFDM modulators, each using N_c sub-carriers. In order to have a fair analysis and comparison between different STBC codes, the signal power at the output of the ST encoder is normalized by $2 \times M_T$.

The double layer encoding matrix is then described by:

$$\mathbf{X}^{(1)} = \begin{pmatrix} \mathbf{X}_{11}^{(2)} & \cdots & \mathbf{X}_{1U}^{(2)} \\ \mathbf{X}_{21}^{(2)} & \cdots & \mathbf{X}_{2U}^{(2)} \end{pmatrix}$$

$$\mathbf{X}_{pq}^{(2)} = \begin{pmatrix} f_{pq,11}(s_1, \dots, s_M) & \cdots & f_{pq,1V}(s_1, \dots, s_M) \\ \vdots & \ddots & \vdots \\ f_{pq,M_T1}(s_1, \dots, s_M) & \cdots & f_{pq,M_TV}(s_1, \dots, s_M) \end{pmatrix} \quad (5)$$

In (5), the superscript indicates the layer, $f_{pq,ii}(s_1, \dots, s_M)$ is a function of the input complex symbols s_m and depends on the STBC encoder scheme. The time dimension of the resulting 3D code is equal to $U \times V$ and the resulting coding rate is $R = \frac{L \times M}{U \times V}$.

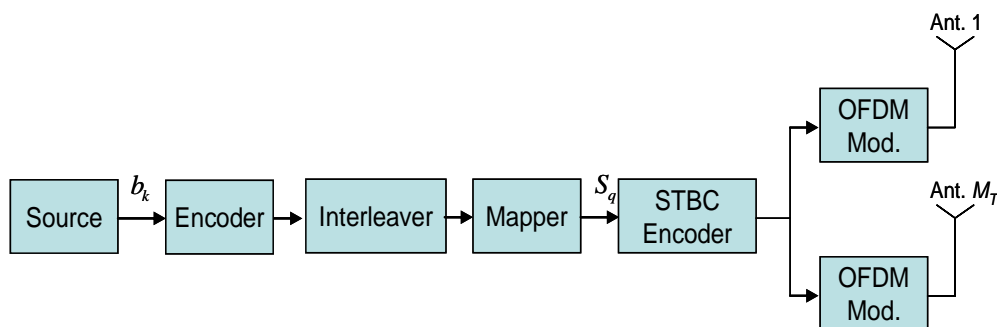


Figure 3- MIMO-OFDM transmitter.

In order to simplify the transmission model, the double layer encoding matrix given in (5) will be represented by $\mathbf{X} = [x_{i,t}]$ where $x_{i,t}$ ($i=1, \dots, 2 \times M_T$; $t=1, \dots, U \times V$) is the output of the double layer STBC encoder on a given sub-carrier n . In other words, the layers construction is transparent from the transmission model viewpoint. Moreover, we set $Q=L \times M$ as the number of the complex symbols at the input of the double layer STBC encoder and we set $T=U \times V$ as the number of the corresponding output symbols. The ST coding rate is then $R = Q/T$.

II.3 SYSTEM MODEL IN HYBRID SATELLITE TERRESTRIAL TRANSMISSION

II.3.1 LAND MOBILE SATELLITE CHANNEL MODEL

One of the main concerns in this hybrid Satellite Terrestrial (SATT) transmission is the LMS channel. In literature, various LMS channel models were proposed based on empirical or statistical models [3]. However, the three-state model proposed by Fontan is widely used within DVB-SH [3] since it is recognized as the most accurate statistical LMS channel model available today, encompassing the widest set of environments and elevation angles. In this model, the direct signal is characterized by a three-state first-order Markov chain where the multi-path component could be in narrow-band or wide-band conditions. These states are defined by:

- S1: LOS conditions
- S2: moderate shadowing conditions
- S3: deep shadowing conditions

Markov chain models can be used to describe the LMS direct propagation channel at a given route position (equivalently given time) by mean of two matrices:

- state transition probability matrix \mathbf{P} whose each element P_{ij} represents the probability of change from state i to state j .
- state probability matrix \mathbf{W} (it could be written as column vector) where W_i is the total probability of being in state i .

The model makes the simplifying assumption of the existence of three-states of the direct signal when traveling a given route. The channel could be in one state according to the probability matrix \mathbf{W} and the transition from one state to another state is achieved according to \mathbf{P} . Typically, each state will last few meters along the traveled distance. In [4], a minimum distance state length called L_{\min} of 3-5 m was observed in the experimentations at S-band. The model proposed by Fontan assumes that the received signal is composed of a superposition of a direct signal and a multipath signal. The joint model of both signals is widely described by a Loo distribution [5]. It is given by a coherent superposition such as:

$$r_T \exp(j\varphi_T) = r_D \exp(j\varphi_D) + r_M \exp(j\varphi_M)$$

where subscript T means total, D direct signal and M multipath signal. For short sections of the traveled route, the received direct signal variations are assumed to vary according to a Ricean distribution with parameters a and σ where a is the mean value and σ is the deviation value. For longer sections, the direct signal is assumed to vary according to a log-normal distribution with parameters μ and Σ describing the mean and standard deviation of the normal distribution. The overall distribution, i.e. for longer stretches of the route, is given by

$$f(r) = \int_0^{\infty} f\left(\frac{r}{a}\right) \cdot f(a) da = \frac{0.6989}{\Sigma \sigma^2 \sqrt{2\pi}} \int_0^{\infty} \frac{1}{a} \exp\left(-\frac{(10 \log a - \mu)^2}{2\Sigma^2}\right) \cdot \exp\left(-\frac{r^2 + a^2}{\sigma^2}\right) I_0\left(\frac{ra}{\sigma^2}\right) da$$

with μ and Σ in dB and $MP \text{ (dB)} = 10 \log(2\sigma^2)$ is the rms squared value of the multipath component expressed in dB.

In this model, the three states of the direct signal corresponds to the very slow variations. The slow variations are generated according to the parameter L_{corr} where L_{corr} is the correlation distance in each state. A distance of $L_{\text{corr}} = 1-3$ m have been observed [6]. In other words, in order to generate the channel coefficients, a sample a should be generated each L_{corr} m according to the Rice distribution. The obtained samples a are then transformed to a lognormal distribution using the transform $A = 10^{a/20}$. In order to ensure a continuity in the resulting direct signal r_D , an interpolation process should be applied each of every $\lambda/8 - \lambda/10$ m [7] where λ is the wavelength. The multipath component samples r_M are generated the same way using the deviation MP . In order to model the Doppler effect due to the mobility of the terminal, the phase of the direct component is assumed to be increased linearly with a random initial phase. The phases of the multipath component are randomly generated and its Doppler effect is modeled by a Butterworth filter which is a common assumption in LMS channels as demonstrated in [6]. Finally, having the different complex samples at each state according to (6), we are now able to generate the overall channel coefficients during a traveling route with different states S1, S2 and S3. In Figure 4, we depict the received signal with the various states.

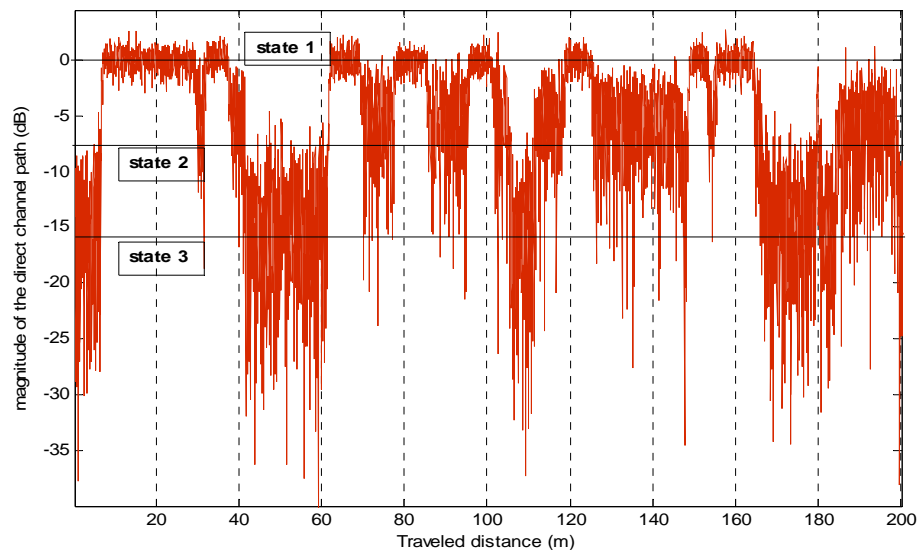


Figure 4- Overall signal level with three states

II.3.2 TRANSMISSION MODEL

It is clear from Figure 4 that when the terminal travels a route, the direct signal from the satellite could be totally lost due to deep or moderate shadowing and hence the performance of the system will be highly degraded if there is no other satellite or terrestrial transmission.

In this section, we describe the MIMO transmission model of the 3D code constructed between the antennas of the satellite and terrestrial sites. The double layer proposed here has to cope with LOS and shadowing states (moderate and deep). The first layer in our proposed code corresponds to the SATT coding while the second corresponds to intra-site coding. Such a system could be implemented using M_T transmit antennas (Tx) by site type as it is done for terrestrial transmission described in previous section. It is clear that the hybrid transmission model is similar to that of terrestrial scheme. The difference here is that the channels of each link are not identical. The receiver will consider the transmitted signal similarly whatever the channel component is. In the following, we will describe the received signal and we will see that this model is independent of the transmission scheme.

II.4 RECEIVING MODEL

II.4.1 RECEIVED SIGNAL

We assume that the transmitter and receiver are perfectly synchronised. Moreover, we assume perfect channel state information (CSI) at the receiver. The signal received on the subcarrier n by the antenna j is a superposition of the transmitted signal by the different antennas multiplied by the channel coefficients $h_{j,i}[n]$ to which white Gaussian noise (WGN) is added. It is given by:

$$y_{j,t}[n] = \sum_{i=1}^{2M_T} \sqrt{P_i} h_{j,i}[n] x_{i,t}[n] + w_{j,t}[n] \quad (8)$$

where $y_{j,t}[n]$ is the signal received on the n^{th} subcarrier by the j^{th} receiving antenna during the t^{th} OFDM symbol duration. $h_{j,i}[n]$ is the frequency channel coefficient assumed to be constant during T symbol durations, $x_{i,t}[n]$ is the signal transmitted by the i^{th} antenna and $w_{j,t}[n]$ is the additive WGN with zero mean and variance $N_0/2$. In the sequel, we will drop the subcarrier index n for simplicity. By introducing an equivalent receive matrix $\mathbf{Y} \in \mathbb{C}^{M_R \times T}$ whose elements are the complex received symbols expressed in (8), we can write the received signal on the n^{th} subcarrier on all receiving antennas as:

$$\mathbf{Y} = \mathbf{H}\mathbf{P}\mathbf{X} + \mathbf{W} \quad (9)$$

where \mathbf{H} is the $(M_R, 2M_T)$ channel matrix whose components are the coefficients $h_{j,i}$, \mathbf{P} is a $(2M_T, 2M_T)$ diagonal matrix containing the signal magnitudes $\sqrt{P_i}$, \mathbf{X} is a $(2M_T, T)$ complex matrix containing the transmitted symbols $x_i[t]$. \mathbf{W} is a (M_R, T) complex matrix corresponding to the WGN.

Let us now describe the transmission link with a general model independently of the ST coding scheme. We separate the real and imaginary parts of the complex symbols input vector $\mathbf{s} \{s_q; q=1, \dots, Q\}$, of the outputs \mathbf{X} of the double layer ST encoder as well as those of the channel matrix \mathbf{H} , and the received signal \mathbf{Y} . Let $s_{q,\Re}$ and $s_{q,\Im}$ be the real and imaginary parts of s_q . The main parameters of the double code are given by its dispersion matrices \mathbf{U}_q and \mathbf{V}_q corresponding (not equal) to the real and imaginary parts of \mathbf{X} respectively. With these notations, \mathbf{X} is given by:

$$\mathbf{X} = \sum_{q=1}^Q (s_{q,\Re} \mathbf{U}_q + js_{q,\Im} \mathbf{V}_q) \quad (10)$$

We separate the real and imaginary parts of \mathbf{S} , \mathbf{Y} and \mathbf{X} and stack them row-wise in vectors of dimensions $(2Q, 1)$, $(2M_R T, 1)$ and $(4M_T T, 1)$ respectively. We obtain:

$$\begin{aligned} \mathbf{s} &= [s_{1,\Re}, s_{1,\Im}, \dots, s_{Q,\Re}, s_{Q,\Im}]^{tr} \\ \mathbf{y} &= [y_{1,\Re}, y_{1,\Im}, \dots, y_{T,\Re}, y_{T,\Im}, \dots, y_{M_R T, \Re}, y_{M_R T, \Im}]^{tr} \\ \mathbf{x} &= [x_{(1,1),\Re}, x_{(1,1),\Im}, \dots, x_{(2M_T, T), \Re}, x_{(2M_T, T), \Im}]^{tr} \end{aligned} \quad (11)$$

where tr holds for matrix transpose.

Since we use linear ST coding, the vector \mathbf{x} can be written as:

$$\mathbf{x} = \mathbf{F}\mathbf{s} \quad (12)$$

where \mathbf{F} has the dimensions $(4M_T T, 2Q)$ and is obtained through the dispersion matrices of the real and imaginary parts of \mathbf{s} . It is given by:

$$\mathbf{F} = \begin{bmatrix} \mathbf{F}_1(1,1) & \cdots & \cdots & \mathbf{F}_Q(1,1) \\ \vdots & \vdots & \vdots & \vdots \\ \mathbf{F}_1(1,T) & \cdots & \cdots & \mathbf{F}_Q(1,T) \\ \vdots & \ddots & \vdots & \vdots \\ \mathbf{F}_1(2M_T, T) & \cdots & \cdots & \mathbf{F}_Q(2M_T, T) \end{bmatrix} \quad (13)$$

\mathbf{F} is composed of $2M_T$ blocks of $2T$ rows each i.e. the data transmitted on each antenna is gathered in one block having $2T$ rows and $2Q$ columns according to the ST coding scheme. The different components of \mathbf{F} are given by:

$$\mathbf{F}_q(m, t) = \begin{bmatrix} \mathbf{U}_{q,\Re}(m, t) & -\mathbf{V}_{q,\Im}(m, t) \\ \mathbf{U}_{q,\Im}(m, t) & \mathbf{V}_{q,\Re}(m, t) \end{bmatrix} \quad (14)$$

As we change the formulation of \mathbf{S} , \mathbf{Y} and \mathbf{X} in (11), it can be shown that the vectors \mathbf{x} and \mathbf{y} are related through the matrix \mathbf{G} of dimensions $(2M_R T, 4M_T T)$ such that:

$$\mathbf{y} = \mathbf{G}\mathbf{B}\mathbf{x} + \mathbf{w} \quad (15)$$

The matrix \mathbf{B} is a $(4M_T T, 4M_T T)$ diagonal matrix whose components are given by:

$$B_{i,i} = \sqrt{P_i} \quad 2T(p-1)+1 \leq i \leq 2T.p \\ p = 1, \dots, 2M_T \quad (16)$$

Matrix \mathbf{G} is composed of blocks $\mathbf{G}_{j,i}$ ($j=1, \dots, M_R; i=1, \dots, 2M_T$) each having $(2T, 2T)$ elements given by:

$$\mathbf{G}_{j,i} = \begin{pmatrix} h_{(j,i),\Re} & -h_{(j,i),\Im} & 0 & \cdots & 0 \\ h_{(j,i),\Im} & h_{(j,i),\Re} & 0 & \cdots & 0 \\ 0 & 0 & h_{(j,i),\Re} & -h_{(j,i),\Im} & 0 & \cdots & 0 \\ 0 & 0 & h_{(j,i),\Im} & h_{(j,i),\Re} & 0 & \cdots & 0 \\ 0 & \cdots & 0 & \ddots & 0 & 0 & 0 \\ 0 & \cdots & 0 & \ddots & 0 & 0 & 0 \\ 0 & \cdots & \cdots & 0 & h_{(j,i),\Re} & -h_{(j,i),\Im} \\ 0 & \cdots & \cdots & 0 & h_{(j,i),\Im} & h_{(j,i),\Re} \end{pmatrix}_{(2T, 2T)} \quad (17)$$

Now, substituting \mathbf{x} from (12) in (15), the relation between \mathbf{y} and \mathbf{s} becomes:

$$\mathbf{y} = \mathbf{G}\mathbf{B}\mathbf{F}\mathbf{s} + \mathbf{w} = \mathbf{G}_{\text{eq}}\mathbf{s} + \mathbf{w} \quad (18)$$

\mathbf{G}_{eq} is the equivalent channel matrix between \mathbf{s} and \mathbf{y} . It is assumed to be known perfectly at the receiving side.

II.4.2 STBC DETECTOR

The detection problem is to find the transmitted data \mathbf{s} given the vector \mathbf{y} . In the case of orthogonal STBC (OSTBC), optimal receiver is made of a concatenation of ST decoder and channel decoder modules. In non-orthogonal (NO-STBC) schemes, there is an inter element interference (IEI) at the receiving side. The optimal receiver in this case is based on joint ST and channel decoding operations. However such receiver is extremely complex to implement and requires large memory to store the different points of the trellis. Moreover, it could not be implemented reasonably in one chip. Thus the sub-optimal solution proposed here consists of an iterative receiver where the ST detector and channel decoder exchange extrinsic information in an iterative way until the algorithm converges. The iterative detector shown in Figure 5 is composed of a parallel interference canceller (PIC), a demapper which consists in computing the soft information of the transmitted bits, i.e. a log likelihood ratio (LLR) computation [8], a soft-input soft-output (SISO) decoder [9], and a soft mapper.

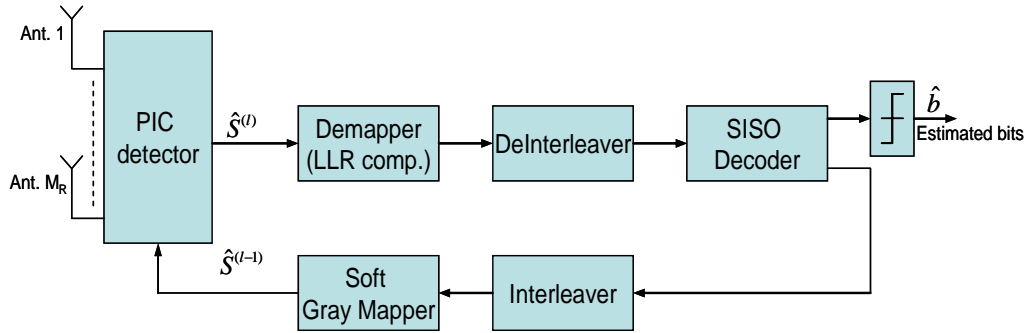


Figure 5- Iterative receiver structure

At the first iteration, the demapper takes the estimated symbols $\hat{\mathbf{s}}$, the knowledge of the channel \mathbf{G}_{eq} and the noise variance, and computes the LLR values of each of the coded bits transmitted per channel use. The estimated symbols $\hat{\mathbf{s}}$ are obtained via minimum mean square error (MMSE) filtering according to:

$$\hat{s}_p = \mathbf{g}_p^{\text{tr}} (\mathbf{G}_{eq} \cdot \mathbf{G}_{eq}^{\text{tr}} + \sigma_w^2 \mathbf{I})^{-1} \mathbf{y} \quad (19)$$

where \mathbf{g}_p^{tr} of dimension $(2M_R T, 1)$ is the p^{th} column of \mathbf{G}_{eq} ($1 \leq p \leq 2Q$) and σ_w^2 is the noise variance. \hat{s}_p is the estimation of the real part (p odd) or imaginary part (p even) of s_q ($1 \leq q \leq Q$). Once the estimation of the different symbols s_q is achieved by the soft mapper at the first iteration, we use this estimation for the next iterations process. From the second iteration, we perform PIC operation followed by a simple inverse filtering (instead of MMSE filtering at the first iteration):

$$\begin{aligned} \hat{\mathbf{y}}_p &= \mathbf{y} - \mathbf{G}_{eq,p} \tilde{\mathbf{s}}_p \\ \hat{s}_p &= \frac{1}{\mathbf{g}_p^{\text{tr}} \mathbf{g}_p} \mathbf{g}_p^{\text{tr}} \hat{\mathbf{y}}_p \end{aligned} \quad (20)$$

where $\mathbf{G}_{\text{eq},p}$ of dimension $(2M_R T, 2Q-1)$ is the matrix \mathbf{G}_{eq} with its p^{th} column removed, $\tilde{\mathbf{s}}_p$ of dimension $(2Q-1, 1)$ is the vector $\tilde{\mathbf{s}}$ estimated by the soft mapper with its p^{th} entry removed.

II.4.3 LLR COMPUTATION

As we consider Gray mapping with QAM modulation of B bits per symbol, the computation of LLRs is done as in [8]. We note that we use the approximation of $\log(\exp(x_1) + \exp(x_2)) \approx \max(x_1, x_2)$. This approximation simplifies considerably the LLR expressions especially for high order constellations. We note also that the total noise variance corresponding to the additive WGN and the IEI is used for LLR computation.

SISO decoder

The deinterleaved soft information ($LLR_{k,p}$) of the k^{th} bit of the p^{th} symbol at the output of the demapper becomes the input of the outer decoder. The outer decoder computes the *a posteriori* information of the information bits and of the coded bits. The *a posteriori* information of the coded bits produces new (and hence) extrinsic information $LLR_{k,p}^{\text{ext}}$ of the coded bits upon removal of the *a priori* information¹ and minimizing the correlation between input values $LLR_{k,p}$. In our work, SISO decoding is based on the Max-Log-MAP algorithm [9]. The extrinsic information at the output of the channel decoder is then interleaved and fed to a soft Gray mapper module.

Soft Gray Mapper

The soft mapper achieves reciprocal operation of soft demapper. Knowing the extrinsic information of the k^{th} bit of the q^{th} complex symbol, the soft estimation of the symbol s_q , noted hereafter \tilde{s}_q , is defined by:

$$\tilde{s}_q = E\left\{s \mid LLR_{1,q}^{\text{ext}}, \dots, LLR_{B,q}^{\text{ext}}\right\} \quad (21)$$

where E holds for expectation function. Let $[c_1, \dots, c_B]$ be the set of bits constituting the constellation point s . Equation (21) yields:

$$\tilde{s}_q = \sum_{s \in \mathcal{V}} s \cdot \Pr(\tilde{s}_q = s) \quad (22)$$

where \mathcal{V} is the set of constellation points and $\Pr(\tilde{s}_q = s)$ is the probability of the event "the estimated symbol \tilde{s}_q takes the point s of the constellation set". Since the different bits of a constellation point are independent, we can write:

$$\Pr(\tilde{s}_q = s) = \prod_{s:=[c_1, \dots, c_B]} \Pr(\tilde{c}_{k,q} = c_k) \quad (23)$$

The probability expressions in (23) are deduced from the LLR expressions as:

¹ when the transmitted bits are likely equal, this information is equal to zero.

$$\Pr(\tilde{c}_{k,q} = 1) = \frac{\exp(LLR_{k,q}^{ext})}{1 + \exp(LLR_{k,q}^{ext})} \quad (24)$$

$$\Pr(\tilde{c}_{k,q} = 0) = 1 - \Pr(\tilde{c}_{k,q} = 1)$$

Once the estimation of the different symbols s_q is achieved by the soft mapper at the first iteration, we use this estimation for the next iterations process.

II.5 CHOICE OF MIMO SCHEMES: TERRESTRIAL TRANSMISSION

The aim of this section is to judiciously build the proposed double layer 3D STS code so that the resulting MIMO scheme behaves efficiently in the SFN context for the both aforementioned open and gap receiving environments. We then need to choose the adequate ST coding scheme, to apply on each layer of our 3D code.

First, we will consider the well-known orthogonal Alamouti ST coding scheme [10] for its robustness and simplicity. The Alamouti scheme provides full spatial diversity gain, no IEI, and requires low complexity maximum likelihood (ML) receiver thanks to the orthogonality of its dispersion matrix. The Alamouti code has a rate R equal to one and its dispersion matrix is given by:

$$\mathbf{X} = \begin{bmatrix} s_1 & s_2 \\ -s_2^* & s_1^* \end{bmatrix} \quad (25)$$

For non-orthogonal schemes, we consider in this work the well-known space multiplexing (SM) scheme [11]. SM is designed to maximize the rate by transmitting symbols sequentially on different antennas. Its coding scheme is given by:

$$\mathbf{X} = [s_1 \quad s_2]^T \quad (26)$$

Finally, we consider the optimized Golden code [12] which is a full rate and fully diverse code. The Golden code is designed to maximize the rate such that the diversity gain is preserved for an increased signal constellation size. It is defined by:

$$\mathbf{X} = \frac{1}{\sqrt{5}} \begin{bmatrix} \beta(s_1 + \theta s_2) & \beta(s_3 + \theta s_4) \\ \bar{\mu}\beta(s_3 + \bar{\theta} s_4) & \bar{\beta}(s_1 + \bar{\theta} s_2) \end{bmatrix} \quad (27)$$

where $\theta = \frac{1 + \sqrt{5}}{2}$, $\bar{\theta} = 1 - \theta$, $\alpha = 1 + j(1 - \theta)$, $\bar{\alpha} = 1 + j(1 - \bar{\theta})$. To identify the most efficient ST code, the OFDM parameters are derived from those of a DVB-T system (see Table 1). Moreover, we have considered the possibility to extend the size of the constellation order up to 256-QAM. The spectral efficiencies 4 and 6 [b/s/Hz] are obtained for different ST schemes as shown in Table 2. In all simulations, we assume that two Rx are used by the MT.

In the simulations results given hereafter, we separate the single layer case and the double layer case. For completeness point overview, we give first simulations results using a Rayleigh channel model in frequency domain i.e. we assume that the transmission from a transmitting antenna i to a receiving antenna j is achieved for each subcarrier n through a frequency non-selective Rayleigh fading channel. The use of the i.i.d. channel model is a first approach to justify our proposed 3D STS code. For this first step, the parameters β_i are chosen arbitrarily². In a second step, we will present results with more realistic channel model like the COST 207 TU-6 channel model [13]. In this case, the results will be given for both, open and gap area environments.

Table 1- Simulations Parameters

FFT size	8K
Sampling frequency ($f_s=1/T_s$)	9.14 MHz
Guard interval (GI) duration	$1024 \times T_s = 112 \mu s$
Rate R_c of convolutional code	1/2, 2/3, 3/4
Polynomial code generator	(133,171) _o
Channel estimation	perfect
Constellation	16-QAM, 64-QAM, 256-QAM
Spectral Efficiencies	$\eta = 4$ and 6 [b/s/Hz]

Table 2- Different MIMO schemes and efficiencies

Spectral Efficiency	ST scheme	ST rate R	Constellation	R_c
$\eta=2$ [bit/Sec/Hz]	Alamouti	1	16-QAM	1/2
	SM	2	QPSK	1/2
	Golden	2	QPSK	1/2
	3D code	2	QPSK	1/2
$\eta=4$ [bit/Sec/Hz]	Alamouti	1	64-QAM	2/3
	SM	2	16-QAM	1/2
	Golden	2	16-QAM	1/2

² Since we model the channel in frequency domain, there is no CIR and hence no CIR delays in this case.

	3D code	2	16-QAM	1/2
$\eta=6$ [bit/Sec/Hz]	Alamouti	1	256-QAM	3/4
	SM	2	64-QAM	1/2
	Golden	2	64-QAM	1/2
	3D code	2	64-QAM	1/2

First, let us characterize the behavior of the iterative receiver. Figure 6 provides the performance of the Golden code with iterative receiver and Rayleigh i.i.d. frequency channel model. The performance is given in terms of bit error rate (BER) versus the E_b/N_0 ratio for different number of iterations. We observe on this figure that the iterative process converges for an E_b/N_0 greater than a limit value, which is equal to 6 dB in this case. Moreover, we observe that the convergence of the iterative receiver is reached after 3 iterations. This implies an acceptable complexity as compared to the ML detection. This can be observed with Golden code, but also with SM scheme. That is, for NO-STBC schemes, we will present in the sequel the performances after 3 iterations only.

II.5.1 SINGLE LAYER CASE: INTER-CELL ST CODING

In the case of single layer reception, we have one antenna by site. Then, the second layer matrix $\mathbf{X}^{(2)}$ in (5) resumes to one element. The multiple input component of the MIMO scheme is then only obtained by the single antenna in each site ($M_T=1$). Due to the mobility, the MT is assumed to occupy different locations and the first layer ST scheme must be efficient face to unequal received powers. For equal received powers, we assume that the powers of the matrix \mathbf{Q} in (15) are equal to 0 dB.

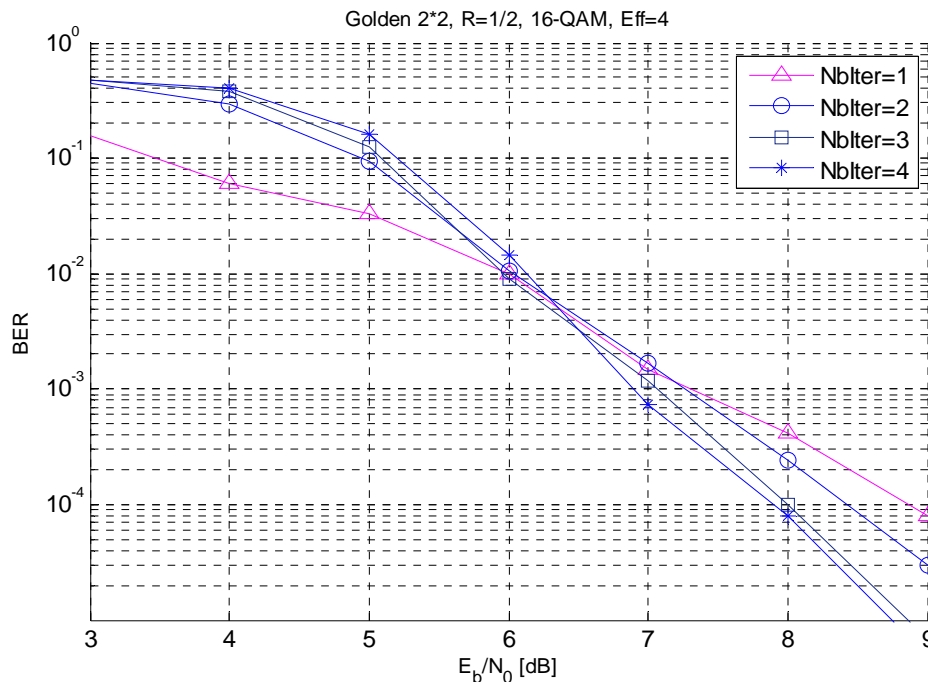


Figure 6- Convergence of the Golden code with respect to the number of iterations, 2Rx.

Figure 7 gives the required E_b/N_0 to obtain a BER equal to 10^{-4} for a spectral efficiency $\eta=4$ [b/s/Hz]. Moreover, since we have one Tx antenna by site, we set $\beta_1=0$ dB and we change $\beta=\beta_2$. As expected, this figure shows that the Golden code presents the best performance when the Rx receives the same power from both sites (i.e. $\beta_1=\beta_2=0$ dB). When β_2 decreases, Alamouti scheme is very efficient and presents a maximum loss of only 3 dB in terms of required E_b/N_0 with respect to equal received powers case. Indeed, for very small values of β , the transmission scenario becomes equivalent to a transmission scenario with one transmitting antenna. In this figure, the value $\beta_{lim} = -6.2$ dB presents the power imbalance limit where the Alamouti and the Golden code schemes have the same performance at a BER= 10^{-4} .

As shown in Figure 8, the same kind of results are observed for a spectral efficiency $\eta=6$ [b/s/Hz]. The Alamouti scheme is more efficient than the Golden code when the power imbalance parameter β becomes less than a given limit value $\beta_{lim} = -11.2$ dB.

II.5.2 DOUBLE LAYER CASE

Considering the whole double layer space domain construction, one ST coding scheme has to be assigned to each layer of the proposed system. The resulting 3D STS code should be efficient for both environments in SFN architectures. In our work, we restrict our study to $M_T=2$ Tx by site. We propose to construct the first layer, i.e. the inter-cell coding, with Alamouti scheme since it is the most resistant for the unequal received powers case. In a complementary way, we propose to construct the second layer, i.e. the intra-cell coding, with the Golden code since it offers the best results in the case of equal received powers. After combination of the two space layers with time dimension, (5) yields:

$$\mathbf{X} = \frac{1}{\sqrt{5}} \begin{pmatrix} \alpha(s_1 + \theta s_2) & \alpha(s_3 + \theta s_4) & \alpha(s_5 + \theta s_6) & \alpha(s_7 + \theta s_8) \\ j\bar{\alpha}(s_3 + \bar{\theta} s_4) & \bar{\alpha}(s_1 + \bar{\theta} s_2) & j\bar{\alpha}(s_7 + \bar{\theta} s_8) & \bar{\alpha}(s_5 + \bar{\theta} s_6) \\ -\alpha^*(s_5^* + \theta^* s_6^*) & -\alpha^*(s_7^* + \theta^* s_8^*) & \alpha^*(s_1^* + \theta^* s_2^*) & \alpha^*(s_3^* + \theta^* s_4^*) \\ j\bar{\alpha}^*(s_7^* + \bar{\theta}^* s_8^*) & -\bar{\alpha}^*(s_5^* + \bar{\theta}^* s_6^*) & -j\bar{\alpha}^*(s_3^* + \bar{\theta}^* s_4^*) & \bar{\alpha}^*(s_1^* + \bar{\theta}^* s_2^*) \end{pmatrix} \quad (28)$$

where $\theta = \frac{1+\sqrt{5}}{2}$, $\bar{\theta} = 1-\theta$, $\alpha = 1 + j(1-\theta)$, $\bar{\alpha} = 1 + j(1-\bar{\theta})$.

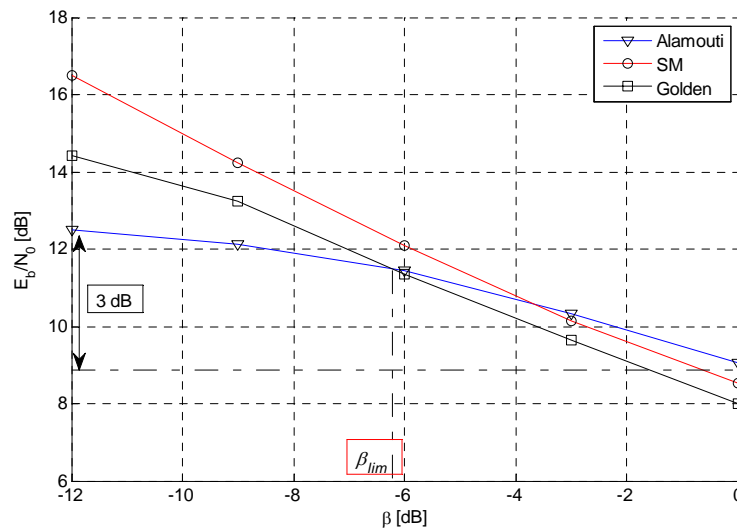


Figure 7- Required Eb/N0 to obtain a BER= 10^{-4} , single layer case, $\eta=4$ [b/s/Hz]

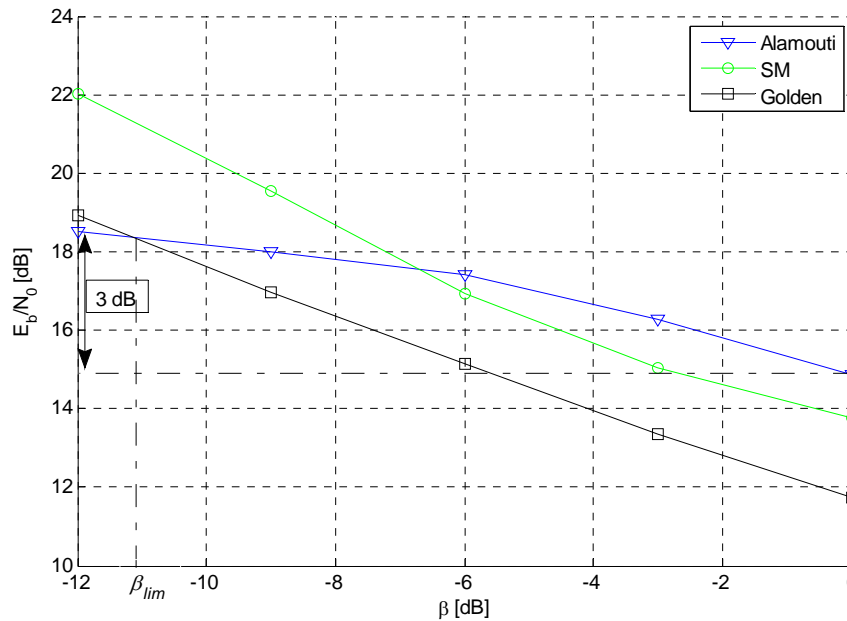


Figure 8- Required E_b/N_0 to obtain a $BER=10^{-4}$, single layer case, $\eta=6$ [b/s/Hz]

II.5.2.1 OPEN AREA ENVIRONMENT

In an open area environment, the MT is in an unobstructed region with respect to each site antennas. Since the distance d between the transmitting antennas in one site is negligible with respect to the distance D (Figure 2), the power attenuation factors in the case of our 3D code are such that $\beta_1=\beta_2= 0$ dB and $\beta=\beta_3=\beta_4$.

Figure 9 shows the results in terms of required E_b/N_0 to obtain a BER equal to 10^{-4} for different values of β and 3 STBC schemes i.e. our proposed 3D code scheme, the single layer Alamouti and the Golden code schemes assuming Rayleigh i.i.d frequency channel coefficients. In this figure, the value β corresponds to β_2 for the single layer case and to $\beta=\beta_3=\beta_4$ for our 3D code. Figure 9 shows that the proposed scheme presents the best performance whatever the spectral efficiency and the factor β . Indeed, it is optimized for SFN systems and unbalanced received powers. For $\beta=-12$ dB, the proposed 3D code offers a gain equal to 1.8 dB (respectively 3 dB) with respect to the Alamouti scheme for a spectral efficiency $\eta=4$ [b/s/Hz] (resp. $\eta=6$ [b/s/Hz]). This gain is greater when it is compared to the Golden code. Moreover, the maximum loss of our code due to unbalanced received powers is equal to 3 dB in terms of E_b/N_0 . This means that it leads to a powerful code for SFN systems.

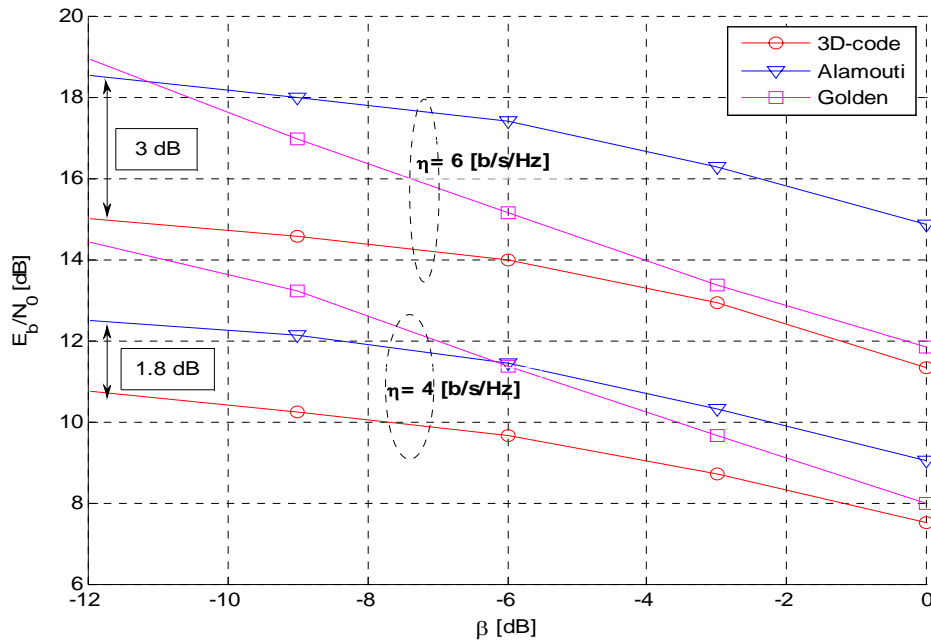


Figure 9- Required E_b/N_0 to obtain a $BER=10^{-4}$, double layer case, $\eta=4$ [b/s/Hz], $\eta=6$ [b/s/Hz], Rayleigh channel

In a MIMO COST 207 TU-6 channel model, we assume that the MT is moving with a velocity of 10 km/h and the distance d_1 of the reference antenna is equal to 5 km. The CIRs between different transmitters and the MT are delayed according to (3).

Figure 10 gives the same kind of results of those given in Figure 9. Once again, these results highlight the superiority of the proposed 3D code in real channel models whatever the spectral efficiency and the factor β i.e. the 3D code outperforms the others schemes in all cases. The gain could reach 1.5 dB for a spectral efficiency $\eta=4$ [b/s/Hz] and 3.1 dB for a spectral efficiency $\eta=6$ [b/s/Hz].

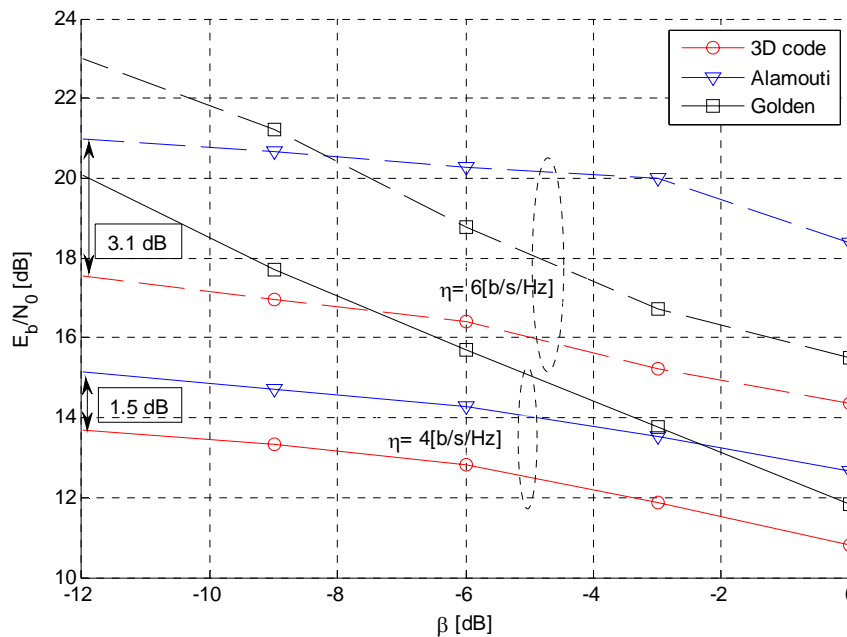


Figure 10- Required E_b/N_0 to obtain a $BER=10^{-4}$, double layer case, $\eta=4$ [b/s/Hz], $\eta=6$ [b/s/Hz], TU-6 channel.

II.5.2.2 GAP AREA ENVIRONMENT

In a gap area environment, the MT is in obstruction with respect to each site antennas. In this case, the gap filler receiving antennas become at the same situation of those of the MT in the open area environment i.e. a power imbalance is observed at the receiving side and it is related to the CIR delays by equation (3). However, due to the gap filler amplification, the power received by the MT in a gap area could be independent of these delays.

In Figure 11, we give the required E_b/N_0 that a MT needs in a gap area to obtain a $BER = 10^{-4}$ with respect to the CIR delays $\Delta\tau$ observed at the gap filler receivers. As expected, we show in this figure that the results are independent of these delays since they are smaller than the guard interval durations ($GI = 1024$ samples). In other words, as these delays are less than the guard interval duration, they produce only a phase rotation which is corrected by the equalizer in the frequency domain. The power imbalance is already corrected by the gap filler amplification.

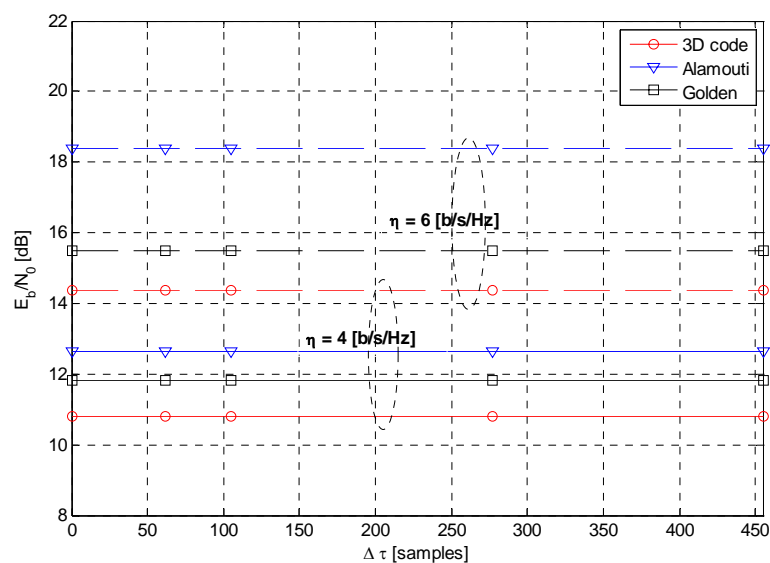


Figure 11- Required E_b/N_0 to obtain a $BER=10^{-4}$, $\eta=4$ [b/s/Hz], $\eta=6$ [b/s/Hz], TU-6 channel, gap area environment.

II.5.3 CHOICE OF MIMO SCHEMES: HYBRID SATT TRANSMISSION

The aim of this section is to judiciously build the proposed DLSTBC so that the resulting MIMO scheme behaves efficiently in an SATT transmission and SFN context as done in previous section for Terrestrial transmission. We recall that the choice of each encoding scheme at each layer should be efficient face to shadowing states in the LMS channel. As a consequence, the same MIMO schemes are considered in this section. The OFDM parameters are given in Table 3. The spectral efficiencies 2, and 6 b/s/Hz are obtained for different ST schemes as shown in Table 4.

The narrow-band LMS channel is used for the satellite link and the COST 207 TU-6 channel model [13] is used for terrestrial link. The Loo model parameters are deduced from the DLR measurements in a suburban area and given in [7] (Table 3). The probability matrices of the Markov chain describing the three states of the received signal are given in Table 4. We note that the probability matrices as well as the Loo parameters are functions of the elevation angle of the receiver relatively to the satellite. We assume that the terminal moves with a velocity of 20 m/s. The properties of the Butterworth filter describing the Doppler effect are specified according to the

maximum Doppler frequency (equal to 56 Hz for a $V_m=20$ m/s). In our simulation, the pass-band ripple of this filter is equal to 3 dB and the stop-band attenuation is equal to 50 dB.

Table 3- Average Loo model parameters in dB for various angles and suburban area (DLR measurements)

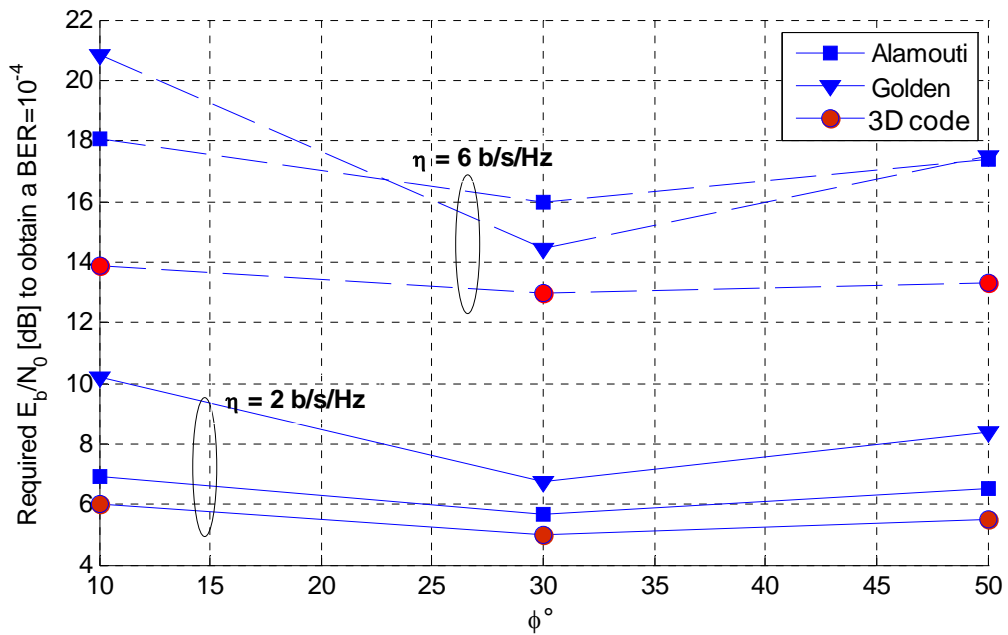
Elevation	S1: LOS			S2: Interm. Shad			S3: Deep Shad.		
	M	Σ	MP	M	Σ	MP	M	Σ	MP
10°	-0.1	0.5	-19	-8.7	3	-12	-12.1	6	-25
30°	-0.5	1	-15	-4.7	1.5	-19	-7	3	-20
50°	-0.5	1	-17	-6.5	2.5	-17	-14	2.5	-20

Table 4- Markov chain matrices **P** and **W** for various elevation angles and suburban area (DLR measurements)

Matrix P (10°)	0.9174	0.0512	0.0314	Matrix W (10°)	0.4389
	0.1064	0.7802	0.1134		0.2599
	0.0285	0.1151	0.8564		0.3012
Matrix P (30°)	0.9531	0.0350	0.0119	Matrix W (30°)	0.7467
	0.1891	0.6198	0.1911		0.1511
	0.0631	0.3065	0.6304		0.1022
Matrix P (50°)	0.7498	0.2462	0.004	Matrix W (50°)	0.1626
	0.0479	0.9160	0.0361		0.7642
	0.0554	0.3296	0.615		0.0732

Considering the whole code construction, we have to assign one ST coding scheme to each layer of the hybrid system. The proposed code should be robust face to the low, moderate and deep shadowing levels.

Figure 12 shows the results in terms of required E_b/N_0 to obtain a BER equal to 10^{-4} for different values of ϕ and 3 STBC schemes including our proposed DLSTBC scheme. This figure shows the superiority of our DLSTBC scheme. Its gain compared to the Alamouti scheme is about 1 dB for a spectral efficiency of 1 bit/s/Hz and reaches 4 dB at 6 bit/s/Hz. Interestingly, its performance remains quasi unchanged whatever the elevation angle ϕ . This definitely demonstrates that the proposed DLSTBC is a powerful code for SFN architecture and NGH systems.

Figure 12- Required E_b/N_0 to obtain a $BER=10^{-4}$

II.6 CONCLUSION

In this work, a new 3D-STBC is proposed and analysed. It is based on a double layer structure combining the Alamouti code and the Golden code. Such a code has been demonstrated to be very efficient in the SFN context where the double layer structure of the code allows inter-cell and intra-cell space-time codes across the multiple antennas of the network. Another field of application has been proposed with the possible hybrid reception of satellite and terrestrial links. In both transmission scenarios, the proposed code outperforms other classical STBC approaches since it not only takes advantage of the robustness of the Alamouti structure but also of the full rate capability of the Golden code. As a consequence, such a code allows achieving high spectral efficiencies while ensuring robust transmission in many broadcasting contexts.

II.7 REFERENCES

- [1] R. Raulefs, A. Dammann, "Relaying and diversity" IEEE Radio and Wireless Symp., pp. 219– 222, 22-24 Jan. 2008.
- [2] Y. Chaehag, "TDM framing for gap filler operation in satellite digital multimedia broadcasting System A", IEEE Vehicular Technology Conf., Vol. 5, pp. 2782-2786, May 2004.
- [3] DVB-SH implementation guidelines, TM-SSP252r9f
- [4] F. Murr, S. Kastner-Puschl, B. Bolzano, E. Kubista, "Land mobile Satellite narrowband propagation measurement campaign at Ka-Band", ESTEC contract 9949/92NL, Final report, 1995
- [5] C.Loo, "A Statistical Model for a Land Mobile Satellite Link", IEEE Trans. Vehicular. Technology, Vol. VT-34, No.3, August 1985
- [6] F. Fontan, M. Vazquez-Castro, S. Buonomo, P. Baptista, and B. Arbesser-Rastburg, "S-Band LMS propagation channel behavior for different environments, degrees of shadowing and elevation angles", IEEE Trans. On Broadcasting, Vol. 44, pp.40-76, March 1998
- [7] F. Fontan, M. Vazquez-Castro, C. Cabado, J. Garcia, E. Kubista, "Statistical modeling of the LMS channel", IEEE Trans. On Vehicular Technology, Vol. 50, No.6, pp. 1549-1567, Nov. 2001

- [8] F. Tosato, and P. Bisaglia, “Simplified Soft-Output Demapper for Binary Interleaved COFDM with Application to HIPERLAN/2”, Proc IEEE Int. Conf. on Communications, pp. 664-668, 2002.
- [9] J. Hagenauer, and P. Hoehner, “A Viterbi algorithm with soft-decision outputs and its applications,” in Proc. of IEEE Global Telecommunications Conf., pp. 1680-1686, Nov. 1989.
- [10] S.M. Alamouti, “A simple transmit diversity technique for wireless communications”, IEEE J. on Selected Areas in Communications, vol. 16, no. 8, pp. 1451-1458, Oct. 1998.
- [11] G. J. Foschini, “Layered space-time architecture for wireless communication in a fading environment when using multi-element antenna,” Bell Labs Tech. J., vol. 1, no. 2, pp. 41–59, 1996.
- [12] J.-C. Belfiore, G. Rekaya, and E. Viterbo, “The golden code: a 2×2 full-rate space-time code with non vanishing determinants”, IEEE Trans. in Information Theory, vol. 51, no. 4, pp. 1432–1436, Apr. 2005.
- [13] COST 207 Report, Digital land mobile radio communications, Commission of European Communities, Directorate General, Telecommunications Information Industries and Innovation, Luxemburg, 1989.

III NEW PREAMBLE FOR EFFICIENT COARSE FREQUENCY SYNCHRONIZATION IN OFDM

One important aspect for future transmission schemes is the efficient and fast synchronization to the data stream. In case of OFDM this especially incorporates the detection of signals and the coarse frequency synchronisation to the data stream. Additionally, the flexibility of the overall signal bandwidth is important, as the available frequency resources get more and more fragmented. One example for a completely flexible signal bandwidth is DVB's second generation standard for cable transmission: DVB-C2 [1]. This system does not rely on any channel raster and the bandwidth of the signal is completely flexible. However, this requires a new synchronisation scheme to the signals. This scheme as presented in this document can also be applied for the next generation handheld system, DVB-NGH. It has to be mentioned that the proposed technique cannot be applied to the preamble only, but is also feasible for the frequency domain pilots within the payload OFDM symbols.

III.1 CONCEPT OF ABSOLUTE OFDM

One basis for the new synchronisation preamble is the so-called concept of absolute OFDM. It has already been introduced in DVB-C2 [1] and allows for flexible assignment of the available spectrum. While normal OFDM is always related to a specific centre frequency, Absolute OFDM is always related to the absolute frequency 0 MHz. The OFDM subcarrier index is counted from the frequency 0 Hz, which corresponds to OFDM subcarrier index 0. The frequency position of the other OFDM subcarrier indexes depends on the OFDM subcarrier spacing that is the main constant of the system. In case of e.g. an OFDM subcarrier spacing of 1 kHz the absolute subcarrier index $k=1000$ corresponds to a frequency of 1 MHz.

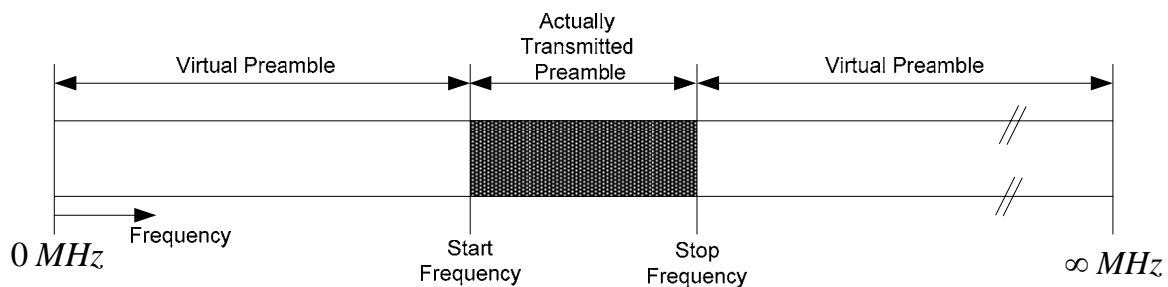


Figure 13: Concept of Absolute OFDM preamble

The same concept can also be used for a synchronisation preamble. Instead of having the same preamble on every channel, the concept of Absolute OFDM only has a single preamble. This preamble does not have a limited bandwidth of e.g. 8 MHz, but covers the complete frequency range from 0 to infinity. Naturally, not the complete preamble is actually transmitted. The transmitted frequency range is limited to the actual channel bandwidth. However, e.g. the modulation of the pilots within the preamble is generated with respect to the absolute frequency 0 MHz. Hence, a unique synchronisation sequence exists for the complete frequency range. If a receiver tries to synchronise on a specific frequency, it already knows the pilot sequence it should correlate to, because this is defined by the frequency itself. Consequently, it can use a correlation window of limited length in order to discover if a signal is present or not. The bandwidth of the correlation window on the pilots in the frequency domain of the OFDM symbol only has to take the accumulated frequency offsets of the transmitter and the receiver into account, which are normally

limited to less than 100 kHz. Thus, it allows a fast synchronisation is signal detection, even if only a very limited part (e.g. 500 kHz) of the transmitted signal are located within the actual tuner window of the receiver. Details are given in the synchronisation subsection, while a possible implementation is given in the following subsection.

III.2 PREAMBLE REALISATION

A possible realisation of the preamble using the Absolute OFDM approach is depicted in Figure 14. It shows an OFDM symbol with its subcarriers in the frequency domain, starting from the absolute frequency 0 MHz. In this example, a pilot is transmitted on every second OFDM subcarrier, while the remaining subcarriers may be used for the transmission of additional signalling data.

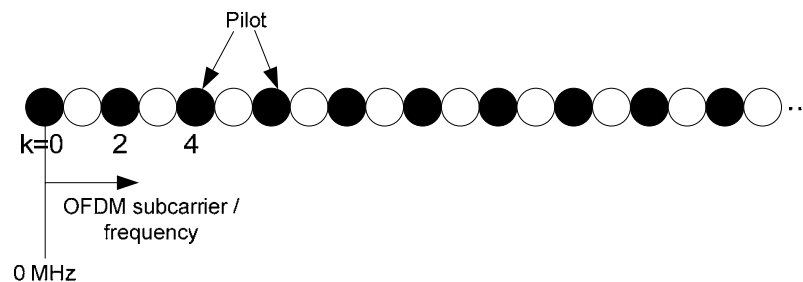


Figure 14: Possible preamble realisation, pilot with PRBS data on every 2nd OFDM subcarrier

The modulation of the pilots is based on a Pseudo Random Binary Sequence (PRBS) that can be generated by means of a Linear Feedback Shift Register (LFSR) as depicted in Figure 15.

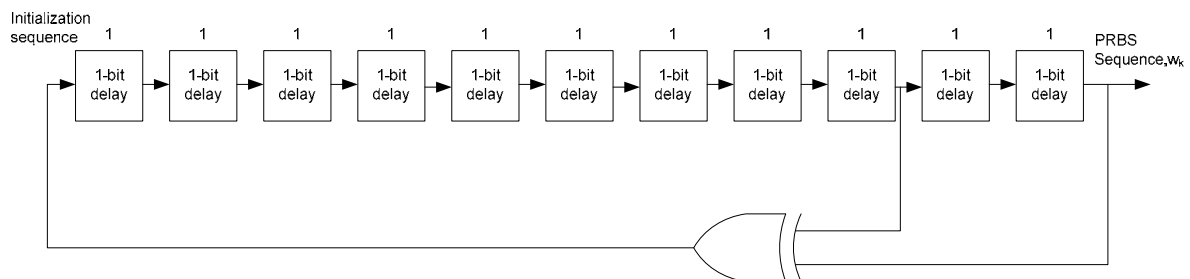


Figure 15: Example for PRBS generator based on a Linear Feedback Shift Register (LFSR)

The shift register is initialised only once (e.g. to all '1') at the frequency 0 MHz, which corresponds to the OFDM subcarrier index 0. Then, the register is running freely over the complete frequency range. The k -th output of the sequence is called w_k . In the depicted case, the generator polynomial

$$X^{11} + X^2 + 1$$

has been used. The resulting length of the sequence until it repeats itself is $2^{11} - 1 = 2047$, as the primitive generator polynomial is of degree 11 [3]. This sequence length may be too short for practical application. However, it is possible to increase the length by means of primitive polynomials of higher degree than can also be found in [3].

The modulation of the pilots itself is finally obtained by mean of differential encoding of the data, which simplifies the correlation process to the data stream. This is reached by:

$$r_k = \begin{cases} w_k & \text{if } k=0 \\ r_{k-2} \oplus w_k & \text{otherwise} \end{cases}$$

for the case of a pilot on every second OFDM subcarrier.

The value k identifies the OFDM subcarrier index, w_k is the k -th output of the PRBS generator, and r_k is the modulation of the pilot on OFDM subcarrier k . The final modulation of the pilot on OFDM subcarrier k is then obtained by:

$$\begin{aligned} \text{Re}\{c_k\} &= A_p \cdot 2(1/2 - r_k) \\ \text{Im}\{c_k\} &= 0, \end{aligned}$$

in which c_k is the complex cell on the OFDM subcarrier k , and A_p is the amplitude of the pilot. The amplitude of the pilot can be adjusted to the requirements. If e.g. no energy is transmitted on every second OFDM subcarrier (as in this example), the amplitude could be chosen as $A_p = \sqrt{2}$ in order to reach a mean power of 1 for the complete OFDM symbol. Additionally, this boosting would increase the robustness of the signal against noise.

III.3 SYNCHRONISATION PROCEDURE

The synchronisation procedure to the preamble is depicted in Figure 16. Firstly, the synchronisation process has to detect the temporal boundaries of the OFDM symbol that carries the preamble and has to do a fractional frequency synchronisation to this OFDM symbol. The fractional frequency synchronisation is the synchronisation to the individual $\sin(x)/x$ functions. The remaining offset is a multiple of the OFDM subcarrier spacing. The fractional frequency synchronisation and the temporal synchronisation can both be achieved by means of the Guard Interval, which is a well-known approach [2].

As shown later on in the simulation results, the required accuracy is very limited and fractional frequency offsets of several 100 Hz for OFDM subcarrier spacing of approx. 1 kHz are still acceptable. The same holds for the temporal synchronisation to the OFDM symbol, as a very low accuracy is required.

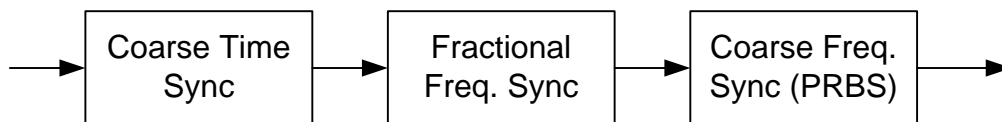


Figure 16: Synchronisation to preamble

The coarse frequency synchronisation is then based on the new preamble structure and works as Figure 17 depicts.

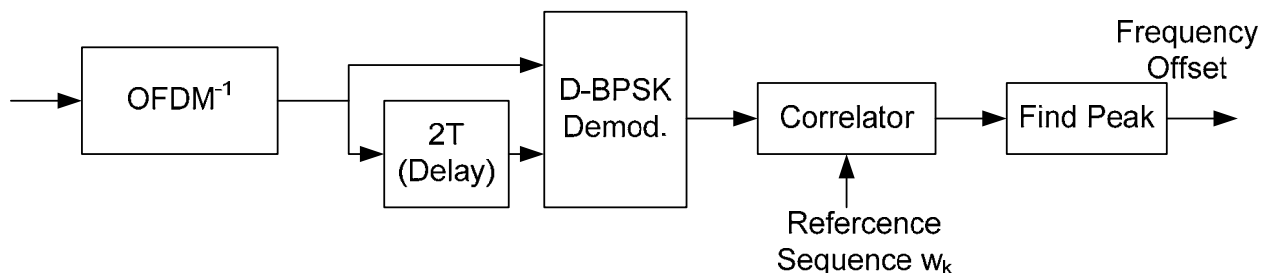


Figure 17: Coarse Frequency Synchronisation

Firstly, the OFDM data is converted from the time into the frequency domain. As already mentioned the synchronisation accuracy has to be quite limited. Then always two consecutive pilots are differentially BPSK demodulated against each other. This is reached by the delay of 2 OFDM subcarriers and the D-BPSK demodulation block. In case of perfect reception the resulting output of the demodulator block is the PRBS sequence w_k with the OFDM subcarrier indices k of the actual receiving window of the receiver. Hence, if this sequence is correlated against the locally generated reference sequence, a peak occurs at the ideal overlapping position and the receiver is able to estimate the coarse frequency offset.

The receiver is able to generate the reference sequence according to its tuning frequency. As the frequency offset between the actual and the intended tuning frequency within the receiver can be expected to less than a few hundreds of kHz, the resulting correlation window could be quite limited.

III.4 TRANSMISSION OF LAYER 1 SIGNALLING DATA

The proposed structure allows for the efficient transmission of Layer 1 signalling data. Therefore, the concept of Absolute OFDM can be applied as well. The complete Layer 1 signalling is grouped into so-called L1 Blocks, which have a fixed number of OFDM subcarrier (i.e. bandwidth). These L1 Blocks are then repeated in the frequency direction starting from the OFDM subcarrier $k=0$, which corresponds to 0 MHz. As the L1 Blocks are repeated, e.g. every 5000 OFDM subcarriers, a new L1 Block starts if the equation $k_{\text{mod}5000}=0$ is fulfilled. Naturally, the repetition of the data in the frequency direction may cause high peak-to-average power ratios in the time domain signal. However, all L1 signalling data on the individual subcarrier can be additionally scrambled by means of the sequence w_k , which mitigates this problem. The resulting structure of the Absolute OFDM concept with the signalling data is depicted in Figure 18.

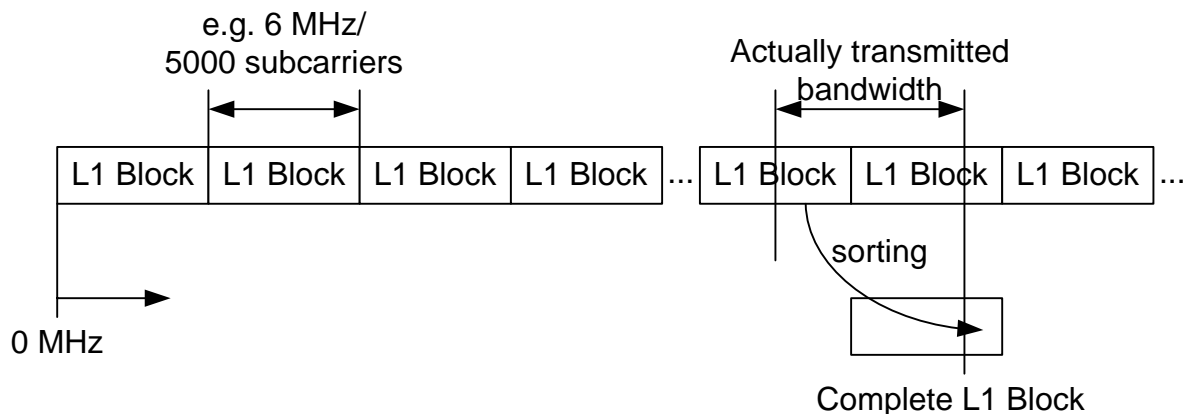


Figure 18: Sorting of Layer 1 Signalling information to obtain complete Layer 1 Signalling Block, only the signals within the transmitted bandwidth are actually transmitted

Interestingly, the bandwidth or channel raster does not have to be aligned to the L1 Block structure. As the receiver knows the carrier indices k in its tuning bandwidth, it knows at which subcarriers the L1 Blocks start. Hence, as all L1 Blocks transmit the very same data, it is able to obtain the complete Layer 1 signalling data out of 2 L1 Blocks, if the signal (or the receiver tuner window) bandwidth is higher than the L1 Block bandwidth.

The modulation of the L1 signalling could be achieved by means of normal QAM constellations. This naturally requires an equalisation process before the data can be decoded. However, as pilots

in the preamble are known data to the receiver, they can be used for the required channel estimation and equalisation.

III.5 EXAMPLE TUNING PROCEDURE

A complete synchronisation process using the new preamble concept is depicted in Figure 19. Firstly, the receiver tunes to the frequency it expects a signal. Then it tries to find out if a signal is present. If a signal has been detected, the receiver tries a Guard Interval correlation. If this has been successful, the receiver uses this correlation information to perform a coarse time synchronisation and a fractional frequency offset compensation. Before this step, the correlation may already work on normal data OFDM symbols. Then, the receiver tries to find the preamble by means of the described correlation process. If this preamble is found, the receiver is able to perform coarse frequency offset compensation and afterwards it can decode the included Layer 1 signalling. Afterwards, the synchronisation process is completed.

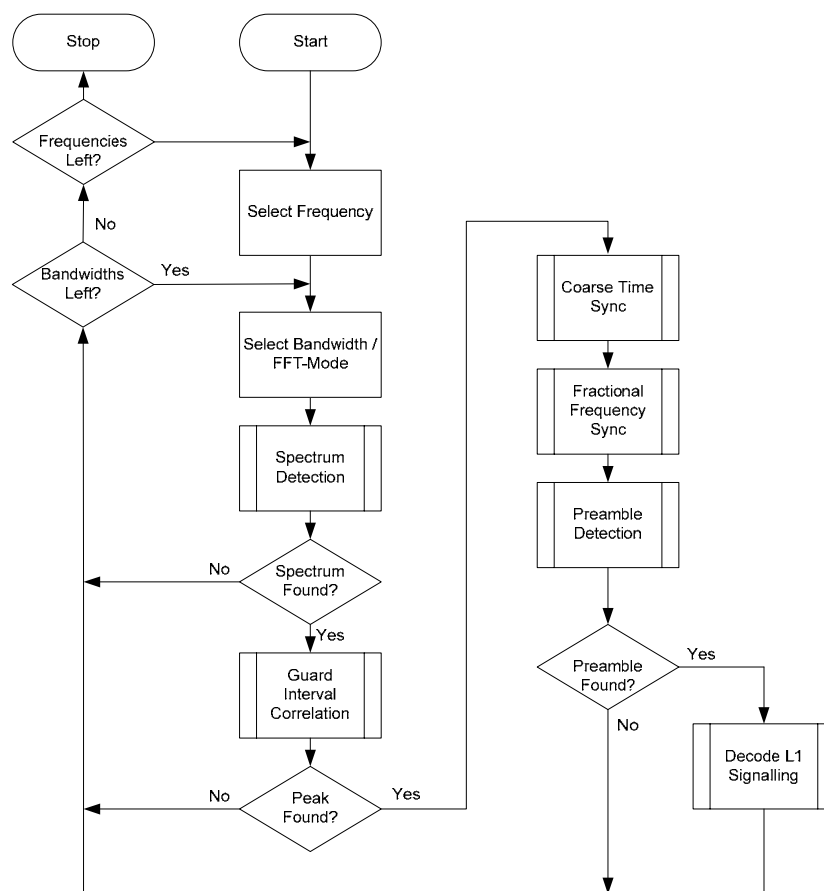


Figure 19: Example flow chart for full synchronisation procedure using the new preamble concept

III.6 SIMULATION RESULTS

Multiple simulations have been performed to show the synchronisation performance of the proposed preamble. The OFDM parameters are an 8K FFT with Guard Interval 1/4 in an 8 MHz channel. A pilot has been placed on every 2nd OFDM subcarrier, while the pilots were boosted by 3dB. Hence, the average power of the OFDM symbol has been 1.

Figure 20a shows the correlation product if a bandwidth of 900 kHz out of the 8 MHz is used in an ideal channel without noise. The unique peak within the output data is clearly visible, and an ideal synchronisation would have been performed. However, also at Signal-to-Noise Ratios (SNR) of -5dB the unique peak within the frequency spectrum is visible and the synchronisation again would have worked perfectly.

Figure 21 additionally shows the correlation peak in case of an additional frequency offset of 400Hz (OFDM subcarrier spacing of 1,116 kHz). Again, the SNR value was chosen to -5dB. However, the correct synchronisation to the preamble is still possible.

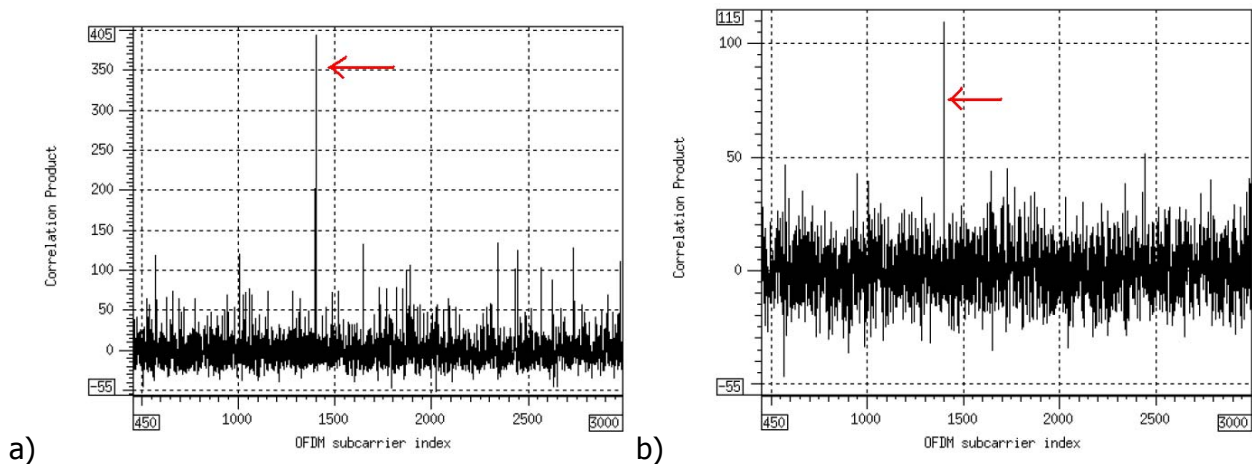


Figure 20: Correlation Product without noise (left hand side) and at -5dB Signal-to-Noise Ratio (right hand side), correlation bandwidth 900 kHz, interleaved structure

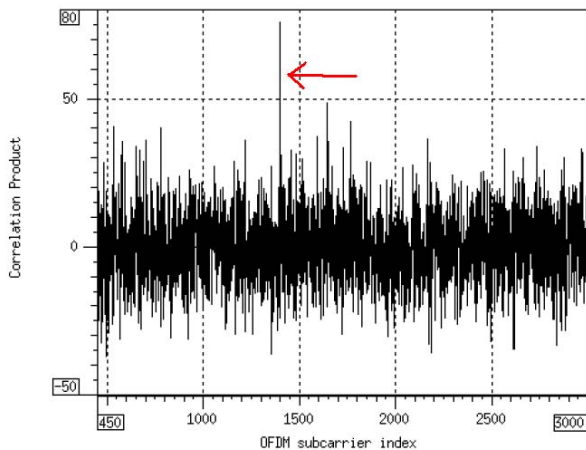


Figure 21: 400 Hz offset, -5dB

III.7 CONCLUSIONS

The presented approach allows for a fast synchronisation to the data stream. This is especially reached by the fact that the receiver knows the sequence it has to expect. Additionally, it allows for a method to transmit Layer 1 signalling within the preamble, which can be received even if the

receiver is not completely tuned to the correct frequencies. Hence, it also allows for variable bandwidth without any need for a fixed channel structure.

III.8 REFERENCES

- [1] Digital Video Broadcasting (DVB); Frame structure channel coding and modulation for a second generation digital transmission system for cable systems (DVB-C2); Draft ETSI EN 302 769, V 1.1.1, July 2009
- [2] Speth, M., Fechtel, S. A., Fock, G., Meyr, H.; Optimum Receiver Design for Wireless Broad-Band Systems Using OFDM – Part I; IEEE Transactions on Communications, Vol. 47, No. 11, November 1999
- [3] Golomb, S.W.; Shift Register Sequences, Holden-Day, 1968

IV PERFORMANCE OF CHANNEL ESTIMATION WITHOUT PILOTS

Pilots are commonly used in OFDM based systems to estimate the channel and perform channel equalization [3]. However, this is known information to the receiver, and thus, contributes to the overhead only. Therefore, DVB-T2 [4] offers a special mode in which the overhead due to the pilots is minimized. Using this Pilot Pattern (PP) 8, the receiver has to employ additional means to estimate the channel. One means, for which the PP8 scheme of DVB-T2 was mainly designed, is the so-called CD3 algorithm [1]. Using this algorithm, the data is used as pilots in order to estimate the channel. However, the data symbols have to be known prior the equalization process in order to estimate the channel correctly. As this is practically impossible, the algorithm introduces a delay of at least one OFDM symbol. Hence, the receiver does not use the correct channel estimates to equalize the channel, but previous ones. This may be uncritical for stationary reception, but gets important for mobile or portable receivers. Additionally, there may be the effect of error propagation. If the PP8 scheme is used for DVB-T2, the application of time interleaving is prohibited, because this would lead to even longer delays than 1 OFDM symbol. However, if the receiver is not able to correct one LDPC FEC block completely, the following channel estimation will include errors that leads to reduced channel estimation performance. This will naturally propagate to the next OFDM symbols, and so on. In extreme situations, this may even lead to loss of synchronization until the next reference symbol is sent.

However, due to the decreased overhead this technique may be a candidate for DVB-NGH as well.

IV.1 DESCRIPTION OF BASIC ALGORITHM

The principle structure of the CD3 algorithm is depicted in Figure 22. After the transformation of the frequency domain into the time domain signal, the channel equalization is performed. In contrast to the "normal" channel estimation based on pilots, this is achieved by means of the data OFDM subcarriers. The channel estimation is obtained by:

$$\hat{H}(l,k) = \frac{y(l,k)}{\hat{x}(l,k)} = \frac{x(l,k) \cdot H(l,k)}{\hat{x}(l,k)} \quad (1),$$

where $y(l,k)$ is the received OFDM subcarrier in OFDM symbol l and subcarrier number k , $x(l,k)$ is the transmitted data, $\hat{x}(l,k)$ is the received and FEC corrected data in the receiver, $H(l,k)$ and $\hat{H}(l,k)$ are the real and the estimated channel transfer function. If equation (1) is without noise and the data in the receiver is estimated correctly, the receiver is hence able to obtain the correct channel transfer function at the specific OFDM subcarrier. However, in order to do this modulation, $\hat{x}(l,k)$ of the data subcarriers has to be known to the receiver. This is achieved by decoding the complete OFDM symbol and encoding it again, which also includes the Forward Error Correction (FEC). Naturally, this process is not possible as the OFDM subcarriers are not decoded during the equalization process. Therefore, the system introduces a delay of a least one OFDM symbol. Hence, the delay is sufficient to decode the data stream of this OFDM symbol and encode it again. However, in some applications a delay of one OFDM symbol may not be sufficient for the receiver. If e.g. an FEC codeblock is transmitted over multiple OFDM symbols, a higher decoding latency may be required. Consequently, the receiver equalizes the channel with an outdated channel transfer function. If the channel is quasi static, this may not cause significant effects. However, in case of mobile reception the equalisation process may lead to errors.

Normally, a noise term has to be included in equation (1). Even if the receiver is able to obtain all values of $\hat{x}(l,k)$ correctly, this noise term will lead to estimation errors. However, this Additive White Gaussian Noise (AWGN) can be reduced by applying an additional filter, which may be some

channel estimation with tenth of dBs. The significant difference compared to the results in [1] can be explained due to the fact that the DVB-T2 LDPC code is more powerful, compared to the DVB-T convolutional code. Hence, the Signal-to-Noise Ratio (SNR) required for error-free reception is lower than in the DVB-T case. Consequently, the data OFDM subcarriers, which are used for channel estimation, carry significantly higher noise levels.

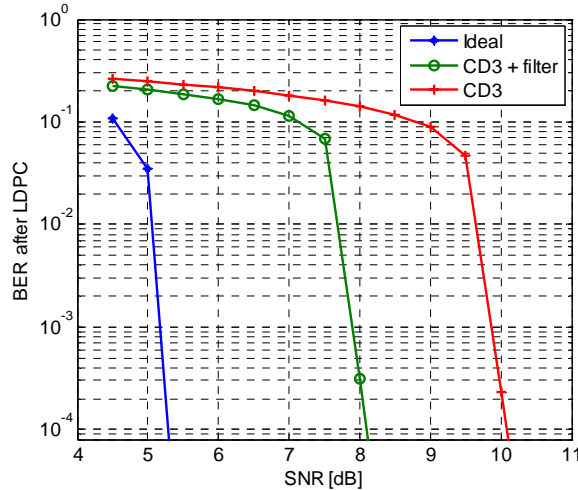


Figure 23: Performance of CD3 in AWGN channel: 8K FFT, Guard Interval 1/4, 16-QAM, LDPC coderate 1/2 (16K), ideal QAM demapping (assumption of Gaussian noise distribution at input of QAM demapper), filter optimized for Guard Interval 1/4

Practically the same holds for the channel estimation in case of the DVB-T Rayleigh channel. The high noise level on the data OFDM subcarriers leads to bad channel estimation. However, it can be improved by means of filtering. Certainly, the performance could be improved by means of filter between different OFDM symbols, but this may lead to additional latency in the decoding process.

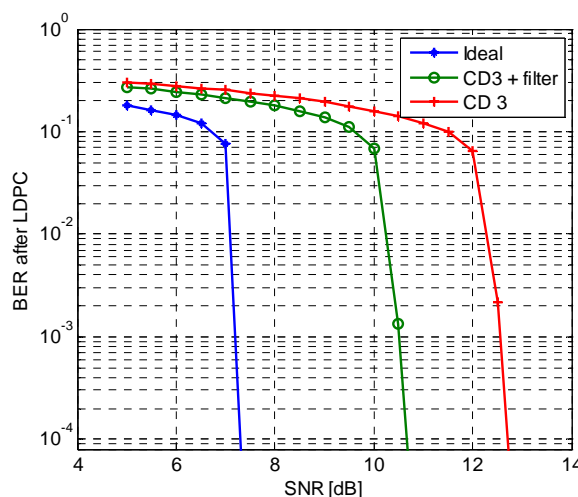


Figure 24: Performance of CD3 in DVB-T2 Rayleigh channel: 8K FFT, Guard Interval 1/4, 16-QAM, LDPC coderate 1/2 (16K), ideal QAM demapping (assumption of Gaussian noise distribution at input of QAM demapper), filter optimized for Guard Interval 1/4

IV.2.2 MOBILE CHANNEL SIMULATION RESULTS

In case of mobile fading channels the channel is no longer static between consecutive OFDM symbols. Hence, if the CD3 algorithm is used with a delay, the channel is equalized with an outdated channel transfer function. The simulation results for 2, 10, 20 and 40 Hz of Doppler are depicted in Figure 25. The channel has been estimated without additional noise. Thus, the degradation is only caused by the delay of the channel transfer function used to equalize the channel. In case of 2 Hz degradation is not visible. The ideal curve nearly overlaps the curves for 1 to 4 OFDM symbols delay. However, if the Doppler frequency is increased, the difference between the ideal and the delayed equalisation is getting bigger. The loss for a delay of one OFDM symbol still remains acceptable for a Doppler frequency of 20 Hz. Though, the 40 Hz Doppler case does not work with only one OFDM symbol delay.

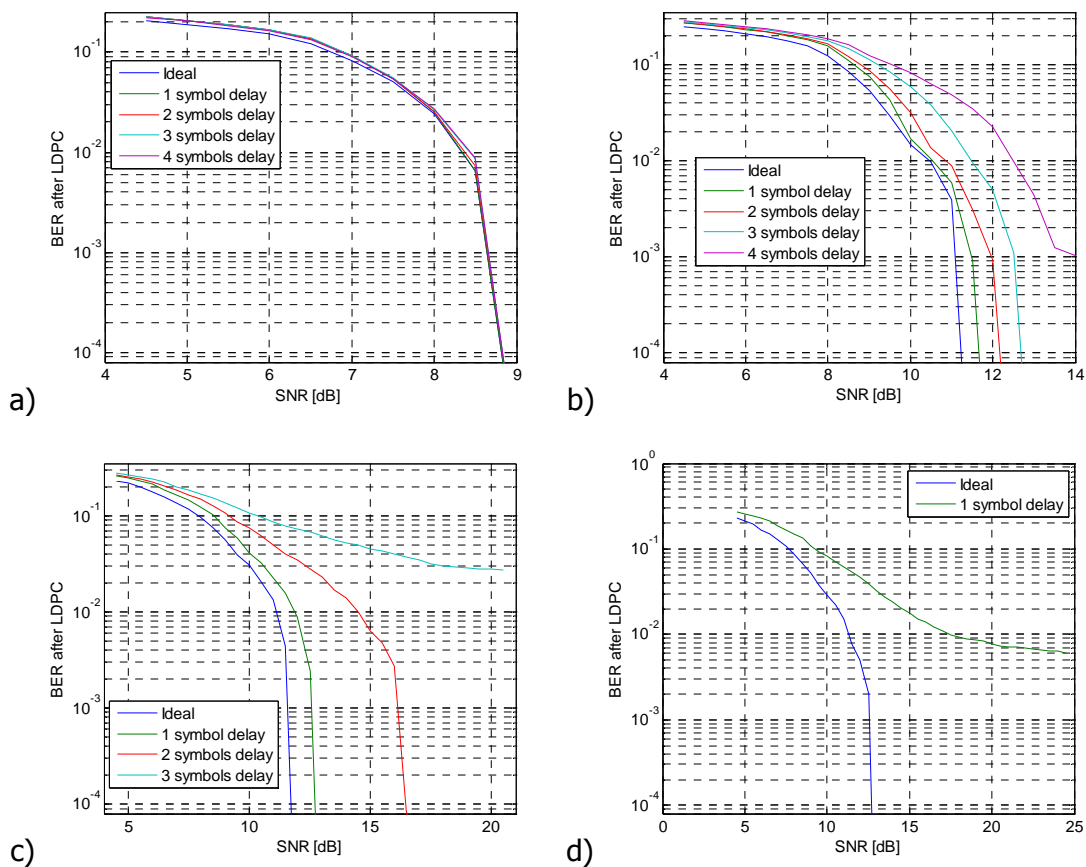


Figure 25: TU-6 channel with 2 Hz (a), 10 Hz (b), 20 Hz (c), 40 Hz (d) Doppler, parameters: 8K FFT (1.116 kHz subcarrier spacing), Guard Interval 1/4, 16-QAM, LDPC coderate 1/2 (16K), noiseless channel estimation

IV.2.3 ERROR PROPAGATION SIMULATION RESULTS

Errors in the decoding process within the receiver lead to estimation errors within the following OFDM symbols, as the estimated QAM constellation \hat{x} is wrong. If the number of errors gets too big this may even lead to loss of synchronisation. The channel estimation quality is reduced, which naturally leads to additional errors in the decoding process that are again fed in the channel estimation of the following OFDM symbol, etc.

Figure 26 shows simulation results for varying bit-error rates in the receiver's feedback loop. This bit-errors lead to wrong values of \hat{x} . Hence, the channel estimation quality is reduced. However, the importance of the bits within the QAM constellations has not been taken into account. An error within the Least Significant Bit (LSB) will naturally lead to less estimation error as an error in the Most Significant Bit (MSB). This is caused by the effect that the MSB defines the sign of \hat{x} , while the LSB only defines small variations. However, the results can be used to give an initial trend.

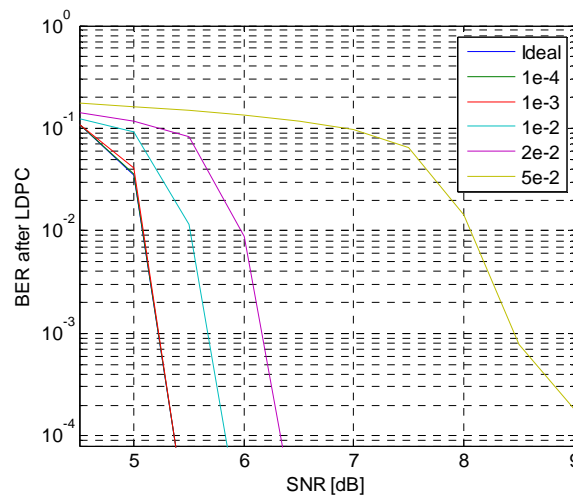


Figure 26: Sensitivity to erroneous bits in the feedback loop, parameters: 8K FFT, Guard Interval 1/4, 16-QAM, LDPC coderate 1/2 (16K), noiseless channel estimation, additional filter optimized for Guard Interval 1/4

Surprisingly, a Bit Error Rate (BER) of $1 \cdot 10^{-3}$ or less does not have any effect on the estimation quality, as the curves ideally overlap. This may be also caused by the fact that additional filtering within the channel estimation of each OFDM symbol is used. If the BER is increased to $1 \cdot 10^{-2}$ a loss of approx. 0.5dB is visible, which may be still acceptable. In case of a BER in the feedback of $5 \cdot 10^{-2}$ no error-free reception is possible. However, this can result may be still improved by means more complex filtering in the channel estimation. Hence, the effect of errors seems to be quite limited.

IV.3 CONCLUSION

The application of CD3 for DVB-NGH allows for channel estimation with almost no pilots. In contrast to DVB-T, for which this technique was initially proposed, the receiver has to cope with higher noise levels. This is caused by the more powerful FEC. In case of mobile channels the technique shows good results for low mobility. However, it fails for higher reception speeds, e.g.

40 Hz Doppler, which corresponds to 20 m/s at 600 MHz transmission frequency. In contrast, the robustness in case of erroneous feedbacks seems to be quite high.

IV.4 REFERENCES

- [1] Mignone, V., Morello, A.; CD3-OFDM: A Novel Demodulation Scheme for Fixed and Mobile Receivers, IEEE Transactions on Communications, Vol. 44, No. 9, September 1996
- [2] Digital Video Broadcasting (DVB); Implementation Guidelines for a second generation digital terrestrial television broadcasting system (DVB-T2); Draft ETSI TR 102 831, January 2009
- [3] L. Hanzo, et.al: OFDM and MC-CDMA for Broadband Multi-User Communications, WLANs and Broadcasting, IEEE Press, 2003
- [4] Digital Video Broadcasting (DVB); Frame structure channel coding and modulation for a second generation digital terrestrial television broadcasting system (DVB-T2); Draft ETSI EN 302 755, October 2008

V CHANNEL MISO CHANNEL ESTIMATION WIHTOUT PILOTS

The application of channel estimation with (almost) no pilots is also an interesting means in case of MISO transmission. This especially holds as the amount of pilots has to be increased significantly compared to SISO channel estimation, because the channel to each transmitter (or transmitter group) has to be estimated separately. However, for the further considerations the number of transmitter groups shall be set to 2, because this is the maximum number of orthogonal sequences offered by the Alamouti scheme [1]. Again, a similar approach as presented in the CD3 paper [2] will be used for the estimation process.

V.1 ESTIMATION OF THE CHANNEL TRANSFER FUNCTIONS

In case of the SISO OFDM transmission, the effect of the channel on the transmitted QAM symbols can be modelled by means of a complex multiplication of the transmitted QAM symbol x with the channel transfer function h at the specific OFDM subcarrier position, i.e.:

$$r = x \cdot h \quad (1)$$

However, for the application of MISO this equation has to take the second transmitter (group) into account, in which two different QAM symbols with different channel transfer functions are received at the same time:

$$r = x_1 \cdot h_1 + x_2 \cdot h_2 \quad (2)$$

This equation is not solvable if r , x_1 and x_2 are known, because it includes two channel transfer functions, instead of one as in (1). However, as (2) is for the general MIMO case (e.g. spatial multiplexing), additional information is known for the Alamouti case. This is due to the fact that each QAM constellation is transmitted twice. If we now assume that the Alamouti scheme is used (in time or in frequency direction), we obtain the equations:

$$\begin{aligned} r_1 &= x_1 \cdot h_{1,1} + x_2 \cdot h_{2,1} \\ r_2 &= -x_2^* \cdot h_{1,2} + x_1^* \cdot h_{2,2} \end{aligned} \quad (3)$$

Again, equation (3) is not solvable as it includes 4 unknown variables in only 2 equations. However, we can assume that the channel transfer function does not vary significantly between the two encoded sequences, i.e.:

$$\begin{aligned} h_{1,1} &\approx h_{1,2} \\ h_{2,1} &\approx h_{2,2} \end{aligned} \quad (4)$$

Hence, the equation (3) can be simplified to:

$$\begin{aligned} r_1 &\approx x_1 \cdot h_1 + x_2 \cdot h_2 \\ r_2 &\approx -x_2^* \cdot h_1 + x_1^* \cdot h_2 \end{aligned} \quad (5)$$

The equations (5) now consist of 2 unknown variables and 2 linear equations, which allows solving the equations. Therefore, the matrix representation of (5) is:

$$\begin{pmatrix} r_1 \\ r_2 \end{pmatrix} = \begin{pmatrix} x_1 & x_2 \\ -x_2^* & x_1^* \end{pmatrix} \cdot \begin{pmatrix} h_1 \\ h_2 \end{pmatrix} = X \cdot \begin{pmatrix} h_1 \\ h_2 \end{pmatrix} \quad (6)$$

Hence, the channel transfer function at the specific OFDM subcarriers can be obtained by:

$$\begin{pmatrix} h_1 \\ h_2 \end{pmatrix} = \frac{1}{\det(X)} \begin{pmatrix} x_1^* & -x_2 \\ x_2^* & x_1 \end{pmatrix} \begin{pmatrix} r_1 \\ r_2 \end{pmatrix} \quad (7)$$

with

$$\det(X) = |x_1|^2 + |x_2|^2$$

Most interestingly, the determinant is constant for BPSK and QPSK mapping, as the transmitted energy of each constellation point is the same. However, this changes for other QAM mappings as 16-QAM or 64-QAM.

V.2 PERFORMANCE RESULTS

The assumption of a static channel between two Alamouti encoded QAM cells is naturally not valid. Results for BPSK/QPSK, 16-QAM and 64-QAM are depicted in Figure 27 and Figure 28, respectively. Here, the Alamouti encoding has been performed in the frequency direction. The DVB-T2 8K FFT mode with Guard Interval 1/4 and 8 MHz channel bandwidth has been chosen for the simulations. This results in a useful OFDM symbol duration of 896 μ s and a Guard Interval length of 224 μ s. The two Alamouti groups are transmitted with the same amplitude, while the second group is delayed w.r.t. the first group. Hence, the criterion of a static channel transfer function for the Alamouti encoded data is more and more violated if the delay of the second group is increased.

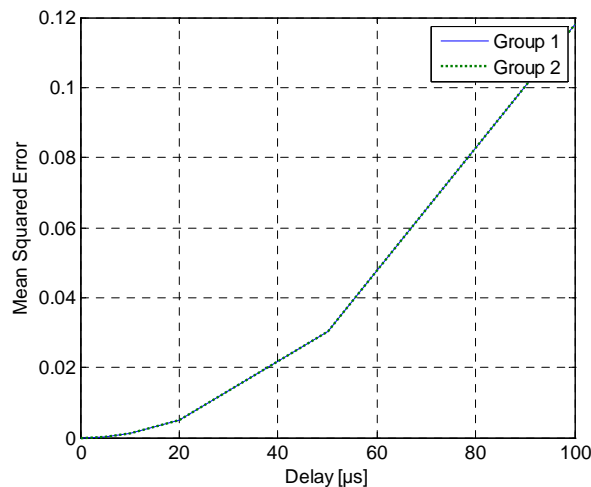


Figure 27: Mean Squared Error (MSE) for varying delay of Group 2; Parameters: BPSK/QPSK mapping, 8K FFT, Guard Interval 1/4, 7.61 MHz bandwidth, useful OFDM symbol duration 896 μ s

Figure 27 shows the simulation results for BPSK and QPSK, which obtain the very same results. The delay of the second Alamouti group is delay, starting from 0 up to 100 μ s, which is far less than the allowed Guard Interval of 224 μ s. However, it turns out that the Mean Squared Error (MSE) between the correct and the estimated channel transfer function rises very quickly, when the delay is increased. As no additional noise is added, the MSE is zero if the second Alamouti group is not delay. However, it increased to 0.12 at 100 μ s. In case of BPSK and QPSK this estimation error may still be tolerable. However, it already turns to significant performance loss, especially if the additional noise is taken into account. In case of delays in the region of the Guard Interval length, no error-free reception of the signal can be expected.

One important aspect is also, that the MSE for each of the two channel transfer functions H_1 and H_2 is the same.

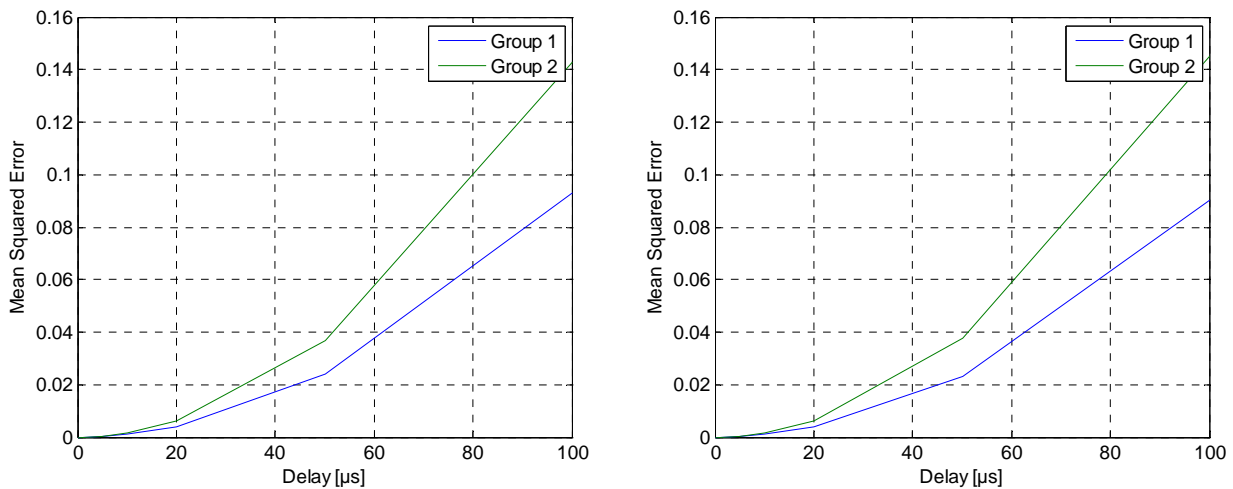


Figure 28: Mean Squared Error (MSE) for varying delay of Group 2; Parameters: 16-QAM (left) and 64-QAM (right) mapping, 8K FFT, Guard Interval 1/4, 7.61 MHz bandwidth, useful OFDM symbol duration 896 μs

The simulation results for the 16-QAM and 64-QAM as depicted in Figure 28 differ from the BPSK/QPSK results. This is caused by the fact that the determinant in equation (7) is no longer constant. Especially the channel estimation quality of the delay path (i.e. Alamouti group 2) shows significantly reduced performance w.r.t. the non-delayed path. Naturally, as 16-QAM and 64-QAM require higher channel estimation accuracies, it is not expected that the signal can be decoded correctly by means of the obtained channel estimation results. Even at echo length of less than 50% of the Guard Interval duration the MSE is already quite high.

V.3 CONCLUSIONS

The application of the proposed scheme does not show interesting results in case of long echo delays. In these cases, the assumption of a constant channel transfer function on consecutive OFDM subcarriers, on which the Alamouti encoded data is transmitted, is not fulfilled. However, the results for short echo durations are quite promising. A possible method for the reduction of the estimation error may be the additional filtering of the channel estimation results.

V.4 REFERENCES

- [1] Alamouti, S. M.; A Simple Transmit Diversity Technique for Wireless Communications; IEEE Journal on Selected Areas in Communications, Vol. 16, No. 8, October 1998
- [2] Mignone, V., Morello, A.; CD3-OFDM: A Novel Demodulation Scheme for Fixed and Mobile Receivers, IEEE Transactions on Communications, Vol. 44, No. 9, September 1996

VI EXTENSION OF ROTATED CONSTELLATIONS FOR MIMO SYSTEMS OVER ERASURE CHANNELS

VI.1 INTRODUCTION

The objective of this document is to present the work performed by Telecom Bretagne in 2009 in the context of TF206 regarding the MIMO studies.

The first part of the document concerns the performance of iterative receivers for MIMO system when the DVB-T2 FEC LDPC encoder is considered. Several space-time block codes (STBC) are studied from the classical spatial multiplexing scheme to more complex linear precoding-based STBC. Regarding the previous work presented in TF206, in particular [8], the system design and the performance evaluation take into account the presence of the powerful FEC encoder/decoder. Moreover, through synthesis charts, this study shows the improvements in terms of spectral efficiency and/or BER performance brought by the MIMO system compared to SIMO or SISO system.

The second part of the document presents the extension of the rotated constellations, a signal space diversity technique adopted in the DVB-T2 standard, for SIMO system. Classical SIMO system is considered except that the conventional mapper is replaced by the rotated mapper. The study shows that the rotated scheme is able to provide much better performance than the non-rotated scheme in the context of Rayleigh fading channels with erasure events. In the future this work should be extended to MIMO systems.

VI.2 PERFORMANCE OF ITERATIVE RECEIVERS FOR MIMO SYSTEM WITH DVB-T2 LDPC CODE

VI.2.1 TRANSMISSION MODEL

We consider a narrow-band radio communication system using simultaneously n_t ($n_t \geq 1$) transmit antennas and n_r ($n_r \geq 1$) receive antennas. A broadband transmission associated with OFDM modulation is implicitly assumed since Rayleigh fading channel is considered. SISO (Single Input Single Output), SIMO (Single Input Multiple Output) and MIMO (Multiple Input Multiple Output) systems are considered.

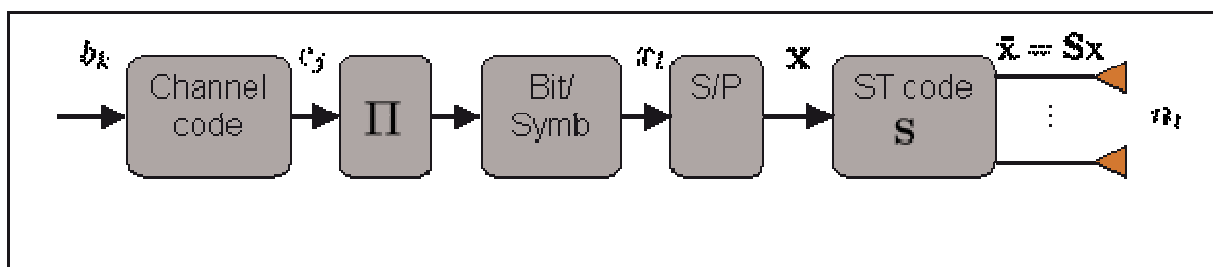


Figure 29: MIMO transmitter scheme.

The generic MIMO transmitter scheme is presented in Figure 29. The information bit stream b_k ($k = 1, 2, \dots, T_{inf}$, where T_{inf} is the number of information bits) is first encoded c_j ($j = 1, 2, \dots, T_{enc}$,

where T_{enc} is the number of encoded bits or frame size) by a rate- R_c LDPC encoder following the DVB-T2 standard. The coded bits are then bit interleaved by a size- T_{enc} random interleaver Π . Following a Gray mapping, the coded bits are base band modulated, according to a constellation χ , to produce the complex symbols stream x_l ($l=1,0,\dots,T_{sym}$), where T_{sym} is the number of symbols per block, i.e, T_{enc}/m where m is the number of bits per complex symbol. The considered constellations are the conventional QPSK and 16QAM. This scheme is called Bit Interleaved Coded Modulation (BICM).

A S/P (Serial to Parallel) conversion generates a stream of complex vectors \mathbf{x}_i of size $Q = n_t \times T$, and $i = 1, \dots, (T_{sym}/Q)$ where T denotes the number of time slots involved in the space-time code. For $n_t=1$, the complex symbols stream is directly transmitted. In the case of MIMO system, \mathbf{x} is space-time coded

$$\bar{\mathbf{x}} = \mathbf{S}\mathbf{x}$$

where \mathbf{S} is the space-time matrix of size $Q \times Q$ (for a full rate code) and $\bar{\mathbf{x}} = [\bar{x}_1 \ \bar{x}_2 \ \dots \ \bar{x}_Q]$ is the result of the linear transformation due to the multiplication by the \mathbf{S} matrix. The space-time code is detailed in section VI.2.2. The MIMO transmitter scheme represented Figure 29 is called ST-BICM (Space-Time Bit Interleaved Coded Modulation).

Then, the received signal is given by:

$$\mathbf{y} = \bar{\mathbf{H}}\bar{\mathbf{x}} + \mathbf{w}$$

or equivalently,

$$\mathbf{y} = \bar{\mathbf{H}}\mathbf{S}\mathbf{x} + \mathbf{w}$$

where $\bar{\mathbf{H}} = \text{diag}(\mathbf{H}^{[1]} \ \dots \ \mathbf{H}^{[T]})$, $\mathbf{y} = [y_1 \ y_2 \ \dots \ y_Q]^T$ and $\mathbf{w} = [w_1 \ w_2 \ \dots \ w_Q]^T$ whose entries are circularly symmetric, complex Gaussian noise samples with zero mean and variance σ_w^2 . We assume that the $n_r \times n_t$ matrix \mathbf{H} has i.i.d Gaussian distributed complex entries with unit variance. Since flat fading is considered, each entries describes the channel gain of the transmission path between the j^{th} transmit antenna and the i^{th} receive antenna. In addition perfect channel estimation and synchronization are considered. An equivalent representation is given by

$$\mathbf{y} = \mathbf{H}_{eq}\mathbf{x} + \mathbf{w} \quad [1]$$

where $\mathbf{H}_{eq} = \bar{\mathbf{H}}\mathbf{S}$ is the equivalent MIMO channel.

VI.2.2 DESCRIPTION OF THE SPACE-TIME CODES

In this section we only consider MIMO systems with $n_t > 1$ and $n_r > 1$. We focus on linear dispersion space-time block codes, introduced in [1]. The space-time block code defines a set of code words that corresponds to the linear combination of complex symbols in the space and time dimension. Full rate codes, such that $R_s = n_t$ are considered as they are able to provide the highest spectral efficiency. Linear precoding, as a diversity technique, improves the reliability of systems impaired by fading channels. The design of the space-time block code in MIMO systems can be based on

linear precoding matrix [2]. In Table 1, we classify different space-time codes with respect to the kind of diversity that can be exploited. Notice that, in this section, we do not take into account the diversity exploited by the FEC encoder/decoder.

Type of diversity	No of spatial diversity	Spatial diversity	Time and space diversities
T	1	n_t	$> n_t$
ST code	Spatial Mux.	Golden code ($n_t=2$) [3], Hassibi code ($n_t=2$) [1], Linear precoding [2], etc	Linear precoding

Table 1. Classification of the used space-time block codes.

- For $T = 1$ (Spatial multiplexing):

$\mathbf{S} = \mathbf{I}_{n_t}$, where \mathbf{I}_{n_t} is the identity matrix of size $n_t \times n_t$.

- For $T = n_t$

The space-time matrix of the LD (Linear Dispersion) code proposed by Hassibi for $n_t = 2, T=2$ is given by:

$$\mathbf{S} = \frac{1}{\sqrt{2}} \begin{bmatrix} 1 & 0 & 1 & 0 \\ 0 & 1 & 0 & 1 \\ 0 & 1 & 0 & -1 \\ 1 & 0 & -1 & 0 \end{bmatrix} \begin{array}{l} \longrightarrow A_1 \\ \longrightarrow A_2 \\ \longrightarrow A_1 \\ \longrightarrow A_2 \end{array} \begin{array}{l} | \\ | \\ | \\ | \end{array} \begin{array}{l} t_0 \\ t_0 \\ t_1 \\ t_1 \end{array}$$

where A_1 and A_2 are the transmit antenna one and two respectively and t_0 and t_1 are the time slot zero and one respectively.

For the same parameters, $n_t = 2, T = 2$ space-time codes based on linear precoding and Hadamard matrix³ can be designed to exploit space diversity, equation (2), or time diversity, equation (3).

³ Hadamard matrix is defined by $\Theta_p = \frac{1}{\sqrt{2}} \begin{bmatrix} \Theta_{p/2} & \Theta_{p/2} \\ \Theta_{p/2} & -\Theta_{p/2} \end{bmatrix}$ with $\Theta_1 = 1$ and p a power of two.

$$\mathbf{S} = \frac{1}{\sqrt{2}} \begin{bmatrix} 1 & 1 & 0 & 0 \\ 1 & -1 & 0 & 0 \\ 0 & 0 & 1 & 1 \\ 0 & 0 & 1 & -1 \end{bmatrix} \quad 2)$$

$$\mathbf{S} = \frac{1}{\sqrt{2}} \begin{bmatrix} 1 & 1 & 0 & 0 \\ 0 & 0 & 1 & 1 \\ 1 & -1 & 0 & 0 \\ 0 & 0 & 1 & -1 \end{bmatrix} \quad 3)$$

- For $T > n_t$

It is possible to design some space-time codes based on linear precoding that exploit space and time diversity jointly.

For $n_t = 2$, $T = 4$ the space-time codes based on Hadamard linear precoding for time and space-time diversity are presented in (4) and (5) respectively.

$$\mathbf{S} = \frac{1}{2} \begin{bmatrix} 1 & 1 & 1 & 1 & 0 & 0 & 0 & 0 \\ 0 & 0 & 0 & 0 & 1 & 1 & 1 & 1 \\ 1 & -1 & 1 & -1 & 0 & 0 & 0 & 0 \\ 0 & 0 & 0 & 0 & 1 & -1 & 1 & -1 \\ 1 & 1 & -1 & -1 & 0 & 0 & 0 & 0 \\ 0 & 0 & 0 & 0 & 1 & 1 & -1 & -1 \\ 1 & -1 & -1 & 1 & 0 & 0 & 0 & 0 \\ 0 & 0 & 0 & 0 & 1 & -1 & -1 & 1 \end{bmatrix} \quad 4)$$

$$\mathbf{S} = \frac{1}{2} \begin{bmatrix} 1 & 1 & 1 & 1 & 0 & 0 & 0 & 0 \\ 1 & -1 & 1 & -1 & 0 & 0 & 0 & 0 \\ 1 & 1 & -1 & -1 & 0 & 0 & 0 & 0 \\ 1 & -1 & -1 & 1 & 0 & 0 & 0 & 0 \\ 0 & 0 & 0 & 0 & 1 & 1 & 1 & 1 \\ 0 & 0 & 0 & 0 & 1 & -1 & 1 & -1 \\ 0 & 0 & 0 & 0 & 1 & 1 & -1 & -1 \\ 0 & 0 & 0 & 0 & 1 & -1 & -1 & 1 \end{bmatrix} \quad 5)$$

In case of frequency selective channels, the exploitation of time diversity can be converted into frequency diversity if the space-time coding is done across the subcarriers of the OFDM modulation. For a L -path channel, the space-time matrix should be dimensioned such that $T \geq L \times n_t$.

VI.2.3 RECEIVER MODEL

VI.2.3.1 SIMO RECEIVER

If CSI is perfectly known the optimal combining technique for the SIMO receiver is the Maximal Ratio Combining (MRC). The output of the MRC receiver is given by [11]

$$\tilde{\mathbf{x}} = \mathbf{g}^T \mathbf{h} \mathbf{x} + \mathbf{g}^T \mathbf{w} = \sum_{i=1}^{n_r} g_i h_i x + \sum_{i=1}^{n_r} g_i w \quad 6)$$

where $\mathbf{g} = \lambda \mathbf{h}^*$ and $\lambda = \left(\sum_{i=1}^{n_r} |h_i|^2 \right)^{-1/2}$.

The MRC detector is followed by a soft demapper (symbol to LLR conversion), detailed in section VI.2.3.3, a bit deinterleaver and the channel decoder.

VI.2.3.2 MIMO ITERATIVE RECEIVER

The MIMO receiver is an iterative (or turbo) receiver based on Minimum Mean Square Error – Interference Cancellation (MMSE-IC) [5] [6].

The iterative receiver is divided into two main parts. The first is the detector, that is updated every each iteration with the information coming from the second part, the channel decoder, as shown in Figure 30. Based on channel observations \mathbf{y} , the detector based on an interference cancellation structure provides an estimation of the complex symbol vector \mathbf{x} according to the MMSE criterion. The estimated vector $\tilde{\mathbf{x}}$ is converted to a stream of symbols. These estimated symbols are transformed to Log-Likelihood Ratios (LLRs) given by

$$L_e(b|\tilde{\mathbf{x}}) = \ln \left(\frac{P\{b=1|\tilde{\mathbf{x}}\}}{P\{b=0|\tilde{\mathbf{x}}\}} \right)$$

The deinterleaved LLR are then processed by the channel decoder that computes the *a posteriori* (L_a) LLR. This information is interleaved again and converted to soft symbols in order to perform MMSE-IC. Thanks to the *a posteriori* LLR provided by the channel decoder, the MMSE-IC detector is able to provide a better estimate of the complex symbol vector. An outer iteration corresponds to detection followed by channel decoding.

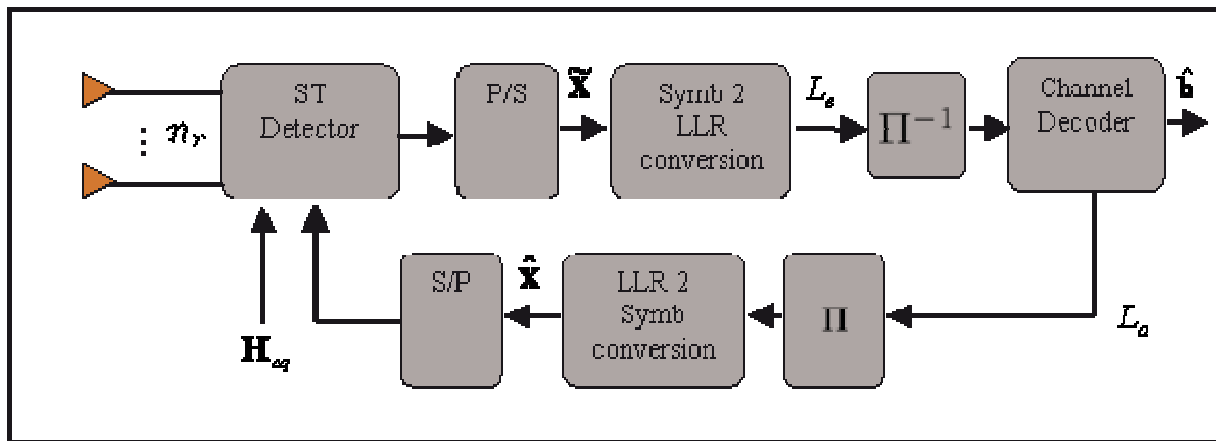


Figure 30. MIMO iterative receiver

The considered FEC encoder is the DVB-T2 LDPC encoder [9]. In this work, the sum-product algorithm is considered at the decoding side. Since this algorithm is based on the message passing concept, it needs several iterations to provide an updated version of the coded bits in terms of LLR L_a . These iterations are called inner iterations contrary to the outer iterations that are performed between the detector and the channel decoder. The input of the channel decoding is a stream of L_c LLR of coded bits. The channel decoder computes the *a posteriori* LLR L_a and the estimated bits \hat{b} .

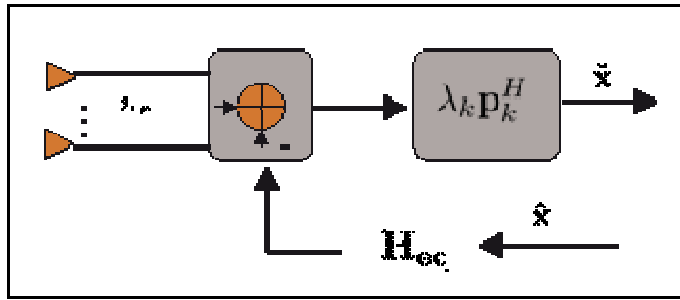


Figure 31. Space-time detector : MMSE-IC scheme

We assume that the equivalent channel \mathbf{H}_{eq} is perfectly known. The space-time detector, depicted in Figure 31, consists in an interference cancellation structure updated according to the MMSE criterion. Based on the transmission model given equation (1), the entries of the estimated vector $\tilde{\mathbf{x}}$ can be derived [5]:

$$\tilde{x}_k = \lambda_k \mathbf{p}_k^H (\mathbf{y} - \mathbf{H}_{eq} \hat{\mathbf{x}} + \hat{x}_k \mathbf{h}_k) \quad (7)$$

where

$$\mathbf{p}_k = \left((\sigma_x^2 - \sigma_{\hat{x}}^2) \mathbf{H}_{eq} \mathbf{H}_{eq}^H + \sigma_w^2 \mathbf{I} \right)^{-1} \mathbf{h}_{eq,k}$$

$$\lambda_k = \frac{\sigma_x^2}{1 + \sigma_{\hat{x}}^2 \beta_k} \quad \beta_k = \mathbf{p}_k^H \mathbf{h}_{eq,k}$$

$$\sigma_{\hat{x}}^2 = \frac{1}{T_{sym}} \sum_{n=0}^{T_{sym}-1} |\hat{x}_n|^2$$

and $k = 0, 1, \dots, n_r$, $\mathbf{h}_{eq,k}$ is the k^{th} column of \mathbf{H}_{eq} , and $(\cdot)^H$ is the conjugate transpose.

At the first iteration, since *a priori* information is not available, we consider $\hat{\mathbf{x}} = \mathbf{0}$ and $\sigma_{\hat{x}}^2 = 0$. Therefore the classical MMSE detector is obtained and the estimated complex symbol is given by

$$\tilde{x}_k = \sigma_x^2 \mathbf{h}_{eq,k}^H (\sigma_x^2 \mathbf{H}_{eq} \mathbf{H}_{eq}^H + \sigma_w^2 \mathbf{I})^{-1} \mathbf{y} \quad (8)$$

VI.2.3.3 SYMBOL TO LLR CONVERSION

The symbol to LLR conversion allows for the conversion of the estimated symbols \tilde{x}_k into LLR of coded bits. The output of the detector (MRC or MMSE-IC) can be written as

$$\tilde{x}_k = g_k x_k + \eta_k \quad (9)$$

where g_k is a real scalar and η_k is a complex Gaussian noise with zero mean and variance σ_{η}^2 . g_k and σ_{η}^2 are computed from the expression of the detector output. Thanks to the max-log approximation ($\ln(\exp(x_1) + \exp(x_2)) \approx \max(x_1, x_2)$), the LLR of the i -th bit of the complex symbol \tilde{x}_k is given by

$$L_e(b_i | \tilde{x}_k) \approx \frac{1}{\sigma_\eta^2} \left[\min_{x \in \mathcal{X}_0^k} (|\tilde{x}_k - g_k x|^2) - \min_{x \in \mathcal{X}_1^k} (|\tilde{x}_k - g_k x|^2) \right] \quad 10)$$

where \mathcal{X}_b^i is composed by the elements of the constellation such that the i -th bit is equal to b .

VI.2.3.4 LLR TO SYMBOL CONVERSION

The LLR to symbol conversion converts the LLR provided by the channel decoder into soft complex symbols. The expression of the soft symbol \hat{x}_k is given by

$$\hat{x}_k = \sum_{x \in \mathcal{X}} x P(x_k = x | L_a(b_i^k), i = 0, \dots, m) \quad 11)$$

where b_i^k is the i -th bit of the symbol x_k .

Assuming that the transmitted bits are statistically independent, we obtain

- For QPSK

$$\Re(\hat{x}_k) = \tanh\left(\frac{L_a(b_0^k)}{2}\right)$$

$$\Im(\hat{x}_k) = \tanh\left(\frac{L_a(b_1^k)}{2}\right)$$

- For 16-QAM

$$\Re(\hat{x}_k) = \frac{3e^{L_a(b_0^k)} e^{L_a(b_1^k)} + e^{L_a(b_0^k)} - 1 - 3e^{L_a(b_1^k)}}{(1 + e^{L_a(b_0^k)})(1 + e^{L_a(b_1^k)})}$$

$$\Im(\hat{x}_k) = \frac{3e^{L_a(b_2^k)} e^{L_a(b_3^k)} + e^{L_a(b_2^k)} - 1 - 3e^{L_a(b_3^k)}}{(1 + e^{L_a(b_2^k)})(1 + e^{L_a(b_3^k)})}$$

VI.2.4 PERFORMANCE BOUNDS

VI.2.4.1 MRC RECEIVER

Assuming that the channel vector \mathbf{h} has i.i.d Gaussian distributed complex entries with unit variance, the probability of error $P(e)$ of the MRC receiver over a Rayleigh channel with n_r receive antennas can be asymptotically approximated by [11]

$$P(e) \approx \left(\frac{N_0}{4E_s}\right)^{n_r} \binom{2n_r - 1}{n_r} \quad 12)$$

The bit error probability decreases inversely with the n_r -th power of the signal-to-noise ratio. This receiver provides the maximum diversity order equal to n_r . At high SNR, the bit error probability of the MRC receiver in the context of a BCIM SIMO system is bounded by

$$P(e) \leq \sum_{d=d_{\min}}^{+\infty} A_d^{(b)} \binom{2Ld - 1}{Ld} \left(\frac{N_0}{4R_c E_b}\right)^{Ld} \quad 13)$$

where $\{(A_d^{(b)}, d), d = d_{\min}, \dots, +\infty\}$ defines the distance spectrum of the channel code and d_{\min} is the minimum distance of the channel code.

VI.2.4.2 MIMO ITERATIVE RECEIVER

Assume that $\hat{\mathbf{x}} = \mathbf{x}$ and $\sigma_{\hat{\mathbf{x}}}^2 = \sigma_x^2$. Then equation (7) becomes

$$\tilde{x}_k = \frac{\sigma_x^2 \mathbf{h}_{eq,k}^H}{\sigma_x^2 \|\mathbf{h}_{eq,k}\|^2 + \sigma_w^2} (\mathbf{h}_{eq,k} \hat{x}_k + \mathbf{w}) \quad (14)$$

This expression corresponds to the genie aided receiver since the complex symbols are supposed to be known. The performance of such a scheme gives a lower bound for the iterative receiver. This bound is achieved when the *a posteriori* information provided by the channel decoder is error-free. It can be shown that this expression is equivalent to the expression of the MRC output, given in section VI.2.3.1, by replacing n_r by T and taking out a scalar. Therefore if the iterative receiver converges towards its lower bound, it is also able to achieve a diversity order equal to T . Finally, the lower bound of the iterative receiver is given by the performance of the MRC detector followed by the channel decoder over a SIMO channel with $n_r = T$ antennas.

VI.2.5 SIMULATION RESULTS

The performance results are given in terms of Bit Error Rate (BER). We assume perfect channel estimation and synchronization. The power is normalized at the transmitter and the receiver so that the ratio E_b / N_0 is given by

$$\frac{E_b}{N_0} = \frac{n_r}{mR_c} \cdot \frac{\sigma_x^2}{\sigma_w^2} \quad (15)$$

where m is the number of bits per symbol and R_c is the channel code rate.

Figure 32 provides the performance of the iterative receiver with the MMSE-IC detector in case of convolutional code or DVB-T2 LDPC for the 8th outer iteration. 5 inner iterations are performed in the case of the LDPC. Both schemes use a linear precoding rate $T=1$ that corresponds to the spatial multiplexing scheme. The simulation parameters are presented in Table 2. For QPSK, at BER= 10^{-5} , the LDPC scheme outperforms the convolutional scheme by 3 dB. For 16-QAM this gain is approximately 2.8 dB.

Number of Tx. × Rx. Antennas	2 × 2
Linear Precoding Rate	T = 1 (Spatial Mux)
Modulation	QPSK and 16QAM
Frame Size	16200
Number of outer iterations (outer)	8
Number of LDPC iterations (inner)	5

Code	Convolutional code and DVB-T2 LDPC
Polynomial code generator	(133,171)o
Convolutional Code rate	1/2
LDPC Code rate	1/2
Type of detector	MMSE-IC

Table 2. Simulation parameters for Figure 32.

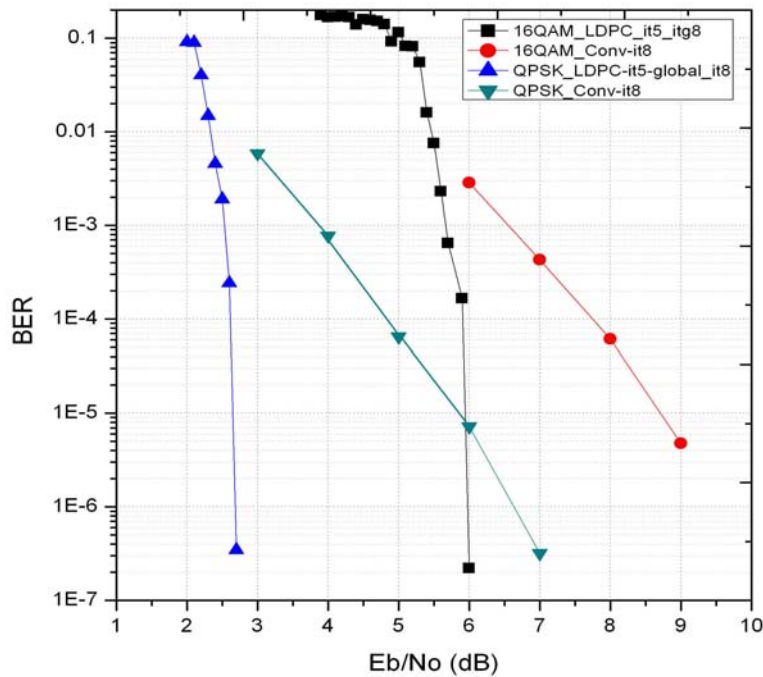


Figure 32. Performance of the MMSE-IC iterative receiver with the convolutional code and the LDPC code. T=1. 8 outer iterations. QPSK and 16-QAM.

Figure 33 shows the performance of the MMSE-IC iterative receiver (LDPC code, 8th outer iteration and 5 inner iterations) with a linear precoding rate of $T=1$ (spatial multiplexing scheme) and $T=2$ (full rate space-time code with the exploitation of transmit spatial diversity, see (2)). The simulation parameters are presented in Table 3. The improvement of the performance brought by linear precoding is due to the addition of diversity in the system - in this case transmit spatial diversity. This improvement is essentially observed for high code rates ($R=3/4$ and $R=4/5$). Indeed the FEC code already exploits time and space diversity thanks to the ST-BICM scheme. Since time diversity is infinite in case of the Rayleigh channel, the diversity order of the ST-BICM, bounded by the minimum distance of the code, is already quite high, even without explicit exploitation of space diversity via STBC. The impact on the performance of the addition of spatial diversity is then visible when the minimum distance of the code is low, that is for high rate codes.

Number of Tx. × Rx. Antennas	2 × 2
------------------------------	-------

Linear precoding rate	$T = 1$ and $T=2$ (Time Diversity)
Modulation	QPSK
Frame Size	16200
Number of outer iterations (outer)	8
Number of LDPC iterations (inner)	5
Code	DVB-T2 LDPC
LDPC Code rate	$(1/2)$, $(11/15 \approx 3/4)$, $(7/9 \approx 4/5)$
Type of detector	MMSE-IC

Table 3. Simulation parameters for Figure 33.

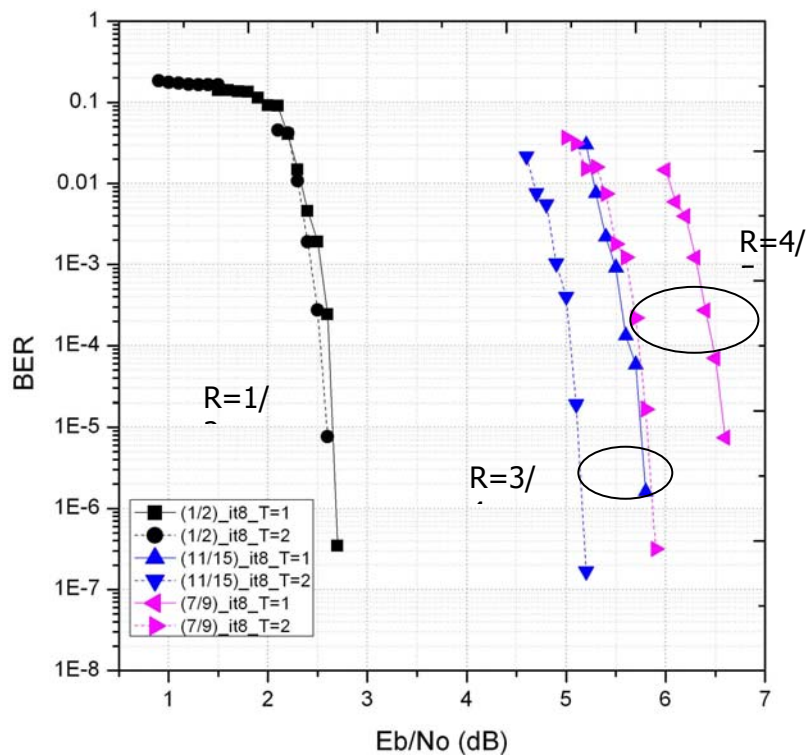


Figure 33. Performance of the MMSE-IC iterative receiver with the LDPC code for different code rates.

$T=1$ and $T=2$. QPSK. 8 outer iterations and 5 inner iterations.

Figure 34 shows the synthesis chart that depicts the spectral efficiencies versus E_b/N_0 at BER equal to 10^{-5} for the MMSE-IC iterative receiver in case of the MIMO system and for the

conventional receiver in case of the SISO system for different code rates and two constellations (QPSK and 16-QAM). Both schemes use the LDPC code. The iterative receiver performs 8 outer iterations and 5 inner iterations that correspond to 40 LDPC iterations. The conventional receiver performs 40 LDPC iterations. The simulation parameters are given in Table 4. We recall that the rotated constellation principle is not implemented yet. Moreover two space-time codes are taken into account: $T=1$ (spatial multiplexing) and $T=2$ (linear precoding along the time dimension, see (3)). By exploiting the spatial dimension through the MIMO system, a gain of several dBs is observed compared to the SISO case for all targeted spectral efficiencies. This gain is due to the use of a lower-order constellation thanks to spatial multiplexing, which is more robust to noise and fading, and to the exploitation of the spatial diversity (at the transmitter and at the receiver) and the time diversity for $T=2$. The impact of the linear precoding on the performance, observed by the comparison between $T=1$ and $T=2$, is less important, from less than 0.5 dB to around 1 dB depending on the couple code rate/modulation.

Number of Tx. × Rx. Antennas	2×2
Linear Precoding Rate	$T = 1$ and $T=2$ (Time Diversity)
Modulation	QPSK and 16-QAM
Frame Size	16200
Number of global iterations (outer)	8
Number of LDPC iterations (inner)	5
Code	DVB-T2 LDPC
LDPC Code rate	$(1/2)$, $(11/15 \approx 3/4)$, $(7/9 \approx 4/5)$
Type of detector	MMSE-IC
SISO LDPC iterations	50

Table 4: Simulation parameters for Figure 34

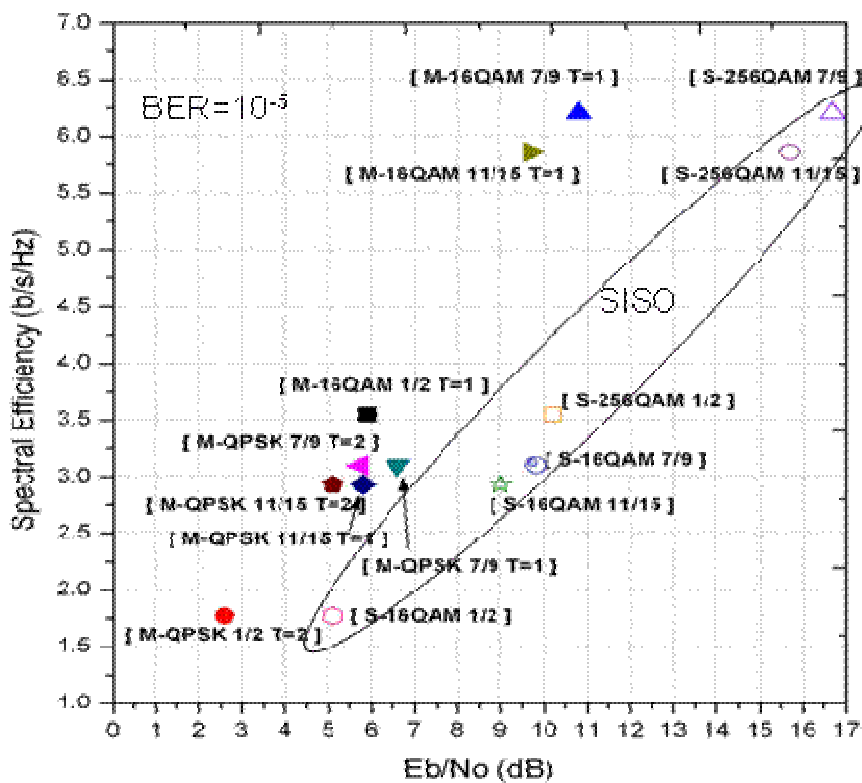


Figure 34. Spectral efficiencies versus Eb/No at BER equal to 10⁻⁵ for the MMSE-IC iterative receiver in the case of the MIMO system and for the conventional receiver in the case of the SISO system.

Figure 35 shows the synthesis chart that depicts the spectral efficiencies versus Eb/No at BER equal to 10⁻⁵ for the MMSE-IC iterative receiver in case of the MIMO system and for the MRC receiver in case of the SIMO system for different code rates and two constellations (QPSK and 16-QAM). Both schemes use the LDPC code. The simulation parameters are presented in Table Table 5. A gain greater than 2 dB is observed between the MIMO and the SIMO system whatever the code rate/modulation. Indeed the spatial multiplexing scheme allows for the use of a more robust lower-order constellation. Moreover the spatial diversity order of the MIMO system is potentially multiplied by n_t compared to the SIMO system.

Number of Tx. × Rx. Antennas	2 × 2 for the MIMO system 1 × 2 for the SIMO system
Linear Precoding Rate	T = 1, and T=2 (Time diversity)
Modulation	QPSK and 16-QAM
Frame Size	16200
Number of outer iterations (outer)	8

Number of LDPC iterations (inner)	5
Code	DVB-T2 LDPC
LDPC Code rate	(1/2), (11/15 ≈ 3/4), (7/9 ≈ 4/5)
Type of detector	MMSE-IC (MIMO) MRC (SIMO)
Number of LDPC iterations (SIMO)	40

Table 5. Simulation parameters for Figure 35.

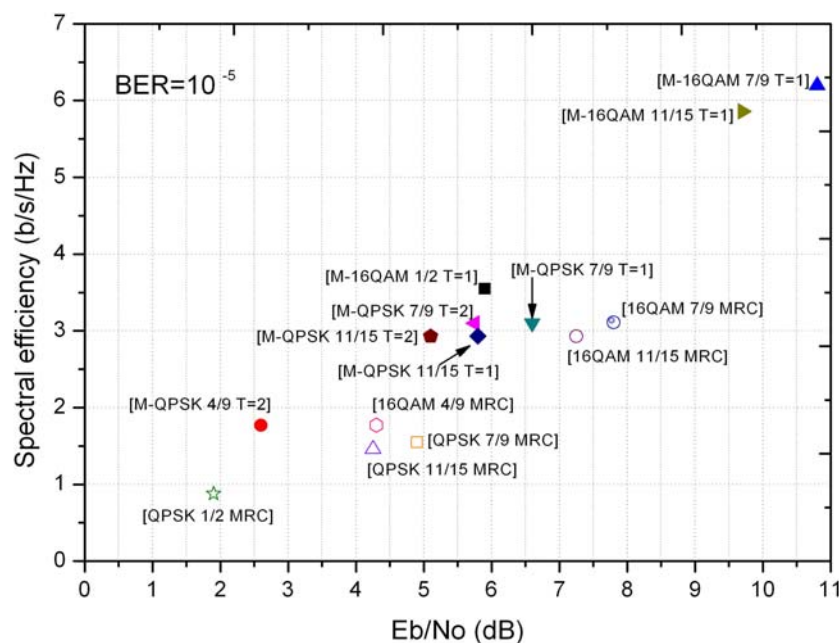


Figure 35. Spectral efficiencies versus E_b/N_0 at BER equal to 10^{-5} for the MMSE-IC iterative receiver in case of the MIMO system and for the MRC receiver in case of the SIMO system.

Figure 36 presents the synthesis chart that depicts the spectral efficiencies versus E_b/N_0 at BER equal to 10^{-5} for the MMSE-IC iterative receiver and for the non-iterative MMSE receiver for different code rates and two constellations (QPSK and 16-QAM). Both schemes use the LDPC code. The linear precoding rate is $T=1$ (spatial multiplexing scheme) and $T=2$ (time diversity). The simulation parameters are presented in Table 6. The iterative receiver achieves a 1dB gain over the non-iterative receiver whatever the couple code rate/modulation.

Number of Tx. × Rx. Antennas	2×2
Linear Precoding Rate	$T = 1$, and $T=2$ (Time

	Diversity)
Modulation	QPSK and 16-QAM
Frame Size	16200
Number of outer iterations (outer)	8
Number of LDPC iterations (inner)	5
Code	DVB-T2 LDPC
LDPC Code rate	(1/2), (11/15 ≈ 3/4), (7/9 ≈ 4/5)
Type of detector	MMSE-IC (iterative receiver) MMSE (non-iterative receiver)
Non-iterative receiver LDPC iterations	40

Table 6. Simulation parameters for Figure 36.

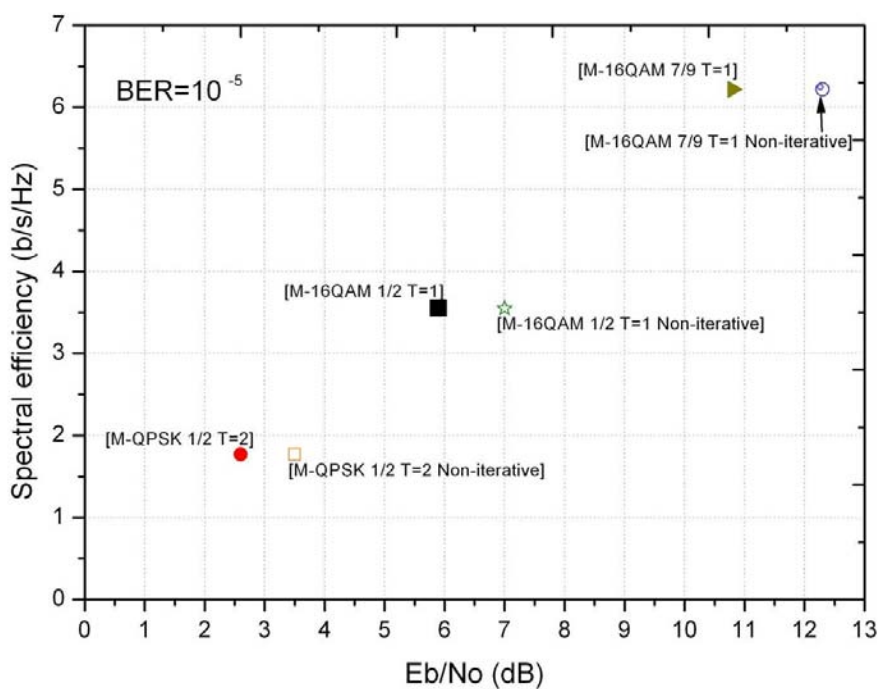


Figure 36. Spectral efficiencies versus E_b/N_0 at BER equal to 10^{-5} for the MMSE-IC iterative receiver with the LDPC code (8 outer iterations and 5 inner LDPC iterations) and the non-iterative MMSE receiver with the LDPC code (40 iterations).

VI.2.6 ITERATIVE RECEIVERS FOR A MIMO SYSTEM WITH DVB-T2 LDPC CODE: CONCLUSION

In this work, we studied the performance of a MIMO system associated with the DVB-T2 LDPC code. The MIMO system involved 2 transmit and 2 receive antennas. In order to achieve high spectral efficiencies we focused on full rate space-time codes such as the spatial multiplexing scheme. To exploit spatial or time diversity, linear precoding was inserted between the bit to symbol conversion and the spatial multiplexing scheme. The resulting scheme can be viewed as a full rate space-time code, classified in the literature under the name of linear dispersion code. To exploit the potentialities of the designed MIMO system at best, an iterative receiver, following the turbo principle and based on the MMSE criterion, was presented. We recall that the rotated constellation was not taken into account and that perfect synchronization and channel estimation were considered at the receiver. Notice also that the scheduling of the iterative process, and in particular the number of inner and outer iterations, was not optimized.

We showed that the proposed MIMO scheme associated with the DVB-T2 LDPC code and the iterative receiver outperformed the same scheme with convolutional code by more than 3 dB at BER equal to 10^{-5} . Moreover, the proposed MIMO scheme allowed for a performance gain, compared to the SISO system, greater than 2 dB for low spectral efficiencies and even 6 dB for high spectral efficiencies. A comparison between the MIMO system and the SIMO system with an MRC receiver is also addressed. A gain greater than 2 dB is observed between the MIMO and the SIMO system whatever the couple code rate/modulation. Finally, the simulation results showed that, for the MIMO system, the iterative receiver, based on the MMSE criterion, achieves a 1dB gain over the non-iterative receiver based on the MMSE detector whatever the couple code rate/modulation.

VI.3 EXTENSION OF ROTATED CONSTELLATIONS FOR A SIMO SYSTEM OVER ERASURE CHANNELS

VI.3.1 SYSTEM MODEL

We consider a narrow-band SIMO radio communication system using $n_t=1$ transmit antennas and n_r ($n_r \geq 1$) receive antennas. The information bits are encoded according to the BICM scheme presented in section VI.2.1. However, the rotated QAM mapper, presented in [12] replaces the conventional mapper. The angles optimized in [12] are chosen. The SIMO channel is represented by a n_r -size vector \mathbf{h} whose entries h_i describe the gain of each transmission path from the transmit antenna to the i th receive antenna. We omit the time index k for the sake of clarity.

The received vector is given by

$$\mathbf{y} = \mathbf{h}x + \mathbf{w} \tag{16}$$

where x is the transmitted complex symbol, the channel vector $\mathbf{h} = [h_1 \ h_2 \ \dots \ h_{n_r}]^T$, the received signal is a complex vector $\mathbf{y} = [y_1 \ y_2 \ \dots \ y_{n_r}]^T$, and $\mathbf{w} = [w_1 \ w_2 \ \dots \ w_{n_r}]^T$ is the circularly symmetric, complex Gaussian noise vector with zero mean and variance σ_w^2 .

If CSI is perfectly known the optimal combining technique for the SIMO receiver is the Maximal Ratio Combining (MRC). The output of the MRC receiver is given by [11]

$$\tilde{\mathbf{x}} = \mathbf{g}^T \mathbf{h}x + \mathbf{g}^T \mathbf{w} = \sum_{i=1}^{n_r} g_i h_i x + \sum_{i=1}^{n_r} g_i w_i \tag{17}$$

where $\mathbf{g} = \lambda \mathbf{h}^*$ and $\lambda = \left(\sum_{i=1}^{n_r} |h_i|^2 \right)^{-1/2}$.

The MRC detector is followed by the soft rotated demapper (symbol to LLR conversion), as presented in [12], a bit deinterleaver and the channel decoder.

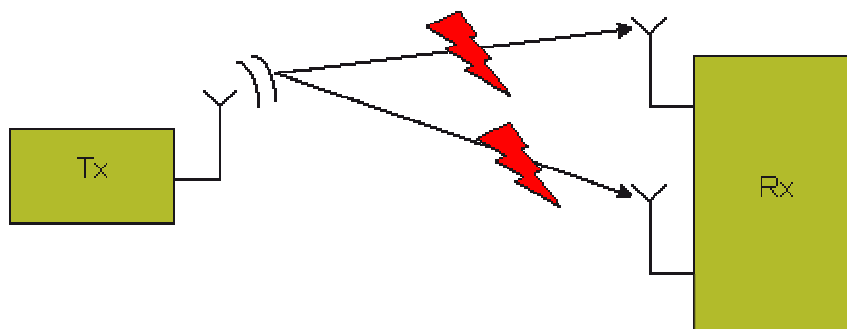


Figure 37a. SIMO fading channel with independent erasure events affecting every received antenna.

Two channel models are considered: the conventional i.i.d Rayleigh fading channel and the i.i.d Rayleigh fading channel with erasures. For the former, the channel gain h_i is an independent Gaussian distributed complex sample with unit variance. For the latter, the channel gain is given by

$$h_i = \rho_i e_i \tag{18)}$$

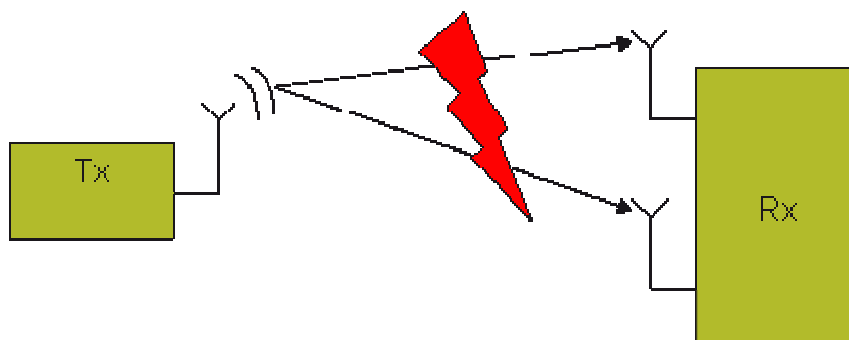


Figure 37b. SIMO fading channel with correlated erasure events affecting every received antenna.

where ρ_i is an independent Gaussian distributed complex sample with unit variance and e_i is the erasure event that takes the value 0 with a probability of P_e and the value 1 with a probability of $1 - P_e$. The erasures can be applied independently or identically over the n_r antennas as shown in figure 10a and 10b. Note that the signal-to-noise ratio has to be normalized by a $\sqrt{1 - P_e}$ factor in order to compensate for the loss of received signal power.

VI.3.2 SIMULATION RESULTS

The performance results are given in terms of Bit Error Rate (BER) w.r.t E_b/N_0 . We assume perfect channel estimation and synchronization. The simulation parameters are reported in Table 7. We compare the performance of the SIMO scheme with and without the rotated constellation.

Number of Tx. × Rx. Antennas	1 × 2
Modulation	16-QAM
Frame Size	16200
Number of LDPC iterations (inner)	40
Code	DVB-T2 LDPC
LDPC Code rate	4/5
Type of detector	MRC

Table 7. Simulation parameters.

VI.3.2.1 OVER I.I.D. RAYLEIGH FADING CHANNEL

Figure 38 presents the performance results of the SIMO system with and without rotated constellation over the i.i.d Rayleigh fading channel. The rotation does not degrade the performance and even leads to a slight improvement of 0.1 dB at BER equal to 10^{-5} .

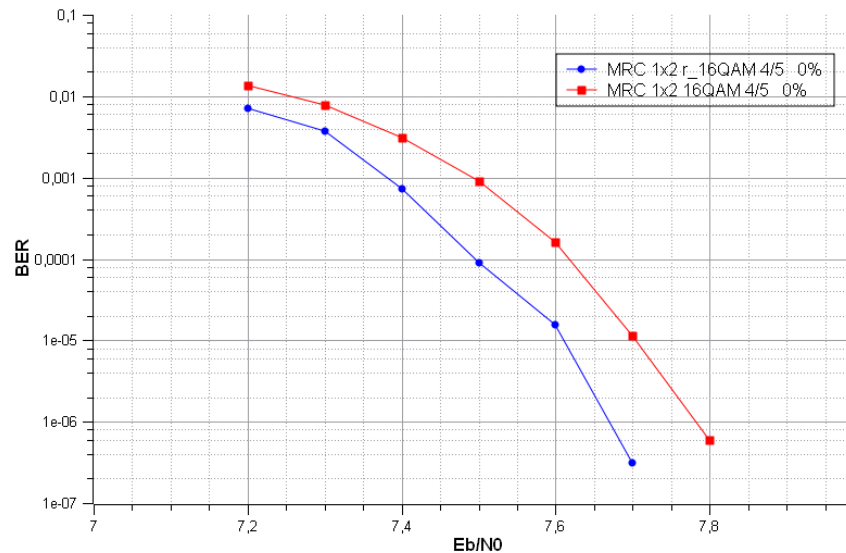


Figure 38. Performance of the SIMO system with/without the rotated constellation over i.i.d. Rayleigh fading channel. MRC detector, DVB-T2 rate-4/5 LDPC, 16QAM, 40 iterations.

VI.3.2.2 OVER I.I.D. RAYLEIGH FADING CHANNEL WITH ERASURES

Four cases are simulated. First, we assume independent erasure events at 20% and 40%. Second, fully correlated erasure events at 15% and 20% are considered.

Figure 39 presents the performance results of the SIMO system with and without rotated constellation over the i.i.d Rayleigh fading channel with independent erasure events at 20%. Thanks to the rotation, the system performance is improved moderately by 0.4 dB at $BER=10^{-5}$. Moreover, the slope of the curve is much steeper in the case of the rotated constellation. The improvement is much more impressive when the erasure events are at 40%, as illustrated in Figure 40. In this context, the performance of the non-rotated SIMO system undergoes severe flattening whereas the rotated one still converges for $E_b/N_0 < 14$ dB. The SIMO system with the rotated constellation is thus able to cope with numerous erasure events.

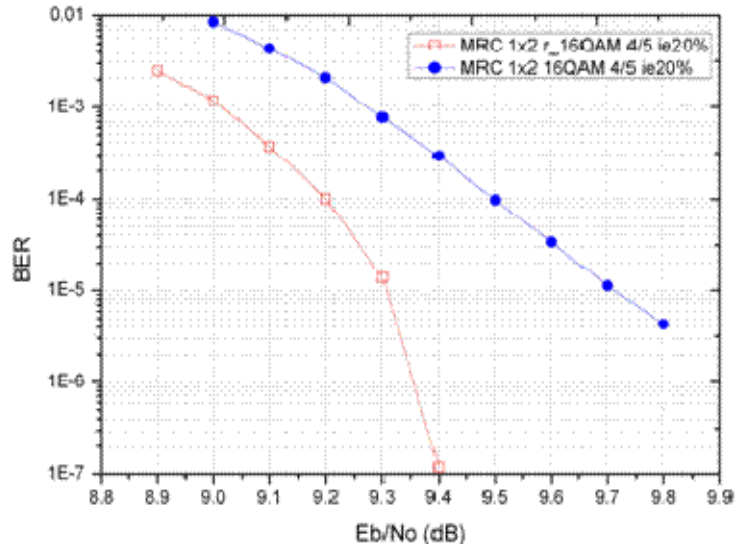


Figure 39. Performance of the SIMO system with/without the rotated constellation over i.i.d. Rayleigh fading channel with independent erasure events at 20%. MRC detector, DVB-T2 rate-4/5 LDPC, 16QAM, 40 iterations.

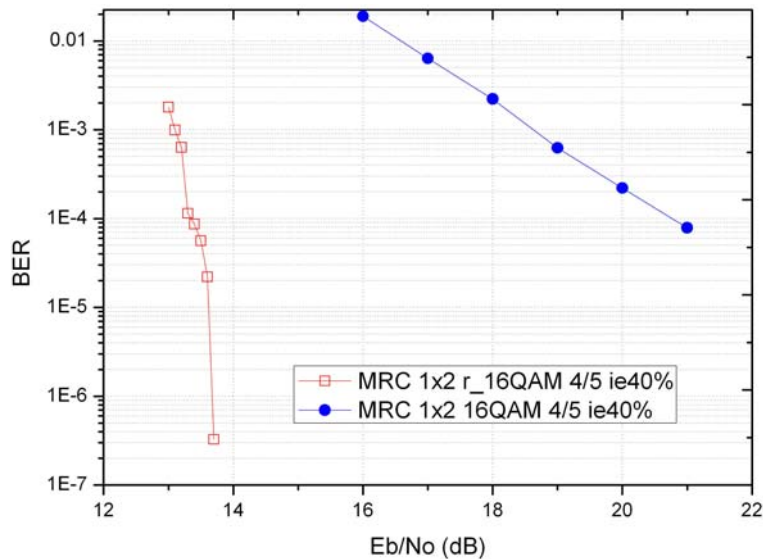


Figure 40. Performance of the SIMO system with/without the rotated constellation over i.i.d. Rayleigh fading channel with independent erasure events at 40%. MRC detector, DVB-T2 rate-4/5 LDPC, 16QAM, 40 iterations.

Figure 41 presents the performance results of the SIMO system with and without rotated constellation over the i.i.d Rayleigh fading channel with fully correlated erasure events at 15%. Again the rotation provides a performance gain of more than 1.5 dB at BER=10⁻⁴. Finally, on Figure 42, we observe the extreme case, corresponding to fully correlated erasure events at 20%, where the SIMO system without rotation does not converge at all since an error floor is observed at 8.10⁻² over the whole simulated SNR range. On the contrary the SIMO system with rotation is still able to provide acceptable BER performance.

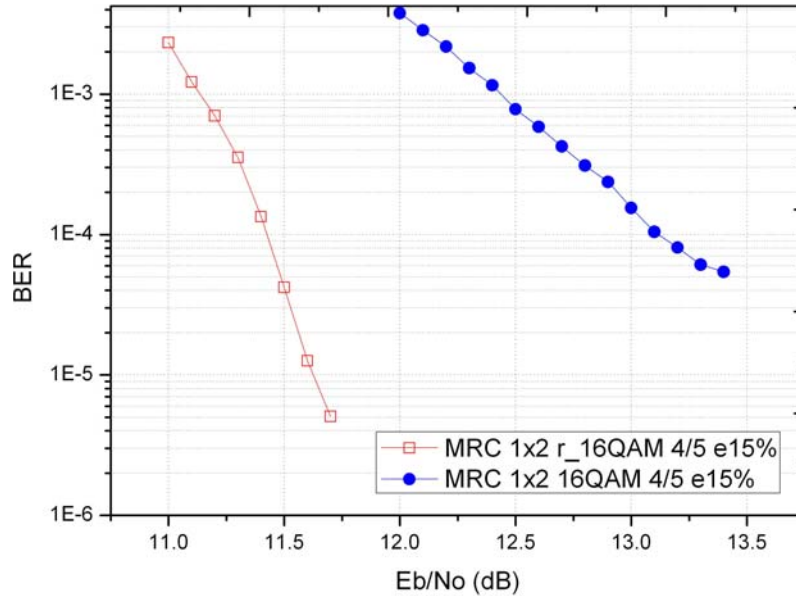


Figure 41. Performance of the SIMO system with/without the rotated constellation over i.i.d. Rayleigh fading channel with fully correlated erasure events at 15%. MRC detector, DVB-T2 rate-4/5 LDPC, 16QAM, 40 iterations.

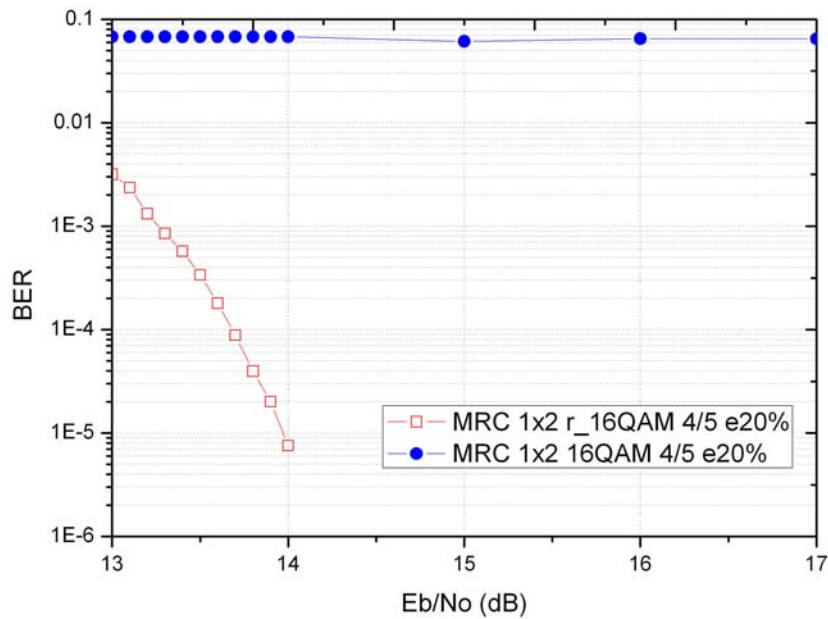


Figure 42. Performance of the SIMO system with/without the rotated constellation over i.i.d. Rayleigh fading channel with fully correlated erasure events at 20%. MRC detector, DVB-T2 rate-4/5 LDPC, 16QAM, 40 iterations.

VI.3.2.3 SUMMARY OF PERFORMANCE OVER I.I.D. RAYLEIGH FADING CHANNEL WITH ERASURES

A summary of the performance over a fading channel with independent erasures is found in Figure 43 and for correlated erasures in

Figure 44.

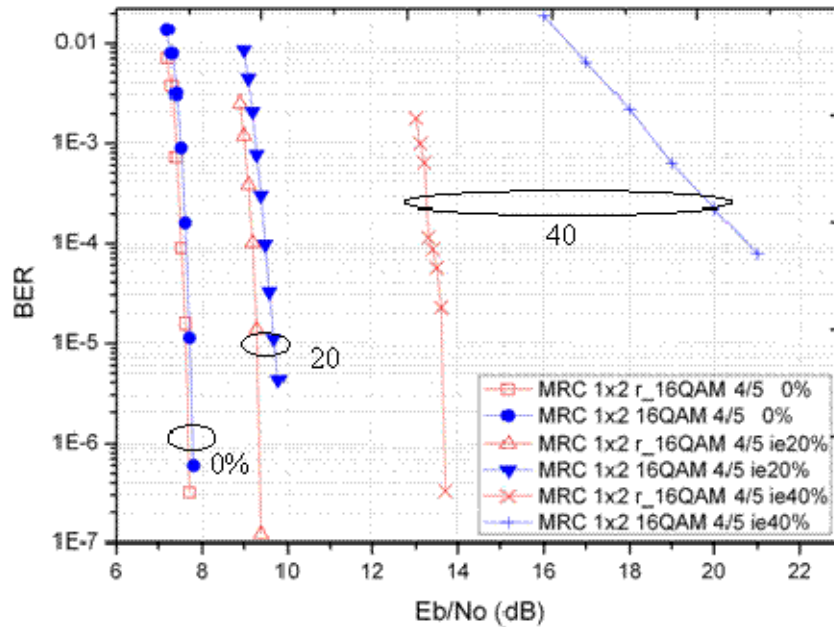


Figure 43. Performance comparison of the SIMO system with/without the rotated constellation over i.i.d. Rayleigh fading channel without/with independent erasure events at 20% and 40%. MRC detector, DVB-T2 rate-4/5 LDPC, 16QAM, 40 iterations.

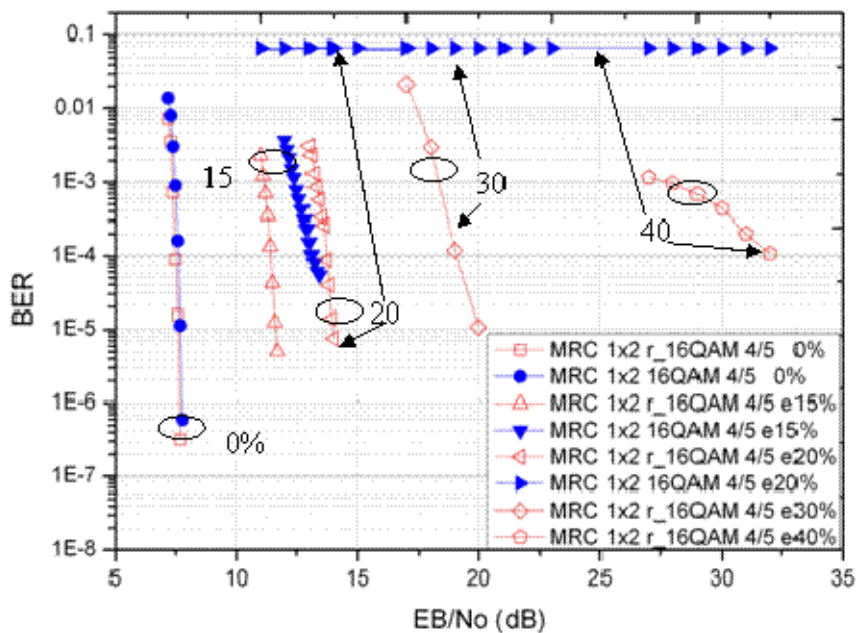


Figure 44. Performance comparison of the SIMO system with/without the rotated constellation over i.i.d. Rayleigh fading channel without/with correlated erasure events at 15%, 20%, 30% and 40%. MRC detector, DVB-T2 rate-4/5 LDPC, 16QAM, 40 iterations.

Figure 44 shows that the non-rotated SIMO system does not achieve iterative process convergence for when suffering from more than 20% of erasure events. Already at 15% of erasure events, several dBs of improvement is seen thanks to the rotated constellation.

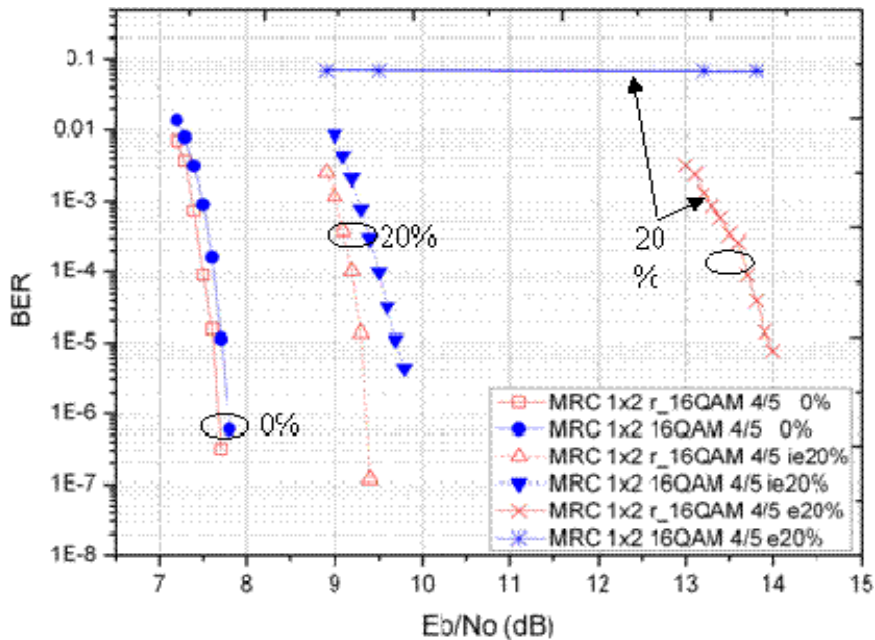


Figure 45. Performance comparison of the SIMO system with/without the rotated constellation over i.i.d. Rayleigh fading channel without/with independent and correlated erasure events at 20%. MRC detector, DVB-T2 rate-4/5 LDPC, 16QAM, 40 iterations.

Figure 45 gives an idea about the performance of a real system. In fact, a real world scenario would have an erasure event with a partial correlation leading to a performance curve in between the curves corresponding to the independent and fully correlated cases.

VI.3.2.4 COMPARISON WITH SISO

Simulations were performed in order to compare the performance of SIMO and SISO schemes over fading channels and fading channels with erasure events. The comparison includes systems with and without rotated constellations.

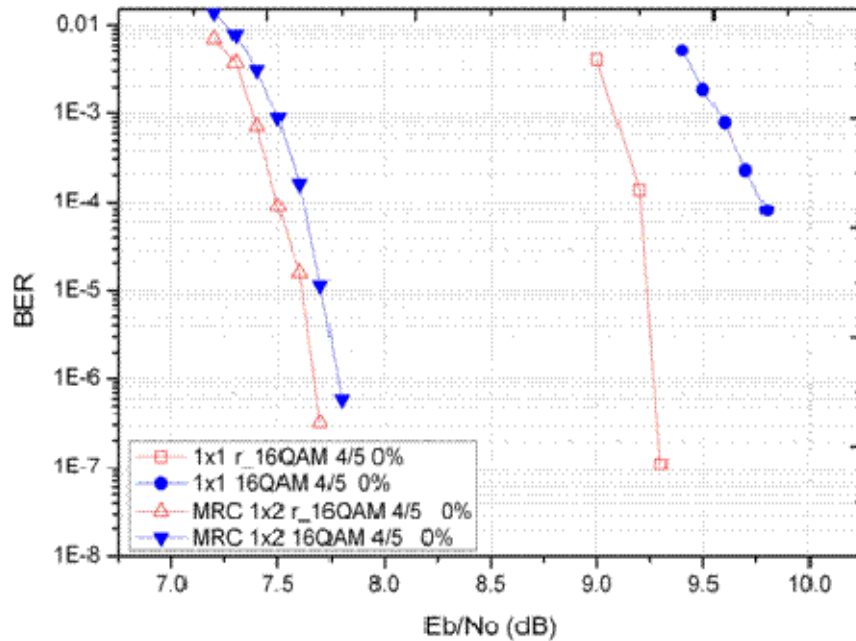


Figure 46. Performance comparison of SIMO and SISO system with/without the rotated constellation over i.i.d. Rayleigh fading channel. MRC detector, DVB-T2 rate-4/5 LDPC, 16QAM, 40 iterations.

Figure 46 shows the results of the above-mentioned comparison over flat fading Rayleigh channels with and without rotation. Note that the received power is also normalized. To obtain the physical SIMO performance, their corresponding curves should be shifted to the left by 3 dB. This shift also applies for the Figure 47 and Figure 48 where the same comparison is performed in the presence of correlated and independent erasure events.

An improvement of 2 dB (to which we add 3dB shift) can be observed for the rotated SIMO system in the presence of 15% of correlated erasure events. Figure 48 shows that the rotated SIMO scheme outperforms in all cases the SISO scheme in the case of independent and correlated erasure events.

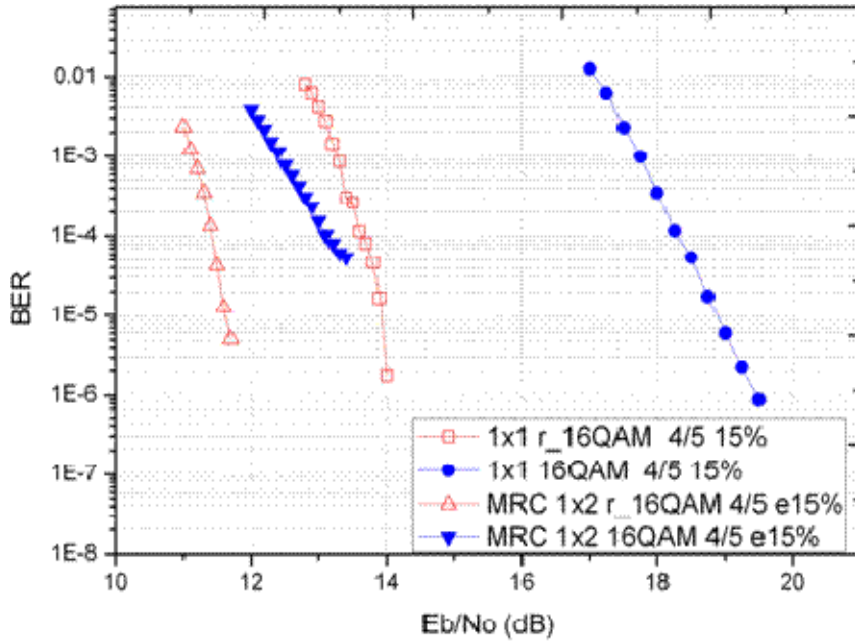


Figure 47. Performance comparison of SIMO and SISO with/without the rotated constellation over i.i.d. Rayleigh fading channel with 15% of correlated erasures. MRC detector, DVB-T2 rate-4/5 LDPC, 16QAM, 40 iterations.

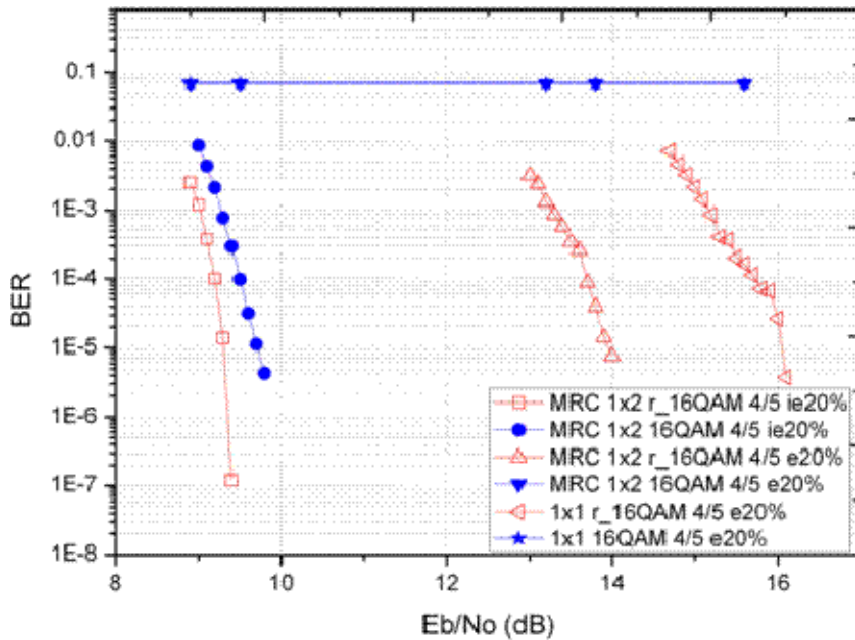


Figure 48. Performance comparison of SIMO and SISO with/without the rotated constellation over i.i.d. Rayleigh fading channel with 20% of independent and correlated erasures. MRC detector, DVB-T2 rate-4/5 LDPC, 16QAM, 40 iterations.

VI.3.3 ROTATED CONSTELLATIONS FOR A SIMO SYSTEM OVER ERASURE CHANNELS: CONCLUSION

In this work we studied the performance of a SIMO system associated with the rotated constellation adopted in the DVB-T2 standard. Two channel models were investigated.

When the i.i.d. Rayleigh fading channel model was considered, the rotation led to a slight improvement of 0.1 dB at BER equal to 10^{-5} . This result is predictable since the combination of a multiple antenna scheme with a powerful outer FEC already takes advantage of the existing diversity over a time invariant channel like the Rayleigh flat fading channel.

However, when erasure events were taken into account, the rotated scheme largely outperformed the non rotated one. The gap between both schemes can range from several tenth of dB to several dBs when the performance of the non rotated scheme leads to an error floor.

VI.4 CONCLUSIONS

The first part of the document concerns the performance of iterative receivers for MIMO system when the DVB-T2 FEC LDPC encoder is considered. Several space-time block codes (STBC) are considered from the classical spatial multiplexing scheme to more complex linear precoding-based STBC. Regarding the previous work presented in TF206, in particular [8], the system design, and then the performance evaluation, take into account the presence of the powerful FEC encoder/decoder. Moreover, through synthesis charts, this study shows the improvements in terms of spectral efficiency and/or BER performance brought by the MIMO system compared to a SIMO or SISO system.

In the first part of the document we evaluated the performance of iterative receivers based on the MMSE criterion and interference cancellation structures when the DVB-T2 FEC LDPC encoder is considered. Through synthesis charts representing spectral efficiency vs E_b/N_0 it was observed that

- compared to the SISO system, the proposed MIMO scheme allowed for a performance gain, greater than 2 dB for low spectral efficiencies and even 6 dB for high spectral efficiencies,
- compared to the SIMO system, the proposed MIMO scheme allowed for a performance gain, greater than 2 dB whatever the couple code rate/modulation

In the second part of the document the principle of rotated constellations that was adopted in the DVB-T2 standard was extended to a SIMO system. The simulation results showed that when erasure events were taken into account, the rotated scheme largely outperformed the non rotated one. The gap between both schemes can range from several tenth of dB to several dBs when the performance of the non rotated scheme leads to an error floor. In the case of i.i.d. Rayleigh fading channel, iterative demapping should be performed to efficiently exploit the signal space diversity provided by the rotated constellation. In the future this work will be extended to MIMO systems.

VI.5 REFERENCES

[1] B. Hassibi, B. Hochwald, "Linear dispersion codes," *IEEE Int. Symp. Inform. Theory (ISIT 2001)*, 2001, p. 325.

- [2] X. Ma et G.B. Giannakis, "Full-diversity full-rate complex-field space-time coding," *IEEE Trans. Signal Process.*, vol. 51, 2003, pp. 2917-2930.
- [3] J.C. Belfiore, G. Rekaya, E. Viterbo, "The golden code: a 2×2 full-rate space-time code with nonvanishing determinants," *IEEE Trans. Inform. Theory*, vol. 51, 2005, pp. 1432-1436.
- [4] A. Tonello, "Space-time bit-interleaved coded modulation with an iterative decoding strategy," *52nd Vehicular Technology Conference (VTC-Fall 2000)*, 2000, pp. 473-478.
- [5] P. Bouvet, M. Helard, J. Le Masson, C. Langlais, "Iterative receivers for linear precoded MIMO system," *4th Int. Symp. on Turbo codes and related topics (ISTC'06)*, 2006.
- [6] M. Sellathurai, S. Haykin, "Turbo-BLAST for wireless communications: theory and experiments," *IEEE Trans. Signal Process.*, vol. 50, 2002, pp. 2538-2546.
- [7] C. Laot, *Égalisation autodidacte et turbo-égalisation. Application aux canaux sélectifs en fréquence*. Ph.D Thesis. Université de Rennes 1, 1997
- [8] M. Crussiere, Y. Nasser, "Analysis of Efficient MIMO-OFDM Systems With Unbalanced Received Powers in the Fixed Digital TV Broadcasting Context", D2.6.1 deliverable, B21C – CELTIC project, December 2007.
- [9] DVB-S2, "Second generation framing structure, channel coding and modulation systems for broadcasting, interactive services, news gathering and other broadband satellite applications," ETSI EN 302 307 V1.1.2, 2006.
- [10] C. Abdel Nour, C. Douillard, "Rotated QAM Constellations to Improve BICM Performance for DVB-T2," *IEEE 10th Int. Symp. on Spread Spectrum Techniques and Applications (ISSSTA 2008)*, 2008, pp. 354-359.
- [11] S. Benedetto, E. Biglieri, *Principles of digital transmission: with wireless applications*, Kluwer academic publishers, 1999.
- [12] C. Abdel Nour, C. Douillard, "Optimisation Of Rotated Constellations For DVB Standards", D06 / D2.4.5 deliverable, B21C – CELTIC project, 2008.

VII MIMO AND OFDM/OQAM

VII.1 INTRODUCTION

The aim of the document is to compare performances between OFDM/OQAM scheme and conventional OFDM one. Since the beginning of the B21C project, Orange Labs has performed a lot of work in order to promote the OFDM/OQAM modulation inside the consortium and also in DVB-T2 standard. The principal interests of OQAM are the improvement of throughput thanks to the lake of the guard interval, the performances against Doppler and the confinement of the spectrum. Of course these advantages are not free since the modem complexity is more than an OFDM one and the performances against long echoes are less than conventional OFDM scheme. It has been shown in [1] and [2] that OFDM/OQAM is suitable for Doppler environments but suffers from large channel delay spreads typical of SFN environments. In addition, we have seen that regarding to the environment, the OFDM/OQAM prototype filter can be adapted since some filters are more suitable for Doppler environments (TFL) and other to large delay spread values (FS). The idea of introducing OFDM/OQAM in a new standard should be very useful for mobile scenario and for networks having delay spread value no more than 10% of the symbol duration. So, the idea is not to entirely stand in conventional CP-OFDM for OFDM/OQAM but to put in as optional to be more robust in mobile environment (train ...).

the point that is introduced in this section is the difficulty to combine OFDM/OQAM with the well known multi-antenna Alamouti coding scheme [3]. *However, is it really a trouble in mobile environment?* After introducing the problem of the association of OFDM/OQAM with Alamouti coding scheme, we compare the performances of OFDM/OQAM regarding OFDM/MISO/Alamouti scheme trough two typical channels:

- additive white Gaussian noise (AWGN) with Doppler;
- channel with an echo at 0dB like single frequency network (SFN) and AWGN.

So, we wish to answer to this question and to quantify the impact of not using Alamouti in mobile scenario.

VII.2 OFDM/OQAM AND ALAMOUTI

VII.2.1 OFDM/OQAM: BRIEF RECALL OF THE BASIC PRINCIPLES

The baseband equivalent of a continuous-time multicarrier OFDM/OQAM signal can be expressed as follows [4]:

$$s(t) = \sum_{m=0}^{M-1} \sum_{n \in \mathbf{Z}} a_{m,n} \underbrace{g(t - n\tau_0) e^{j2\pi m F_0 t}}_{g_{m,n}(t)} \nu_{m,n} \quad \text{Eq.(1)}$$

with \mathbf{Z} the set of integers, $M = 2N$ an even number of sub-carriers, $F_0 = 1/T_0 = 1/2\tau_0$ the sub-carrier spacing, g the prototype function assumed here to be a real-valued and even function and $\nu_{m,n}$ an additional phase term such that $\nu_{m,n} = j^{m+n} e^{j\phi_0}$ where ϕ_0 can be chosen arbitrarily. The transmitted data symbols $a_{m,n}$ are real-valued. They are obtained from a 2^{2K} -QAM constellation,

taking the real and imaginary parts of these complex valued symbols of duration $T_0 = 2\tau_0$, where τ_0 denotes the time offset between the two parts [4].

Assuming a distortion-free channel, the Perfect Reconstruction (PR) of the real data symbols is obtained owing to the following real orthogonality condition:

$$\Re\{\langle g_{m,n} | g_{p,q} \rangle\} = \Re\left\{ \int g_{m,n}(t)g_{p,q}^*(t)dt \right\} = \delta_{m,p}\delta_{n,q},$$

where * denotes conjugation, $\langle . | . \rangle$ denotes the inner product and $\delta_{m,p} = 1$ if $m = p$ and $\delta_{m,p} = 0$ if m different of p . Otherwise said $\langle g_{m,n} | g_{p,q} \rangle$ is a pure imaginary number for $(m, n) \neq (p, q)$.

For a sake of brevity, we set

$$\langle g \rangle_{m,n}^{p,q} = -j \langle g_{m,n} | g_{p,q} \rangle$$

The orthogonality condition for the prototype filter can also be conveniently expressed using its ambiguity function. Indeed, defining it by

$$A_g(n, m) = \int_{-\infty}^{\infty} g(u - n\tau_0)g(u)e^{2j\pi mF_0u} du,$$

it is known [4] that to be orthogonal the OFDM/OQAM prototype has to be such that

$$A_g(2n', 2m') = 0 \text{ if } (n', m') \neq (0, 0) \text{ and } A_g(0, 0) = 1.$$

In practical implementations the baseband signal is directly generated in discrete-time sampling the continuous-time signal at the critical frequency, i.e. with $F_e = MF_0 = 2NF_0$.

Then, based on [5], the discrete-time baseband signal taking the causality constraint into account, is expressed as:

$$s[k] = \sum_{m=0}^{M-1} \sum_{n \in \mathbf{Z}} a_{m,n} \underbrace{g(k - nN)e^{j2\pi m(k - \frac{Lg-1}{2})}}_{g_{m,n}[k]} v_{m,n}. \tag{Eq.(2)}$$

The parallel between (1) and (2) shows that the overlapping of duration τ_0 also corresponds to N discrete-time samples. For sake of simplicity, we will assume that the prototype filter length, denoted L_g , is such that $L_g = bM = 2bN$ with b a positive integer.

With the discrete-time formulation the real orthogonality condition can also be expressed as:

$$\Re\{\langle g_{m,n} | g_{p,q} \rangle\} = \Re\left\{ \sum_{k \in \mathbf{Z}} g_{m,n}[k]g_{p,q}^*[k] \right\} = \delta_{m,p}\delta_{n,q}.$$

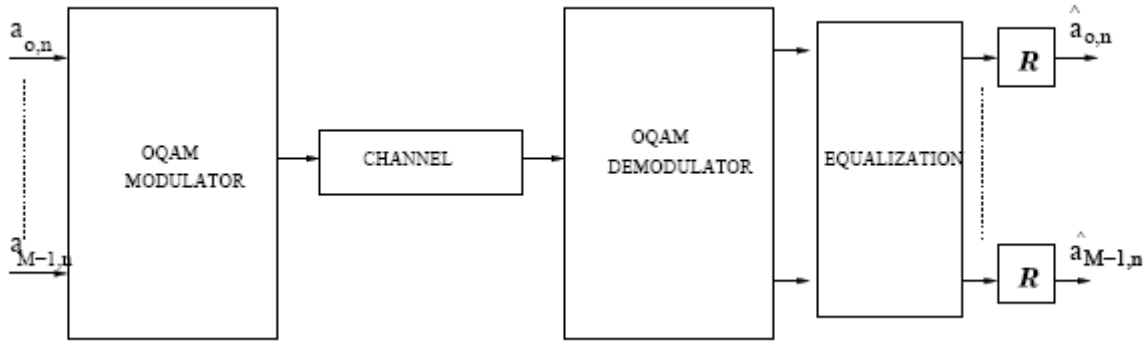


Figure 1: The transmission scheme based on OFDM/OQAM

The above block diagram illustrates our OFDM/OQAM transmission scheme. The propagation channel breaks the real orthogonality condition thus an equalization must be performed at the receiver side to restore this orthogonality.

Let us consider a channel $h(t, \tau)$ that can also be represented by a complex-valued number $H^{(c)}_{m,n}$ for sub-carrier m at symbol time n . At the receiver side, the received signal is the summation of the $s(t)$ signal convolved with the channel impulse response and of a noise component $\eta(t)$. For a locally invariant channel, we can define a neighborhood, denoted $\Omega_{\Delta m, \Delta n}$, around the (m_0, n_0) position, with

$$\Omega_{\Delta m, \Delta n} = \{(p, q), |p| \leq \Delta m, |q| \leq \Delta n | H^{(c)}_{m_0+p, n_0+q} \approx H^{(c)}_{m_0, n_0} \}$$

And we also define

$$\Omega_{\Delta m, \Delta n}^* = \Omega_{\Delta m, \Delta n} - \{(0, 0)\}$$

Note also that Δn and Δm are chosen according to the time and bandwidth coherence of the channel, respectively. Then, assuming

$$g(t - \tau - n\tau_0) \approx g(t - n\tau_0), \forall \tau \in [0, \Delta]$$

The demodulated signal can be expressed as

$$y_{m_0, n_0}^{(c)} = H_{m_0, n_0}^{(c)} (a_{m_0, n_0} + ja_{m_0, n_0}^{(i)}) + J_{m_0, n_0} + \eta_{m_0, n_0}$$

With $a_{m_0, n_0}^{(i)}$, the interference created by the neighbor symbols, is given by

$$a_{m_0, n_0}^{(i)} = \sum_{(p, q) \in \Omega_{\Delta m, \Delta n}^*} a_{m_0+p, n_0+q} \langle g \rangle_{m_0+p, n_0+q}^{m_0, n_0}$$

and, finally, J_{m_0, n_0} the interference created by the data symbols outside $\Omega_{\Delta m, \Delta n}$.

It can be shown that, even for small size neighborhoods, if the prototype function g is well localized in time and frequency, J_{m_0, n_0} becomes negligible when compared to the noise term η_{m_0, n_0} . Indeed a good localization means that the ambiguity function of g , which is directly related to the $\langle g \rangle_{m_0+p, n_0+q}^{m_0, n_0}$ terms, is concentrated around its origin in the time-frequency plane, i.e. only takes small values outside the $\Omega_{\Delta m, \Delta n}$ region. Thus the received signal can be approximated by:

$$y_{m_0, n_0}^{(c)} \approx H_{m_0, n_0}^{(c)} (a_{m_0, n_0} + j a_{m_0, n_0}^{(i)}) + \eta_{m_0, n_0} \quad \text{Eq.(3)}$$

For the rest of the study, we consider equation (3) as the expression of the signal at the output of the OFDM/OQAM demodulator.

VII.2.2 ALAMOUTI SCHEME: GENERAL CASE

In order to describe the Alamouti scheme [3], let us consider the one-tap channel model described as follows: when an antenna u transmits a complex symbol $s_{k,u}$, this symbol is received by the antenna without interference, i.e. the received sample at time instant k , named y_k , is given by:

$$y_k = h_{k,u} s_{k,u} + n_k$$

where $h_{k,u}$ is linked to the channel and corresponds to the channel coefficient between antenna u and the receive antenna, at time instant k . The index k indicates that the channel coefficient can be time variant. The channel coefficients are supposed to have a normal distribution with unitary variance. η_k represents the noise component at time k at the receive antenna. One transmit antenna and one receive antenna is generally referred as SISO model. We consider coherent detection by assuming a perfect knowledge of the channel coefficients at the receiver side.

Originally, the Alamouti scheme has been implemented with 2 transmit and one receive antennas, i.e. 2×1 and symbols are processed by couples. Let us consider s_{2k} and s_{2k+1} to be the two symbols to transmit at time $2k$ and time $2k + 1$, respectively. At time $2k$, the antenna 0 transmits $\frac{s_{2k}}{\sqrt{2}}$ whereas the antenna 1 transmits $\frac{s_{2k+1}}{\sqrt{2}}$. At time $2k + 1$, the antenna 0 transmits $\frac{-(s_{2k+1})^H}{\sqrt{2}}$ whereas the antenna 1 transmits $\frac{s_{2k}}{\sqrt{2}}$ where H stands for the transpose conjugate operation. The term $\frac{1}{\sqrt{2}}$ is used to normalize the total transmitted power. The received samples at time instants $2k$ and $2k + 1$ are given by:

$$\begin{cases} y_{2k} = \frac{1}{\sqrt{2}}(h_{2k,0}s_{2k} + h_{2k,1}s_{2k+1}) + n_{2k} \\ y_{2k+1} = \frac{1}{\sqrt{2}}(-h_{2k+1,0}(s_{2k+1})^* + h_{2k+1,1}(s_{2k})^*) + n_{2k+1} \end{cases}$$

Assuming the channel to be constant between the time instant $2k$ and $2k + 1$, we get

$$\begin{bmatrix} y_{2k} \\ y_{2k+1}^* \end{bmatrix} = \frac{1}{\sqrt{2}} \underbrace{\begin{bmatrix} h_{2k,0} & h_{2k,1} \\ (h_{2k,1})^* & -(h_{2k,0})^* \end{bmatrix}}_{\underline{H}_{2k}} \begin{bmatrix} s_{2k} \\ s_{2k+1} \end{bmatrix} + \begin{bmatrix} n_{2k} \\ n_{2k+1}^* \end{bmatrix} \quad \text{Eq.(4)}$$

Where \underline{H}_{2k} is an orthogonal matrix with $\underline{H}_{2k}\underline{H}_{2k}^H = \frac{1}{2}(|h_{2k,0}|^2 + |h_{2k,1}|^2)\underline{I}_2$ and \underline{I}_2 the identity matrix of size $(2,2)$. Thus using the Maximum Ratio Combining (MRC) equalization, the estimates of s_{2k} and s_{2k+1} are obtained by:

⁴ Time and frequency axis can be permuted in multicarrier modulation

$$\begin{aligned} \begin{bmatrix} \hat{s}_{2k} \\ \hat{s}_{2k+1} \end{bmatrix} &= \frac{\sqrt{2}}{|h_{2k,0}|^2 + |h_{2k,1}|^2} \begin{bmatrix} h_{2k,0}^* & h_{2k,1} \\ (h_{2k,1})^* & -(h_{2k,0}) \end{bmatrix} \begin{bmatrix} y_{2k} \\ y_{2k+1} \end{bmatrix} \\ &= \begin{bmatrix} s_{2k} \\ s_{2k+1} \end{bmatrix} + \begin{bmatrix} \mu_{2k} \\ \mu_{2k+1} \end{bmatrix} \end{aligned}$$

with,

$$\begin{bmatrix} \mu_{2k} \\ \mu_{2k+1} \end{bmatrix} = \frac{\sqrt{2}}{|h_{2k,0}|^2 + |h_{2k,1}|^2} \begin{bmatrix} h_{2k,0}^* & h_{2k,1} \\ (h_{2k,1})^* & -(h_{2k,0}) \end{bmatrix} \begin{bmatrix} n_{2k} \\ n_{2k+1}^* \end{bmatrix}.$$

As the noise components η_{2k} and η_{2k+1} are uncorrelated, we have

$$E(|\mu_{2k}|^2) = E(|\mu_{2k+1}|^2) = \frac{2N_0}{|h_{2k,0}|^2 + |h_{2k,1}|^2}$$

where N_0 denotes the monolateral noise density.

VII.2.3 OFDM/OQAM WITH ALAMOUTI SCHEME

Equation (3) means that we can consider the transmission of OFDM/OQAM on a given sub-carrier as a flat fading transmission even if $a_{m_0, n_0}^{(i)}$ is an inter-carrier and intersymbol term. Thus, let us try to apply the Alamouti scheme on each sub-carrier. As OFDM/OQAM transmits real data, transmitting a complex data $d_{m,n}^{(c)}$ results in OFDM/OQAM to the transmission of its real part $\Re\{d_{m,n}^{(c)}\}$ and its imaginary part $\Im\{d_{m,n}^{(c)}\}$. Let us denote by $a_{m,n,i}$ the real data transmitted by antenna i at time instant m and sub-carrier n . Therefore, if we apply the previous Alamouti scheme to OFDM/OQAM at a particular sub-carrier m , it will result in the transmission of:

$$\left\{ \begin{array}{l} a_{m,2n,0} = \Re\{d_{m,2n}^{(c)}\} \\ a_{m,2n,1} = \Re\{d_{m,2n+1}^{(c)}\} \\ a_{m,2n+1,0} = \Im\{d_{m,2n}^{(c)}\} \\ a_{m,2n+1,1} = \Im\{d_{m,2n+1}^{(c)}\} \\ a_{m,2n+2,0} = -\Re\{(d_{m,2n+1}^{(c)})^*\} = -\Re\{d_{m,2n+1}^{(c)}\} = -a_{m,2n,1} \\ a_{m,2n+2,1} = \Re\{(d_{m,2n}^{(c)})^*\} = \Re\{d_{m,2n}^{(c)}\} = a_{m,2n,0} \\ a_{m,2n+3,0} = -\Im\{(d_{m,2n+1}^{(c)})^*\} = \Im\{d_{m,2n+1}^{(c)}\} = a_{m,2n+1,1} \\ a_{m,2n+3,1} = \Im\{(d_{m,2n}^{(c)})^*\} = -\Im\{d_{m,2n}^{(c)}\} = -a_{m,2n+1,0}. \end{array} \right.$$

Again, we assume the channel to be constant between the time instant $2n$ and $2n + 1$.

This means that in OFDM/OQAM, the channel is assumed to be constant between the time instant $2n$ and $2n+3$, since the time scale in OFDM/OQAM is $\tau_0 = T_0/2$ (transmission

of real symbols). Let us denote by $h_{m,n,i}$ the channel coefficient between transmit antenna i and the receive antenna at sub-carrier m and time instant n . Therefore, at the single receive antenna we have

$$\begin{cases} y_{m,2n} &= h_{m,2n,0}(a_{m,2n,0} + ja_{m,2n,0}^{(i)}) + h_{m,2n,1}(a_{m,2n,1} + ja_{m,2n,1}^{(i)}) + n_{m,2n,0} \\ y_{m,2n+1} &= h_{m,2n,0}(a_{m,2n+1,0} + ja_{m,2n+1,0}^{(i)}) + h_{m,2n,1}(a_{m,2n+1,1} + ja_{m,2n+1,1}^{(i)}) + n_{m,2n+1,1} \\ y_{m,2n+2} &= h_{m,2n,0}(a_{m,2n+2,0} + ja_{m,2n+2,0}^{(i)}) + h_{m,2n,1}(a_{m,2n+2,1} + ja_{m,2n+2,1}^{(i)}) + n_{m,2n+2,0} \\ y_{m,2n+3} &= h_{m,2n,0}(a_{m,2n+3,0} + ja_{m,2n+3,0}^{(i)}) + h_{m,2n,1}(a_{m,2n+3,1} + ja_{m,2n+3,1}^{(i)}) + n_{m,2n+3,1}. \end{cases} \text{Eq.(5)}$$

Setting

$$\begin{cases} z_{m,2n} &= y_{m,2n} + jy_{m,2n+1} \\ z_{m,2n+1} &= y_{m,2n+2} + jy_{m,2n+3}, \end{cases}$$

And using Eq.(5)

$$\begin{cases} z_{m,2n} &= h_{m,2n,0}d_{m,2n}^{(c)} + h_{m,2n,1}d_{m,2n+1}^{(c)} + h_{m,2n,0}x_{m,2n,0} + h_{m,2n,1}x_{m,2n,1} + \kappa_{m,2n,0} \\ z_{m,2n+1} &= -h_{m,2n,0}(d_{m,2n+1}^{(c)})^* + h_{m,2n,1}(d_{m,2n}^{(c)})^* \\ &\quad -h_{m,2n,0}(x_{m,2n+2,0})^* + h_{m,2n,1}(x_{m,2n+2,1})^* + \kappa_{m,2n+2,0}. \end{cases}$$

With

$$\begin{cases} x_{m,2n,0} &= -a_{m,2n+1,0}^{(i)} + ja_{m,2n,0}^{(i)}, x_{m,2n,1} = -a_{m,2n+1,1}^{(i)} + ja_{m,2n,1}^{(i)} \\ \kappa_{m,2n,0} &= n_{m,2n,0} + jn_{m,2n+1,0}, \kappa_{m,2n,0} = n_{m,2n+2,0} + jn_{m,2n+3,0} \\ x_{m,2n+2,0} &= a_{m,2n+3,0}^{(i)} + ja_{m,2n+2,0}^{(i)}, x_{m,2n+2,1} = -a_{m,2n+3,1}^{(i)} - ja_{m,2n+2,1}^{(i)}. \end{cases}$$

This results in the following equation:

$$\underbrace{\begin{bmatrix} z_{m,2n} \\ (z_{m,2n+1})^* \end{bmatrix}}_{z_{2n}} = \underbrace{\begin{bmatrix} h_{m,2n,0} & h_{m,2n,1} \\ (h_{m,2n,1})^* & -(h_{m,2n,0})^* \end{bmatrix}}_{Q_{2n}} \underbrace{\begin{bmatrix} d_{m,2n}^{(c)} \\ d_{m,2n+1}^{(c)} \end{bmatrix}}_{d_{2n}} + \underbrace{\begin{bmatrix} h_{m,2n,0} & h_{m,2n,1} & 0 & 0 \\ 0 & 0 & (h_{m,2n,1})^* & -(h_{m,2n,0})^* \end{bmatrix}}_{K_{2n}} \underbrace{\begin{bmatrix} x_{m,2n,0} \\ x_{m,2n,1} \\ x_{m,2n+2,0} \\ x_{m,2n+2,1} \end{bmatrix}}_{x_{2n}} + \underbrace{\begin{bmatrix} \kappa_{m,2n} \\ (\kappa_{m,2n+1})^* \end{bmatrix}}_{\kappa_{2n}}$$

Q_{2n} is an orthogonal matrix that is similar to the one found in Eq.(4) for the conventional 2X1 Alamouti scheme. However, the $K_{2n}x_{2n}$ term appears, which is an interference term due to the fact that OFDM/OQAM has only a real orthogonality. Therefore, even without noise and assuming a distortion-free channel, we cannot achieve a good error probability since $K_{2n}x_{2n}$ is an inherent “noise” component.

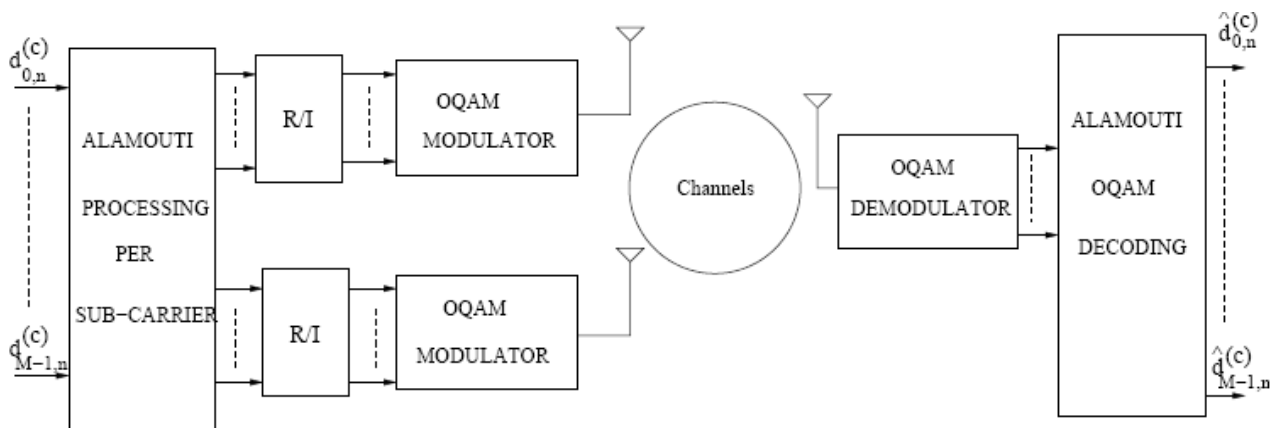


Figure 2: Alamouti transmission scheme with OFDM/OQAM.

Otherwise said, the Alamouti OFDM/OQAM transmission scheme depicted in Fig. 2, where the R/I blocks implement the staggering rule that leads, taking separately the real and imaginary parts of the complex numbers, to the $a_{m,n}$ data symbols, is naturally impaired by an “extra” noise component. This can be seen as a consequence of the absence of a complex orthogonality property of the OFDM/OQAM. To tackle this drawback some research studies are being carried out [6] [7] and [8]. Now, having introduced the trouble of the combination of OFDM/OQAM with Alamouti, we propose to compare SISO OFDM/OQAM versus MISO Alamouti CP-OFDM in order to see if Alamouti is suitable and more resistant for mobile environment and large delay spread values.

VII.3 SISO OFDM/OQAM VERSUS MISO ALAMOUTI CP-OFDM

VII.3.1 CONTEXT

In this part we present the performances of the OFDM/OQAM (Orthogonal Frequency Division Multiplex/ Offset Quadrature Amplitude Modulation) modulation compared to OFDM/MISO /Alamouti through two typical channels, one tap with Doppler and AWGN (Additive White Gaussian Noise) and SFN model (Single Frequency Network) with AWGN.

For these evaluations we use a modem implementing DVB-T framing and Turbo coding scheme. After a presentation of OFDM/OQAM, we present different OQAM filter family with their performances in terms of Doppler and delay spread robustness.. Then, we select the best solution for the comparison with OFDM/MISO/Alamouti.

In the last part we present the performances obtained with the OFDM/MISO/Alamouti decoder either by using the simple ZF (Zero Forcing) decoder or the MMSE (Minimum Mean Square Error) one. Comparison is carried out by considering a SISO OFDM/OQAM transmission with the TFL1 prototype filter.

VII.3.2 SIMULATION CHAIN DESCRIPTION

The software validation chain is similar to the VHDL prototyping developed at Orange Labs in Rennes. It is based on the DVB-T framing in 2K mode. It is composed of:

- A random data generator;
- A duo binary turbo coder of 1504 info size bits;
- A specific bit interleaver of the same size for the systematic and redundancy parts;
- A puncturing component in order to achieve the 1/2, 7/12, 2/3, 5/6 and 11/12 coding rates;
- A pre-mapping block that optimizes the results for low SNR values (LSB and MSB bit partitioning);
- A mapping component allowing to generate the QPSK, 16QAM, 64QAM and 256QAM mappings;
- A framing module that inserts the scattered pilots (and that will allow to process the OFDM/OQAM intrinsic interference produced by the pilot on the neighbourhood data);
- A phase component that corresponds to the ambiguity function of the OFDM/OQAM filters;
- A 2K FFT modulation;
- The OFDM/OQAM prototype filter is the **TFL1** one since it proposes the best compromise between Doppler shift and resistance against large delay spreads.

At the reception side, the dual transmitter functions are implemented by considering the perfect channel estimation either with Zero Forcing or MMSE equalization for MISO scenario. The sampling frequency is equal to 9.14 MHz has defined in DVB-T/H standards for the 8MHz bandwidth.

The Figure 3 depicts the simulation chain block diagram.

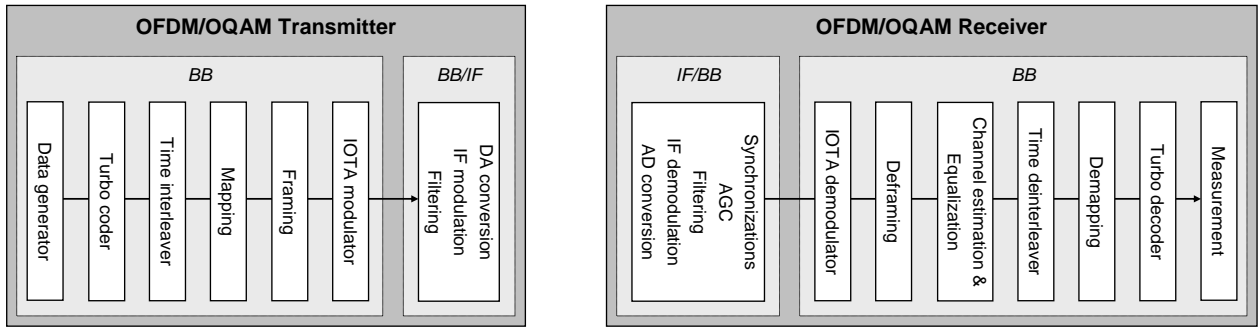


Figure 3: Simulation chain block diagram

VII.3.3 PRESENTATION OF THE DIFFERENT OFDM/MISO/ALAMOUTI SCHEMES

To compare conventional MISO/OFDM based on the Alamouti STBC scheme and SISO/OQAM, we are tested two different structures of MISO/Alamouti. The first one is the classical STBC (Space Time Block Coding) solution that performs the Alamouti coding in the time domain and the second was proposed and accepted by the DVB-T2 consortium that carries out the Alamouti coding in the frequency domain. The fact not to combine Alamouti with OQAM is deliberately done, due to the fact that technical troubles are not solved.

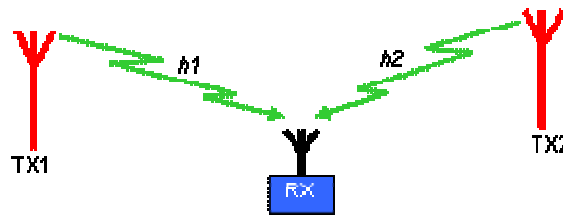


Figure 4: MISO description

VII.3.4 TIME APPROACH (CLASSICAL)

This approach is the simple explanation of the transmission scheme with Alamouti Space Time Block coding that is represented in the following table.

	n	$n+1$
S_1	$X_{n,m}$	$X_{n+1,m}^*$
S_2	$-X_{n+1,m}$	$X_{n,m}^*$

n : time index

S_1 : signal out for the first antenna

S_2 : signal out for the second antenna

(*): complex conjugate

Alamouti decoder is:

$$R_1 = H_1 X_{m,n} + H_2 X_{n,m+1} + N_1$$

$$R_2 = -H_1 X_{n,m+1}^* + H_2 X_{n,m}^* + N_2$$

Where H_1 and H_2 describe the channel transfer functions between T_{X1} and R_x and T_{X2} and R_x respectively, and with N_1 and N_2 characterizing the noise terms.

VII.3.5 FREQUENCY APPROACH (INCLUDED IN DVB-T2)

For the frequency approach the transmission scheme is described below:

	m	m+1
S_1	$X_{n,m}$	$X_{n,m+1}$
S_2	$-X_{n,m+1}^*$	$X_{n,m}^*$

m: frequency index

S_1 : signal out for the first antenna

S_2 : signal out for the second antenna

(*): complex conjugate

Accordingly, the signal components can be recovered at the receiver side, as follows. The received complex values for the cells of a MISO pair, R_1 and R_2 are given by:

$$R_1 = H_1 X_{m,n} - H_2 X_{n,m+1}^* + N_1$$

$$R_2 = H_1 X_{n,m+1} - H_2 X_{n,m}^* + N_2$$

VII.3.6 PERFORMANCES RESULTS

The performances obtained through the modem presented in §VII.3.2 between SISO/OFDM/OQAM and OFDM/MISO/Alamouti against Doppler are presented below.

VII.3.6.1 RESULTS WITH DOPPLER SHIFT

The principle of the simulation is for one Doppler shift, we look at a target BER (Bit Error Rate) around 10^{-4} according to a variation of the SNR (Signal to Noise Ratio) value.

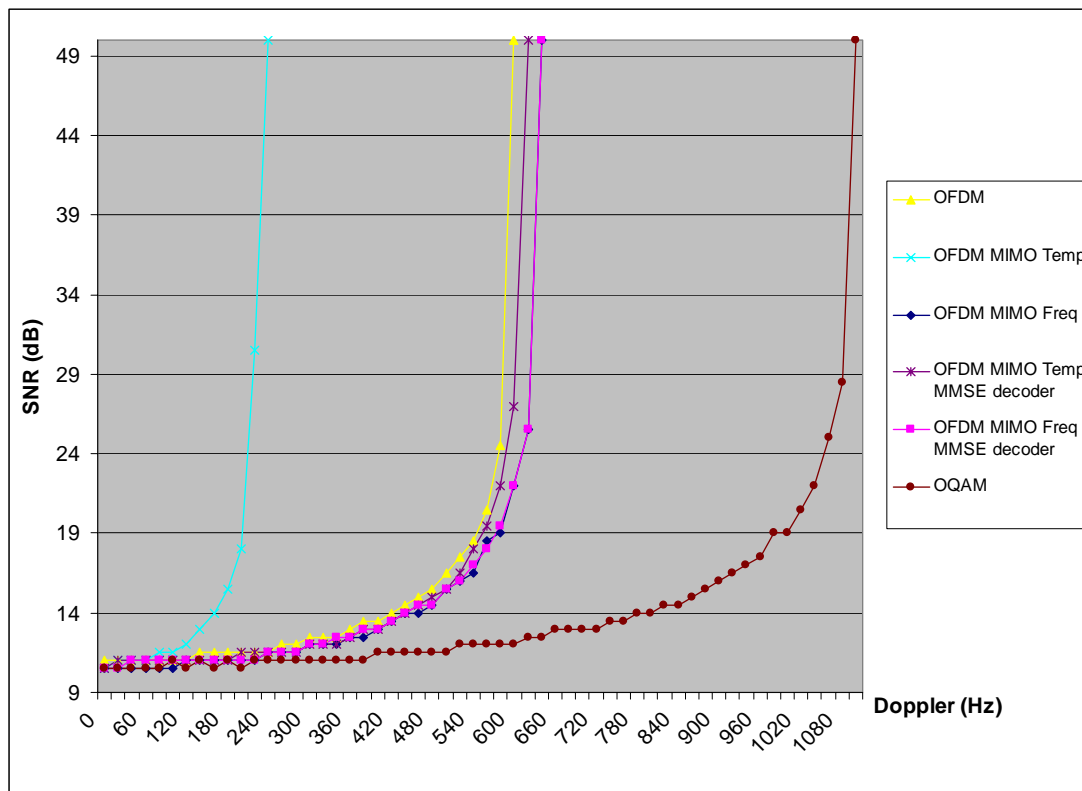


Figure 5: Performance results comparing the OFDM/OQAM, OFDM conventional and OFDM/MISO/Alamouti in Doppler environment

First, we notice, in Figure 5 that the gain is around 1.7 for OQAM against conventional OFDM that confirms the previous results. For the implementation corresponding to the STBC structure carried out in the time domain, it is essential to use a MMSE decoder. Indeed, the implementation of STBC Alamouti coding assumes that the channel must be invariant in the direction where the coding is applied. In the case of time varying channel (subject to velocity impact), the implementation of ZF decoding doesn't allow to restore the STBC orthogonality. The main conclusion is that adding a MISO component to conventional OFDM is not sufficient to achieve the SISO/OQAM performance in terms of Doppler impact. In addition, it is more suitable to implement Alamouti in the frequency domain when considering time varying channel as proposed by DVB-T2 consortium and in that case ZF decoder is sufficient enough (not necessary to implement MMSE decoder).

VII.3.6.2 RESULTS WITH SFN CHANNEL

The characteristic of SFN is a two paths channel with 0dB coefficients. For the simulation we change the delay (in μs) of the second path. It's like for Doppler the target is a BER around 10^{-4} according to a variation of SNR in decibel. In this simulation scenario, we considered a channel without Doppler.

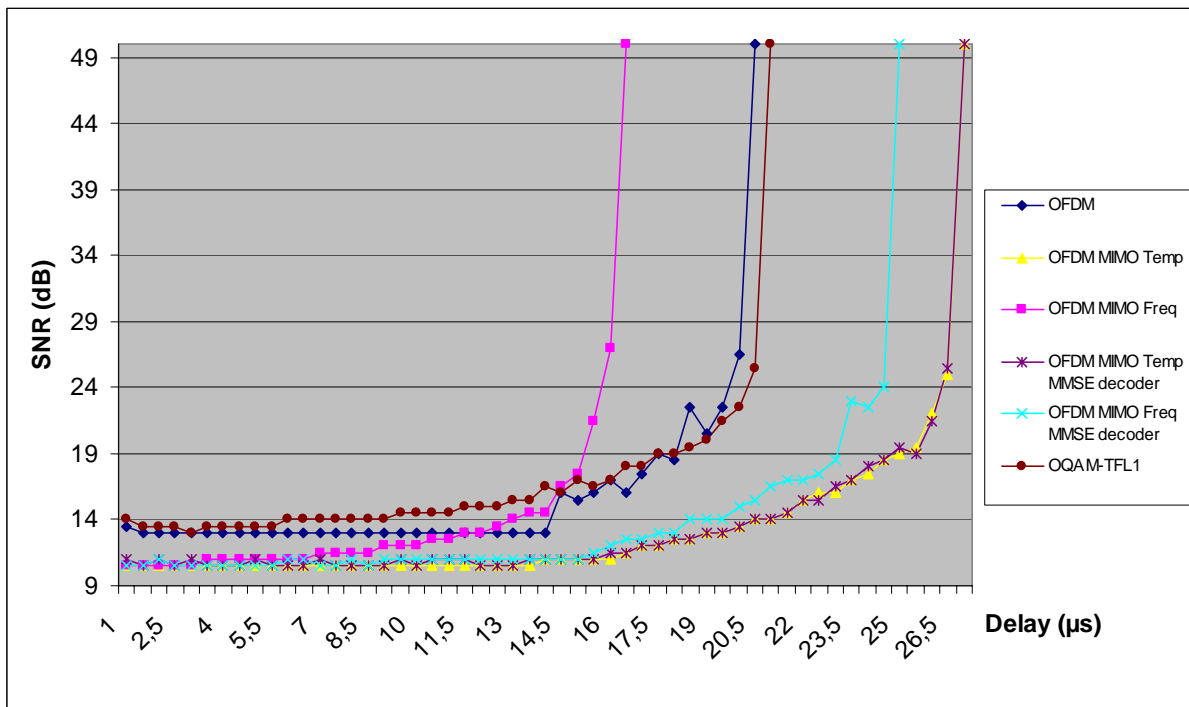


Figure 6: Performance results comparing the OFDM/OQAM, OFDM conventional and OFDM/MISO/Alamouti in SFN

Figure 6 shows that performance results between conventional OFDM with guard interval of 1/16 and OFDM/OQAM with TFL1 filter are equivalent. For the low delays we notice the gain from MISO/Alamouti around 3dB against conventional OFDM and OFDM/OQAM; this gain comes from the antenna diversity. Between the two schemes of MISO/Alamouti applied either in the time or in the frequency domains for SFN channel the classical structure (STBC in time) is required. Indeed, SFN scenario leads to very selective channel that induces channel variations between consecutive sub-carriers. Then, the Alamouti hypothesis is not ensured as explained previously and needs to apply MMSE decoder. We can also notice that the MISO component allows the conventional OFDM system to be more robust against large echoes and that for SFN environment, time domain MISO/OFDM is more suitable than frequency one. Then, the STBC solution done in DVB-T2 is less robust than classical time domain Alamouti coding scheme when considering SFN environment.

VII.4 CONCLUSION

The first part of this document was to introduce the difficulty of combining OFDM/OQAM with Alamouti and also to evaluate the performances of OFDM/OQAM against OFDM/MISO/Alamouti through two typical channels affected either by Doppler or SFN environments. After referring to some contributions already presented in the B21C framework and recalling that the OFDM/OQAM is well adapted to mobile environment with delay spread values less than 10% of the symbol duration, we give a comparison between conventional OFDM with MISO/Alamouti and SISO/OQAM. We have shown that MISO transmission doesn't improve the OFDM performances in Doppler environment. In the case of time varying channel, it has been shown that Alamouti performed in the frequency domain as proposed in DVB-T2 is more suitable than Alamouti carried out in the time domain, that allows the system to only implement a ZF decoder. This conclusion can be reversed when considering SFN environment where MMSE decoder is necessary when performing the DVB-T2 solution. In addition, MISO transmission in SFN scenario has shown that

OFDM is more robust against frequency selective channel mainly when implementing classical time domain Alamouti. However, performing Alamouti doesn't improve the performance in case of Doppler effect and doesn't allow to reach the performances of a SISO OFDM/OQAM system.

However, in SFN environment, the Alamouti coding scheme brings some improvements, especially when implementing it in the time domain. The last remark concerns the proposition of DVB-T2 consortium with a MISO/Alamouti coded in frequency, the results have shown that this solution doesn't bring anything with regard to the Doppler effect. In SFN environment, it obliges to use MMSE decoder whereas it gives worst performance than classical Alamouti scheme

VII.5 REFERENCES

- [1] D06 Report – B21C deliverable – "Report on waveform and channel coding studies" March 2009.
- [2] Internal D06 deliverable – B21C deliverable – " MODULATION AND WAVEFORM STUDIES ABOUT ADVANCED MULTI-CARRIER MODULATION SCHEME: OFDM/OQAM" – March 2009
- [3] S. M. Alamouti, "A simple transmit diversity technique for wireless communications," IEEE Journal on Selected Areas in Communications, vol. 16, no. 8, pp. 1451–1458, Oct. 1998.
- [4] B. Le Floch, M. Alard, and C. Berrou, "Coded Orthogonal Frequency Division Multiplex," Proceedings of the IEEE, vol. 83, pp. 982–996, June 1995.
- [5] P. Siohan, C. Siclet, and N. Lacaille, "Analysis and design of OFDM/OQAM systems based on filterbank theory," IEEE Transactions on Signal Processing, vol. 50, no. 5, pp. 1170–1183, May 2002.
- [6] M. Bellanger, "Transmit diversity in multicarrier transmission using OQAM modulation," in ISWPC 2008, Santorini, Greece, May 2008.
- [7] H. Lin, C. L   , and P. Siohan, "A pseudo alamouti transceiver design for OFDM/OQAM modulation with cyclic prefix," in SPAWC, Perugia, Italy, June 2009.
- [8] C. L   , P. Siohan and R. Legouable, "The Alamouti scheme with CDMA-OFDM/OQAM" to be published in EURASIP JASP: "FILTER BANKS FOR NEXT GENERATIONS MULTICARRIER WIRELESS COMMUNICATIONS".